Study on root system development by modeling approach(Dissertation_全文)

AUTHOR(S):

Tsutsumi, Daizo

CITATION:

Tsutsumi, Daizo. Study on root system development by modeling approach. 京都大学, 2003, 博士(農学)

ISSUE DATE:

2003-03-24

URL:

https://doi.org/10.14989/doctor.k10236

Study on Root System Development by Modeling Approach

Daizo Tsutsumi

2003

Study on Root System Development by Modeling Approach

Daizo Tsutsumi

Kyoto University, Kyoto, Japan

2003

CONTENTS

CHAPTER 1

INTRODUCTION

The plant root system, which is the underground part of the plant body, consists of numerous individual roots, and has some important functions. First, roots absorb water and nutrients from the soil. The water and nutrient absorption efficiency affects the crop yield, which is one of the greatest interests in crop science. Also, the circulation of water through the soil, plant, and atmosphere plays an important role in the hydrological process in a field or forest. Second, the root system architecture resists and supports loading of the aboveground part of a plant. This function contributes to preventing trees from being felled by strong winds. Third, the root system increases the stability of the soil structure. This function contributes to controlling the erosion of the soil surface layer and preventing a hillside slope from being collapsed by landslides. The root system development is affected by its surrounding environments, namely gravity, water, temperature, nutrients, and soil structure. As a result of these effects on the root system development, the root system changes its morphological architecture to adapt to changes in the surrounding environment. Therefore, understanding the mechanism of the root system development is fundamental to understand the physiological and morphological functions of the root system itself. However, studies of the root system, which is hidden under the ground, are lagging when compared to the studies of plant shoots or leaves. The reason for this may be that it is hard and time-consuming labor to reveal the root system in the soil because the root system exists under the ground. Even if the root system can be excavated from the ground, it is almost impossible to observe continuous root system development. In this sense, a modeling approach may help in promoting the study of the root system.

In general, root system development may be considered as a combination of root branching and root elongation. In a root system development model, the root branching and root elongation are represented with mathematical descriptions and are calculated by means of numerical simulation. The root system development model is, therefore, a useful tool to predict the root system morphology and to understand the process or the mechanism of root system development as affected by the surrounding environments. Furthermore, root system development models which are combined with water or nutrient uptake models can be used for simulating synchronized root system development and its soil water uptake or nutrient uptake behaviors. As a pioneer study of modeling plant root system development, Lungley (1973) proposed a

two-dimensional model. Diggle (1988) and Pages et al. (1989) developed three-dimensional root system architecture models. They successfully simulated the crop plant root system development and morphological architecture three-dimensionally. It seems that the fundamental part of root system development modeling has been completed by these models. Recently, root system development models focus on the interactions between the plant root systems and soil water flow (Clausnitzer and Hopmans, 1994; Doussan et al., 1998), or nutrient supply (Dunbabin et al., 2002; Somma et al., 1998), which combines the water uptake models or nutrient uptake models. Many other models have been proposed and some of them have succeeded in simulating root system development in various plant species, under various conditions (e.g. Jourdan and Rey, 1997; Lynch et al., 1997; Shibusawa, 1994). However, All applications of these models were made to the root systems developing on plane, and no applications on slopes can be found. It is empirically known that a plant that grows on a slope has an asymmetric root system, and this asymmetric architecture of the root system has been confirmed in some experimental studies (Scippa et al., 2001; Yamadera, 1990). Recently, the contribution of plant root system architecture to slope stability has become one of the primary interests in the fields of erosion-control and re-vegetation-technology. Some studies suggest that plant root systems growing under hillside slope contribute to slope stability, increasing soil resistance against shear stress, and decreasing the soil water content through their water uptake (Greenway, 1987; Tsukamoto, 1987). These effects of root systems have been investigated extensively, considering root strength, growth and rate of decay (Abe, 1996; Kato and Syuin, 2001; Syuin, 1998; Syuin et al., 1998; Tsukamoto, 1987; Watson et al., 1999). Modeling the root system development and soil water flow on slopes may contribute greatly to slope stability analysis. To simulate root system development and soil water flow on a slope, it is necessary to take into account the effect of environmental conditions of the slope on root growth. It is also necessary to understand the mechanism of root system development itself. Some experimental results show that root growth is influenced by hydrotropism, which is root elongation toward water (Takahashi, 1994; Takahashi and Scott, 1993; Takano et al., 1995). Because soil moisture distributes asymmetrically on a slope, root hydrotropism can be one of the important factors in causing asymmetric root system development.

Root hydrotropism, which is root elongation bending toward moisture according to a water gradient, has been known empirically and had been reported in earlier published studies (Darwin, 1880; Hooker, 1915). However, little attention had been paid to hydrotropism for many years, partly because some earlier workers failed to detect the occurrence of hydrotropism (Dutrochet, 1824; Keith, 1815). Their failure was due to an inability to control appropriate moisture gradient, and due to the counteracting effects of gravity (Takahashi, 1994). Recently, experimental methods

have been improved and their results were reported in studies. Takahashi and Scott (1993) strictly controlled the gradient of air humidity in a closed chamber and observed that the roots of pea (*Pisum sativum* L.) and corn (*Zea may* L.) grew bending toward the direction of moisture. Takano et al. (1995) applied a water potential gradient to the root cap of an agravitropic pea mutant *ageotropumi*, that does not respond to gravity, and observed that the root elongated bending toward the side of the higher water potential. By these studies, the existence of hydrotropism was confirmed and accepted as a genuine plant tropism. Together with other root tropisms, i.e. gravitropism, thigmotropism, thermotropism, root hydrotropism may ultimately contribute to establishment of a root system, by which roots avoid environmental risks such as drought conditions, and support the growth and development of the whole plant. However, in all the experiments on root hydrotropism, the effect of hydrotropism on only the elongation of an individual root was investigated. There seems to have been no studies investigating the effect of hydrotropism on the entire plant root system development. Although the effect of soil moisture conditions or drip irrigation on entire root system development and its morphological architecture in various crop plants (Galamay et al., 1992; Kono et al., 1987) or vegetables (Morita and Toyoda, 1998) were investigated, these effects were not considered as root hydrotropism, and sufficient theoretical considerations were not carried out.

The objectives of this study are (1) to develop a new model, which can simulate and analyze root system development and soil water flow both on plane and slope, by considering the effect of hydrotropism which is not considered in conventional models and (2) to understand the mechanism of plant root system development for the purpose of investigating the effect of soil water conditions on root system development by measuring the quantitative root system morphological architecture and distribution of soil water content.

The objectives of Chapter 2 are to classify the models on root system and to review some conventional root system development models. After the reviews, those items which of necessity must be included into any new model are summarized.

In Chapter 3, a two-dimensional root system development model considering hydrotropism is proposed, and applied to root system development on a slope. The outputs from the model are then compared to those from a conventional model, in which hydrotropism is not considered.

In Chapter 4, an experiment on the root system development in a root box was carried out in order to investigate the effect of hydrotropism on actual plant root growth, and the results are presented. From the experimental results, the effect of hydrotropism on root system development and its importance on root system

morphological architectures were investigated.

In Chapter 5, the two-dimensional root system development model was applied for simulating the experimental results of root system development and soil water flow in the root box, presented in Chapter 4. And hypothesis that employed in the model was examined.

In Chapter 6, a three-dimensional root system development model is proposed. The model is based on the two-dimensional model previously shown in Chapter 3 and 5. Actual plant root system architectures that were developed on slopes were observed and simulated by the model incorporating the actual soil and weather conditions into the model.

Chapter 7 summarizes the conclusions of each chapter. The general conclusions are then presented.

REFERENCES

Abe T. 1996 In-situ Direct Shrear Test for Study on Tree Root Function of Preventing Landslides J. Jpn. Soc. Reveget. Tech. 22(2), 95-108

Clausnitzer V. and Hopmans J.W. 1994 Simultaneous modeling of transient three-dimensional root growth and soil water flow. Plant and Soil 164, 299-314

Darwin C. 1880 The power of Movement in Plants. John Murray, London

Diggle A. J. 1988 ROOTMAP —a model in three-dimensional coordinates of the growth and structure of fibrous root systems. Plant and Soil 105, 169-178

Doussan C., Pages L. and Vercambre G. 1998 Modeling of the hydraulic architecture of root systems: An integrated approach to water absorption – model description. Annals of Botany 81, 213-223

Dunbabin V.M., Diggle A.J., Rengel Z. and van Hugten R. 2002 Modelling the interactions between water and nutrient uptake and root growth. Plant and Soil 239, 19-38

Durtochet H. 1824 Physiologische Untrsuchungen uber die Beweglichkeit der Pflanzen. Ubersetzt von Nathansohn. Ostwald's Klassiker der exacten Wissenschaften, 144 Cited by von Sachs.

Galamay T.O., Yamauchi A., Nonoyama T. and Kono Y. 1992 Acropetal lignification in protective tissues of cereal nodal root axes as affected by different soil moisture conditions. Jpn. J. Crop Sci. 61(3), 511-517

Greenway D.R. 1987 Vegetation and slope stability, In Slope Stability, edited by Anderson M. F. and Richards K. S. New York, Wiley, 187-230

Hooker H.D.Jr. 1915 Hydrotropism in roots of Lupinus albus. Ann. Bot. 29, 265-283

Jourdan C. and Rey H. 1997 Modeling and simulation of the architecture and development of the oil-palm (Elaeis guineensis Jacq.) root system I. The model. Plant and Soil 190, 217-233

Kato N. and Syuin Y. 2001 Effects of Soil Suction on Root Reinforcement in Unsaturated Forest Soil J. Jpn. Soc. Erosion Control Eng. 54(2), 32-37

Keith P. 1815 On the development of the seminal germ. Trans. Linn. Soc. 11, 252-269

Kono Y., Yamauchi A., Nonoyama T., Tatsumi J. and Kawamura N. 1987 A revised experimental system of root-soil interaction for laboratory work. Environ. Control in Biol. 25(4), 141-151

Lungley D.R. 1973 The growth of root systems –A numerical computer simulation model. Plant and Soil 38, 145-159

Lynch J.P., Nielsen K.L., Davis R.D. and Jablokow A.G. 1997 SimRoot: Modelling and visualization of root systems. Plant and Soil 188, 139-151

Morita S. and Toyota M. 1998. Root system morphology of pepper and melon at harvest stage grown with drip irrigation under desert conditions. Jpn. J. Crop Sci. 67(3), 353-357 (in Japanese with English summery)

Pages L., Jordan M.O. and Picard D. 1989 A simulation model of the three-dimensional architecture of the maize root system. Plant and Soil 119, 147-154

Scippa G.S., Baraldi A., Urciouli D. and Chiatante D. 2001 Root response to slope condition. Which are the factors involved? Analysis at biochemical and molecular level. Proceedings of the 6th symposium of the international society of root research (Nov. 2001, Nagoya, Japan), Jpn. Soc. Root Res., Nagoya, Japan 128-129

Shibusawa S. 1994 Modelling the Branching Growth Fractal Pattern of the Maize Root

System Plant and Soil 165, 339-347
Somma F., Hopmans J.W. and Clausnitzer V. 1998 Transient three-dimensional modeling of soil water and solute transport with simultaneous root growth, root water and nutrient uptake. Plant and Soil 202, 281-293
Syuin Y. 1998 A Model for the Effect of Soil Moisture Fluctuation on Soil Reinforcement by Root －Application of the Model to the Results of Direct Shear Test Using Substitute Materials Simulating a Root System－ J. Jpn. Soc. Erosion Control Eng. 51(4), 11-20
Syuin Y., Kato H., Suzuki M. and Ohta T. 1998 Effects of Soil Moisture Fluctuation on Soil Reinforcement by Root －Direct Shear Tests with Materials Simulating a Root system－ J. Jpn. Soc. Erosion Control Eng. 51(1), 23-30
Takahashi H. 1994 Hydrotropism and its interaction with gravitropism in roots. Plant and Soil 165, 301-308
Takahashi H. and Scott T.K. 1993 Intensity of hydrostimulation for the induction of root hydrotropism and its sensing by the root cap. Plant Cell Environ 16, 99-103
Takano M., Takahashi H., Hirasawa T. and Suge H. 1995 Hydrotropism in roots: sensing of a gradient in water potential by the root cap. Planta 197, 410-413
Tsukamoto Y. 1987 Evaluation of the Effect of Tree Roots on Slope Stability. Bulletin of the Experiment Forest, Tokyo Univ. of Agric. And Tech. 23, 65-123
Watson A., Phillips C. and Marden M. 1999 Root strength, growth, and rates of decay: root reinforcement changes of two tree species and their contribution to slope stability. Plant and Soil 217, 39-47
Yamadera Y. 1990 Experimental study for improving the revegetation technique on steep hillside slopes. Tokyo, Japan (In Japanese)

CHAPTER 2

A REVIEW OF ROOT SYSTEM DEVELOPMENT MODELS

2.1 CLASSIFICATION OF MODELS OF ROOT SYSTEM

All the models of root systems can be divided into three types, "development models", "morphometric models", and "distribution models". The development models and the morphometric models can be sub-classified into smaller categories. The root system development model that will be considered in this study is regarded as a development model. However, in order to make the objectives of the study clear, the author shows the classification of the root system models, first.

2.1.1 Development Model

In development model, roots are distinguished by their hierarchy, that is first-order, second-order, etc., and their growths are represented by defined specific rules. The development models can be sub-classified into two categories, "algebraic models" and "numerical models".

2.1.1.1 Algebraic model

In algebraic model, root growth is described by algebraic equations, in which factors considering root growth are represented by basic parameters. By solving the equations, the characteristics of root system development, such as total root numbers or total root length can be analyzed. However, the algebraic model can only describe the specific root system development using constant elongation rates and constant branching intervals. Hackett and Rose (1972a, b) proposed one of the algebraic models.

2.1.1.2 Numerical model

In the numerical model, root growth is described as a set of equations, which is similar to the algebraic model. However, the equations are solved numerically by the use of a computer. Therefore, every individual root growth can be obtained as a trajectory of each root tip. Because of the numerical calculation, the elongation rate or branching interval needs not to be of a constant value parameter. Therefore, it is also possible to simulate more complicated root growths and to obtain more variable information by the numerical models rather than the algebraic models. The pioneer of the numerical model is a model by Lungley (1973). Then Diggle (1988) and Pages et

al. (1989) proposed advanced three-dimensional models. After that, many other models were proposed (e.g., Clausnitzer and Hopmans, 1994; Jourdan and Rey, 1997; Lynch et al., 1997; Shibusawa, 1994; Somma et al., 1998), and are being used extensively.

2.1.2 Morphometric Model

The objective of the morphometric models is not to represent the actual shapes or architecture of a root system, but rather to analyze the root system morphologies with the aid of mathematical theories as "graph theory" or " fractal theory". Therefore, the morphometric model can be sub-classified into two categories, "topology model" and "fractal model", according to their theories used.

2.1.2.1 Topology model

Fitter et al. (1991a, b) proposed a model that describes root system morphological architecture by a graph theory. The graph is a diagram consists of points and links that connect the points, and the graph theory is a part of the topology that analyzes graph as an interaction between the points and links. Fitter et al. (1991a, b) distinguished root systems into herringbone type and dichotomous type, and predicts which type of root system is beneficial to acquire resources from soil, under different nutrient conditions.

2.1.2.2 Fractal model

Tatsumi (1989) analyzed root systems by fractal theory, and described complexity of the root system as a fractal dimension. The advantage of describing a root system by a fractal model is to estimate the total root system characteristics from a part of the root system.

2.1.3 Distribution Model

Distribution of roots, that is the length density and rooting depth, is empirically known and represented with simple mathematical equations. Gerwits and Page (1974) represented the one-dimensional distribution of root length density with a liner function and an exponential function. Gandar and Hughes (1988) represented them with an elliptical function. Brog and Grimes (1986) estimate the rooting depth by using a sine-function and an exponential function. Barley (1970) represented microscopic distribution of roots, that is spatial relationship between roots, by using an exponential function.

2.2 CONVENTIONAL ROOT SYSTEM DEVELOPMENT MODEL

In this study, a "numerical model" that describes root system development and its morphological architecture will be developed. Hereafter, the conventional numerical

models that describe root system development will be reviewed.

The pioneer study of the root system development model is the two-dimensional model proposed by Lungley (1973). In this model, roots are classified into a main root and first and second order lateral roots, and each root is described as a set of short, straight filaments whose length is determined by an elongation rate and a calculation time step. Each filament has a specified slope, which may be altered along with root elongation representing root curvature. Only the effect of gravity on the root curvature is considered. The root branching is described as a simple rule, i.e. roots branch with constant intervals and do not generate in apical non-branching zones. Diggle (1988) proposed a three-dimensional model that describes growth and structure of fibrous root systems in wheat. In that model, roots are classified into seminal roots, nodal roots, first order lateral roots, second order lateral roots, and third order lateral roots. The model principle of root elongation and branching is similar to that of the model by Langley (1973). However, orientation of the root elongation is determined according to a vector that has a deflection angle and an orientation angle against the root orientation at previous time steps. The deflection angle and the orientation angle are determined by probability indexes D and G, and the effect of gravity on the root orientation is taken into consideration by the index G. Pages et al. (1989) also proposed a three-dimensional model that describes the architecture of a fibrous root system in maize. The model principle of root elongation and branching is also similar to the Langley's model (1973), and consequently to the Diggle's model (1989). However, Pages et al. employed three vectors representing gravitropism, the mechanical constraint of the soil, and the previous root orientation in order to determine the root elongation and orientation.

It may be said that the model of Diggle (1988) and the model of Pages (1989) are the first models that describe the dynamic growth and architecture of a complicated three-dimensional root system quantitatively, and that the fundamental part of root system development modeling has been completed by these models. Recently, root system development models focus on the interactions between plant root systems and soil water or nutrient flow, which combines the water uptake models or nutrient uptake models. Clausnitzer and Hopmans (1994) proposed a three-dimensional model of simultaneous root growth and soil water flow, which combines the root system development model based on the model proposed by Pages et al. (1989) and the water uptake model by Feddes et al. (1978). In the model simulation, the three-dimensional form of Richards' equation for soil water pressure is solved in order to obtain soil water flow and water uptake by a root system. Not only the effect of gravity on root elongation but also the effect of soil water content on root elongation are taken into consideration by the model by assuming that roots respond to a soil strength gradient that is defined as a function of the soil water content. Furthermore, the interaction

between root and shoot growth is analyzed by assuming the amount of assimilate allocation. Doussan et al. (1998) proposed a model that combines the root system development model proposed by Pages (1989) and detailed water absorption by considering hydraulic conductivity in and between roots. Somma et al. (1998) proposed a three-dimensional model that combines a three-dimensional solute transport model with a three-dimensional transient model for soil water flow and root growth proposed by Clausnitzer and Hopmans (1994). Dunbabin et al. (2002) also proposed a three-dimensional model that simulates the interaction between root system development and water and nitrate uptake, in which the root system development is simulated based on the model proposed by Diggle (1988).

As we have seen previously, many studies of root system development modeling are based on the model of Pages (1989) and the model of Diggle (1988). Some other models were proposed independently from them. Shibusawa (1994) proposed a two-dimensional root system growth model that simulates the maize root system development, and mainly analyzed the root branching fractal patterns using a method called L-system. Lynch et al. proposed a three-dimensional model in which root elongation and orientation are determined by a vector method, that is similar to the method by Pages et al. (1989), however, considering not only the architecture of the root system but also the root thickness and surface area. His model was combined with the topology model (Fitter et al., 1991a, b) mentioned previously, and the effects of root system topological architecture on nutrient uptake and carbon allocation was analyzed in some other studies (Ge et al., 2000; Nielsen et al., 1994). Jourdan and Rey (1997) proposed a three-dimensional model that simulates the architecture and development of the oil-palm root system, which is based on the theory developed by de Reffye (1979) for the modeling of coffee tree aboveground architecture.

2.3 REQUIREMENTS FOR A NEW ROOT SYSTEM DEVELOPMENT MODEL

As we have seen so far, many conventional models have been constructed in order to simulate the root system development of various plant species and the interaction with the soil water and nutrient flows, mainly in the field of agronomy. For this reason, all the models dealt with the root system development of herbaceous plant species (i.e. maize, wheat or soybean), except the model that simulates the oil-palm root system, by Jourdan and Rey (1997). For the same reason, the ground conditions were limited to plane in the application of the models. The other thing that is common to all conventional models is that the modeling methods for root elongation is expressed using a vector or a segment of the root. Farther more, all models considered the effect of gravity on root growth, which is called "gravitropism (or geotropism)", whereas no model considered the effect of soil water on root growth, which is called

"hydrotropism". Although the effect of soil water on root growth is implicitly considered as the response to the soil strength gradient that is defined as a function of the soil water content in the model proposed by Clausnitzer and Hopmans (1994), no explicit effect of hydrotropism was considered.

In this study, a new root system development model, in which the following points are necessarily satisfied, will be developed.

(1) The model can be applied for the root system development of woody plant species.
(2) The model can be applied for the root system development on slopes.
(3) The root elongation is modeled using a differential-growth mechanism, which reflects actual plant root growth accurately.
(4) Hydrotropism is included into the root elongation modeling as well as gravitropism.

REFERENCES

Barley K.P. 1970 The configuration of the root system in relation to nutrient uptake. Adv. Agron. 22, 159-201

Brog H. and Grimes D.W. 1986 Depth development of roots with time: An empirical description. Trans. ASAE 29(1), 194-197

Clausnitzer V. and Hopmans J.W. 1994 Simultaneous modeling of transient three-dimensional root growth and soil water flow. Plant and Soil 164, 299-314

de Reffye P., Houllier F., Barthelemy D., Dauzat J. and Auclair D. 1995 A model simulating above- and below-ground tree architecture with agroforestry applications. Agrofor. Syst. 30, 175-197

Diggle A.J. 1988 ROOTMAP —a model in three-dimensional coordinates of the growth and structure of fibrous root systems. Plant and Soil 105, 169-178

Doussan C., Pages L. and Vercambre G. 1998 Modeling of the hydraulic architecture of root systems: An integrated approach to water absorption – model description. Annals of Botany 81, 213-223

Dunbabin V.M., Diggle A.J., Rengel Z. and van Hugten R. 2002 Modelling the interactions between water and nutrient uptake and root growth. Plant and Soil 239, 19-38

Feddes R.A., Kowalik P.J. and Zaradny H. 1978 Simulation of field water use and crop yield. Simulation Monographs, Pudoc, Wageningen, The Netherlands.

Fitter A.H., Stickland T.R., Harvey M.L. and Wilson G.W. 1991a Architectural analysis of plant root systems 1. Architectural correlates of exploitation efficiency. New Phytol. 118, 375-382

Fitter A.H., Stickland T.R., Harvey M.L. and Wilson G.W. 1991b Architectural analysis of plant root systems 2. Influence of nutrient supply on architecture in contrasting plant species. New Phytol. 118, 383-389

Gandar P.W.and Hughes K.A. 1988 Kiwifrut root system 1. Root-length densities. N.Z. J. Exp. Agric. 16, 35-46

Ge Z., Ruvio G. and Lynch J.P. 2000 The importance of root gravitropism for inter-root competition and phosphorus acquisition efficiency: results fro a geometric simulation model. Plant and Soil 218, 159-171

Gerwits A. and Page E.R.1974 An empirical mathematical model to describe plant root systems. J. Appl. Ecol. 11, 773-782

Hackett C. and Rose D.A. 1972a A model of the extesion and branching of a seminal root of barley, and its use in studying relations between root dimensions. I. The model. Aust. J. Biol. Sci. 25, 669-679

Hackett C. and Rose D.A. 1972b A model of the extesion and branching of a seminal root of barley, and its use in studying relations between root dimensions. II. Results and inferences from manipulation of the model. Aust. J. Biol. Sci. 25, 681-690

Jourdan C. and Rey H. 1997 Modeling and simulation of the architecture and development of the oil-palm (Elaeis guineensis Jacq.) root system I. The model. Plant and Soil 190, 217-233

Lungley D. R. 1973 The growth of root systems –A numerical computer simulation model. Plant and Soil 38, 145-159

Lynch J.P., Nielsen K.L., Davis R.D. and Jablokow A. G. 1997 SimRoot: Modelling and visualization of root systems. Plant and Soil 188, 139-151

Nielsen K.L., Lynch J.P., Jablokow A.G. and Curtis P.S. 1994 Carbon cost of root systems: an architectural approach. Plant and Soil 165, 161-169

Pages L., Jordan M.O. and Picard D. 1989 A simulation model of the three-dimensional architecture of the maize root system. Plant and Soil 119, 147-154

Shibusawa S. 1994 Modelling the Branching Growth Fractal Pattern of the Maize Root System Plant and Soil 165, 339-347

Somma F., Hopmans J.W. and Clausnitzer V. 1998 Transient three-dimensional modeling of soil water and solute transport with simultaneous root growth, root water and nutrient uptake. Plant and Soil 202, 281-293

Tatsumi J., Yamauchi A. and Kono Y. 1989 Fractal analysis of plant root system. Annals of Botany 64, 499-503

CHAPTER 3

A TWO-DIMENSIONAL ROOT SYSTEM DEVELOPMENT AND WATER EXTRACTION MOMDEL CONSIDERING HYDROTROPISM

3.1 INTRODUCTION

The interaction between plant root systems and soil, especially soil with moisture, is very important in many respects. For example, root water uptake from the soil plays an important role in the hydrological process of water flow through soil, plants and air. In the field of crop science, many experimental studies indicate that variations in soil water conditions affect the root system architecture of various kinds of crops, and that architecture affects absorption efficiency. However, the interaction between the roots and soil, which is hidden under the ground, is difficult to investigate and studies of them are lagging when compared to the studies of shoots or leaves. The modeling of plant root system development and of soil water extraction by plant roots is therefore very useful for understanding the interaction between plant root systems and soil.

The water extraction by plant root system can be calculated by adding a term of water extraction intensity S [s^{-1}] to the Richards' equation, which is the fundamental equation of water flow in unsaturated soil. Various models that give the extraction intensity S have been proposed (Feddes et al., 1978; Gardner, 1964; Herkelrath et al., 1977). Herkelrath et al. (1977) proposed that the extraction intensity S is proportional to the potential difference between roots and soil, volume saturation of the soil space, and root length per unit soil volume. Feddes et al. (1978) introduced water extraction efficiency as a function of soil water potential and succeeded in showing the behavior of soil water extraction by plant root system under certain conditions. However, because root system development is not considered in these water extraction models, the root length per unit soil volume should be given a priori as a function of soil depth. That is, the water extraction model alone cannot simulate the behavior of soil water extraction by roots with active growth, which changes the distribution of the root system over time.

As a pioneer study of modeling plant root system development, Lungley proposed a two-dimensional model (Lungley, 1973). Diggle and Pages developed three-dimensional root system architecture models, and they successfully simulated crop plant root system development and morphological architecture three-

dimensionally (Diggle, 1988; Pages et al., 1989). It seems that the fundamental part of root system development modeling has been completed by these models. Recently, root system development models focus on the interactions between plant root systems and soil water flow (Clausnitzer and Hopmans, 1994; Doussan et al., 1998), or nutrient supply (Somma et al., 1998), which combines the water uptake models or nutrient uptake models. The models shown above are not the only ones that exist. Many other models have been proposed and some of them have succeeded in simulating root system development in various plant species, under various conditions (e.g. Jourdan and Rey, 1997; Lynch et al., 1997).

However, all applications of these models were made to the root systems developing on planes, and no application on slopes can be found. It has been generally known that a plant that grows on a slope has an asymmetric root system, and this asymmetric architecture of the root system has been confirmed by some experimental studies (Scippa et al., 2001; Yamadera, 1990). Recently, the contribution of plant root system architecture to slope stability has become one of the main interests in the fields of erosion control and re-vegetation technology. Some studies have shown that plant root systems growing under hillside slope contributes to the slope stability, increasing the soil strength by the their architecture, and decreasing the soil water content by water uptake (Greenway, 1987). This contribution has been investigated, considering root strength, growth and rate of decay (Watson et al., 1999).

To simulate the root system development and soil water flow on a slope, it is necessary to take into account the effect of the slope on root growth. Some experiment results have shown that root growth is influenced by hydrotropism, which is the root elongation toward water (Takahashi, 1994, Takano et al., 1995). Because soil moisture exhibits asymmetric distribution on a slope, root hydrotropism can be one of the main factors that causing the asymmetric root system development.

The objective of this study is to propose a root system development model, which can analyze root system development and soil water extraction both on a plane and slopes, by considering the effect of hydrotropism that was not considered in previous models. After reviewing previous studies on root system development on slopes and on hydrotropism, a two-dimensional model that combines soil water extraction and root system development employing both root gravitropism and hydrotropism is proposed. The model is applied to root system growth both on a plane and slopes, and the results are compared with those obtained using a conventional model. Also, the author tries to explain root system morphology with plagiogravitropism, which is a lateral root elongation deviating from the vertical direction, and especially the asymmetric plagiogravitropic response of roots growing on slopes.

3.2 REVIEW OF PREVIOUS STUDIES

3.2.1 Root Development on Slopes

Figure 3.1a, b show the projected root systems of seedlings in Japanese red pine (*Pinus densiflora*) experimentally developed on a plane, and a slope (Yamadera, 1990). The experiments were conducted in Yoga experimental farm of Tokyo University of Agriculture (Tokyo, Japan), from April 1983 to November 1984. Seeds were sown in boxes (1.0m in length, 0.5m in depth and width), which were filled with loamy soil (under 20mm mesh). During the growth period, water was supplied from the soil surface. After 2-years of growth, the root systems were excavated from the soil and schematic drawings were made. In Figure 3.1a, the root system on a plane has roughly symmetric architecture. On the other hand, the root system on a slope has asymmetric architecture, with larger angles between the main and lateral roots in the up-slope direction than those in the down-slope direction (Figure 3.1b). The experimental observations by Yamadera (1990) are not the only studies. Some other observations showed that the root systems in various species have asymmetric architectures under slopes (Karizumi, 1979; Scippa et al., 2001). Although Scippa et al. (2001) explained the asymmetric root system architecture of a plant by the resistance to the loading of its own weight to ensure better anchorage on a slope, the detailed mechanism on how the roots sense and respond to the loading, is not yet fully understood.

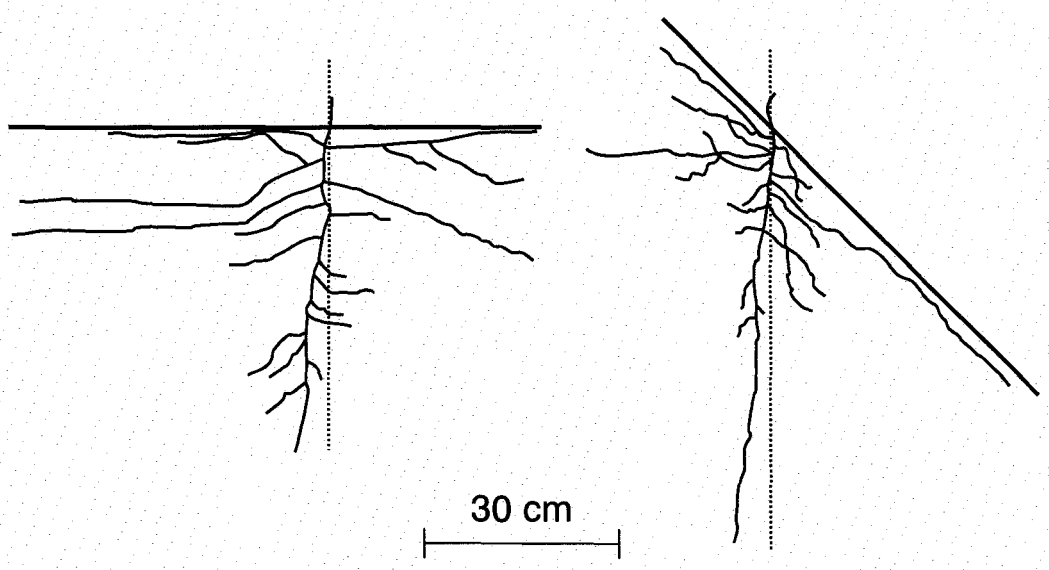

Figure 3.1 Projected root systems of seedlings in Japanese red pine (*Pinusdensiflora*) in a) plane, b) slope $\delta = 45^{\circ}$ (Modified from Yamadera, 1990).

3.2.2 Hydrotropism

Hydrotropism, that is the bending of roots in the direction of increasing moisture in a moist gradient, has been reported in many plant species from earlier studies (Darwin, 1880; Hooker, 1915). However it had not ever been confirmed that hydrotropism truly exists, because of the failure in controlling the appropriate gradient of moisture, or of the counteracting effects of gravity (Takahashi, 1994). Recently, some studies have succeeded in proving the existence of hydrotropism (Takahashi and Scott, 1993; Takano et al., 1995). Takahashi and Scott (1993) investigated the behavior of root hydrotropism in pea and corn roots. In their experiment, they controlled the gradient of air humidity in the closed chamber, and observed the roots bending in the direction of increasing moisture. Takano *et al.* (1995) investigated the behavior of root hydrotropism in an agratropic pea mutant *ageotropum*, which does not respond to gravity. In their experiment, they applied two agar blocks, each having different water potential, to the bilateral sides of the root cap, and found that the root curves away from the lower water potential side (drier side) toward the higher water potential side (wetter side), and that the curvature became larger when the agar blocks had even greater differences in water potential. They also found that the root part that senses water stimuli is the root cap.

However, root hydrotropism has not been employed in most of the previous root system development models. Only in the model by Clausnitzer and Hopmans (1994), has the root hydrotropic effect been considered implicitly; they assumed that roots respond to the soil strength gradient that is defined as a function of the soil moisture content.

In the model proposed in this chapter, root hydrotropism is employed explicitly; it is assumed that the root hydrotropism is the key factor that reflects environmental water conditions upon the root system morphology in order to explain the asymmetric root system development on a slope.

3.3 MODEL

3.3.1 Type of Root System and Branch

Japanese red pine, one of pioneer wood species in Japan, widely inhabits and is often seen on bared hillside slopes. For this reason, the root system development in the Japanese red pine is dealt with, as an object of model simulation in this study. Figure 3.2 shows the projected root system of a 1-year old seedling in Japanese red pine, showing the typical characteristics of the main root system (Karizumi, 1979). When the main root system is considered, roots may be classified into the main root which is derived from a seed, the first order lateral roots which are derived from the main root, the second order lateral roots which are derived from the first order lateral roots and so on. In this paper, only the main root system will be dealt with, and more than fourth order lateral roots will not be considered.

Following the definition in literature (Pages et al., 1989), the root branch

parameters are defined as shown in Figure 3.3. When the first order lateral roots branching from the main root are considered, the main root corresponds to the parent root and the first order lateral roots corresponds to the lateral roots in Figure 3.3. In the same manner, when the second order lateral roots branching from the first order lateral root are considered, the first order lateral root correspond to the parent root and the second order lateral roots correspond to the lateral roots. Because the first lateral root arises at some distance from the parent root base, the basal non-branched zone L_b [cm] is introduced. Because the latest lateral root cannot be found close to the root tip (root

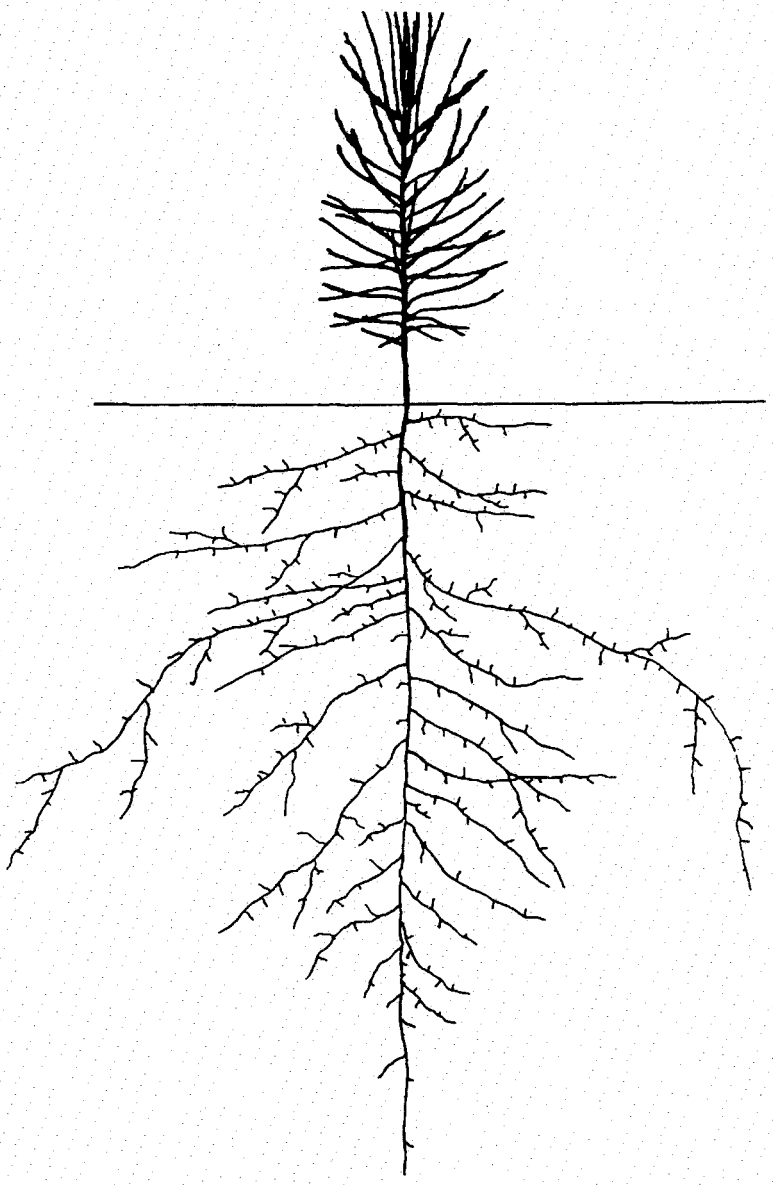

Figure 3.2 Projected root system of 1-year old seedling in Japanese red pine (*Pinus densiflora*) (Karizumi, 1979).

apex), the apical non-branching zone L_a [cm] is introduced. Hence, no root branch occurs until the root has become longer than L_b+L_a [cm]. After the root grows longer than L_b+L_a, lateral roots appear at regular interval I_b [cm]. Moreover, it is assumed that the lateral roots alternatively branch to both side of the parent root, and defined angle between the parent and lateral roots as insertion angle ϕ_i [degree].

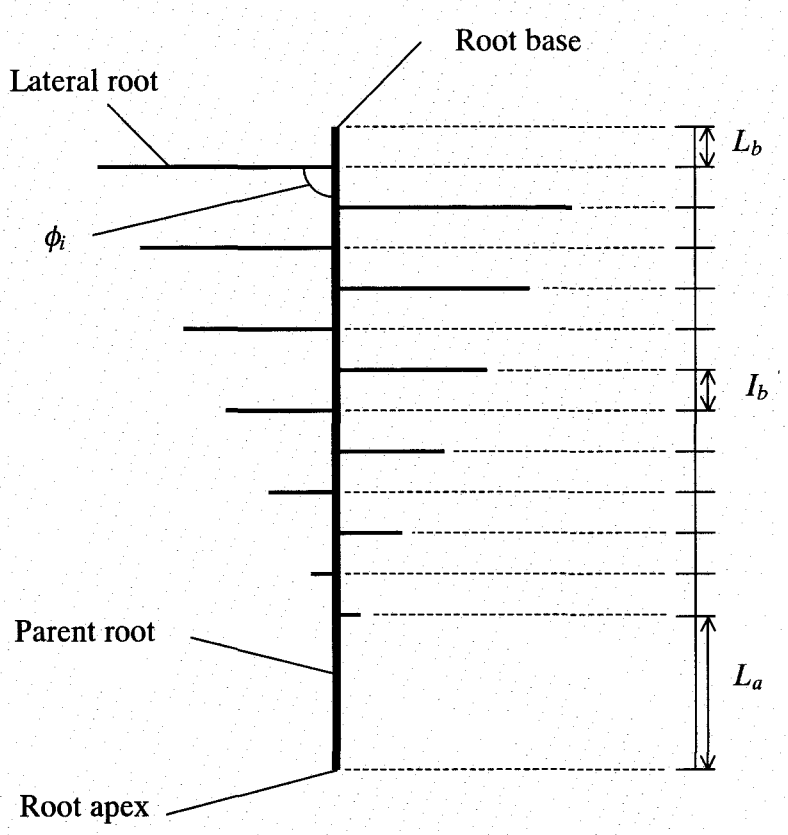

Figure 3.3 Branches along the root axis.

3.3.2 Proposed Root Elongation Model

Following the experimental results (Ishikawa et al., 1991, Takahashi, 1994, Takano et al., 1995), the mechanism of root tropism can be shown as Figure 3.4. The tropism is caused by the difference in elongation rates ER [cm/s], at the elongation points P_1 and P_2, which are located opposite to each other. In Figure 3.4, $ER(P_1)$ is larger than $ER(P_2)$, so the root deflects toward the right side from the former direction of elongation. Inversely, If $ER(P_1)$ is smaller than $ER(P_2)$, the root deflects toward the left side from the former direction of elongation. Here, we can obtain the radius r [cm] and the angle α [rad] within the time Δt [s] as follows,

$$r = \left| \frac{ER(P_1) + ER(P_2)}{ER(P_1) - ER(P_2)} \right| \frac{d}{2} \tag{3.1}$$

$$\alpha = \frac{|ER(P_1) - ER(P_2)|}{d} \Delta t \tag{3.2}$$

where, d [cm] is the diameter of the root at the elongation point. Also, the elongation rate of the center of the root, ER_c [cm/s], can be obtained as follows;

$$ER_c = \frac{ER(P_1) + ER(P_2)}{2} \tag{3.3}$$

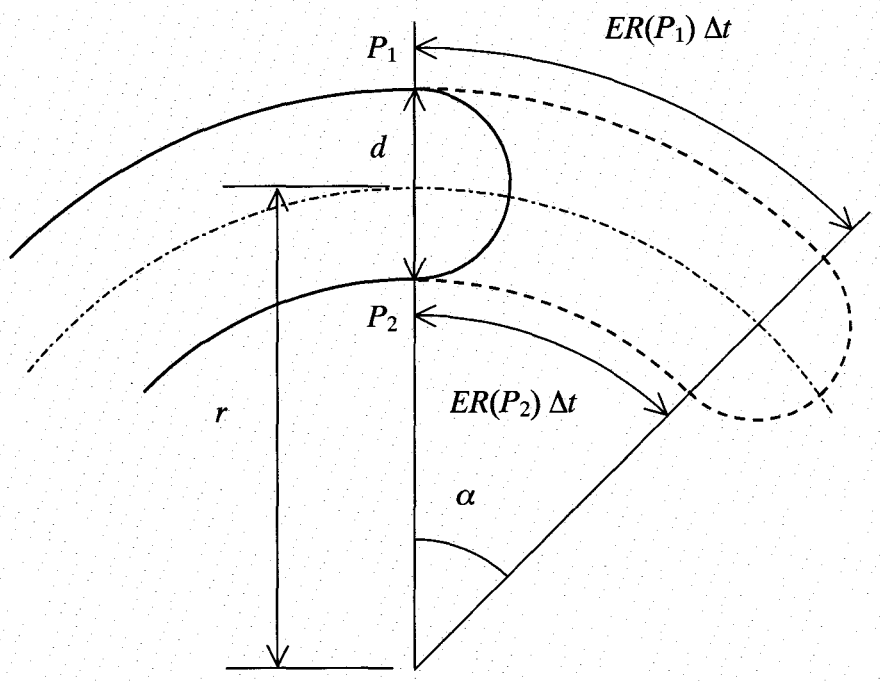

Figure 3.4 Schematic figure showing the principle of the mechanism of root tropism.

From Figure 3.4 and Equation (3.1), (3.2) and (3.3), we can see that the behavior of the tropism is determined by the elongation rate ER at each of the elongation points. Thus, to determine the tropism, it is necessary to describe the elongation rate as a function of the tropism factors. Because gravitropism and hydrotropism are dealt with, the elongation rate functions of gravitropism and hydrotropism are written as ER_g [cm/s] and ER_h [cm/s], respectively, and the elongation rate ER is written,

$$ER = ER_g + ER_h \tag{3.4}$$

Ishikawa et al. (1991) investigated the elongation behavior of the main root in maize that was orientated horizontally, and found that the elongation rate of the upper side became greater, and that of the lower side became lesser than the elongation rates when the root was orientated vertically. Moreover, they found that this difference of

elongation rates between the upper side and lower side became greater when the angle between the direction of gravity and root orientation was larger. From these results, the elongation rate function of gravitropism for the upper and lower elongation points may be defined as shown in Figure 3.5,

For the upper side elongation point:

$$ER_g = ER_{g,0} + \Delta ER_g \sin\gamma \qquad 0 \leqq \gamma \leqq \pi/2 \qquad (3.5)$$

$$ER_g = ER_{g,0} + \Delta ER_g \qquad \pi/2 < \gamma \leqq \pi \qquad (3.6)$$

For the lower side elongation point:

$$ER_g = ER_{g,0} - \Delta ER_g \sin\gamma \qquad 0 \leqq \gamma \leqq \pi/2 \qquad (3.7)$$

$$ER_g = ER_{g,0} - \Delta ER_g \qquad \pi/2 < \gamma \leqq \pi \qquad (3.8)$$

where, γ [rad] is the angle between the directions of gravity and root orientation, $ER_{g,0}$ [cm/s] gives the value of the gravitropic elongation rate when the root directs toward gravity (γ = 0), ΔER_g [cm/s] is the constant that determines the intensity of gravitropism.

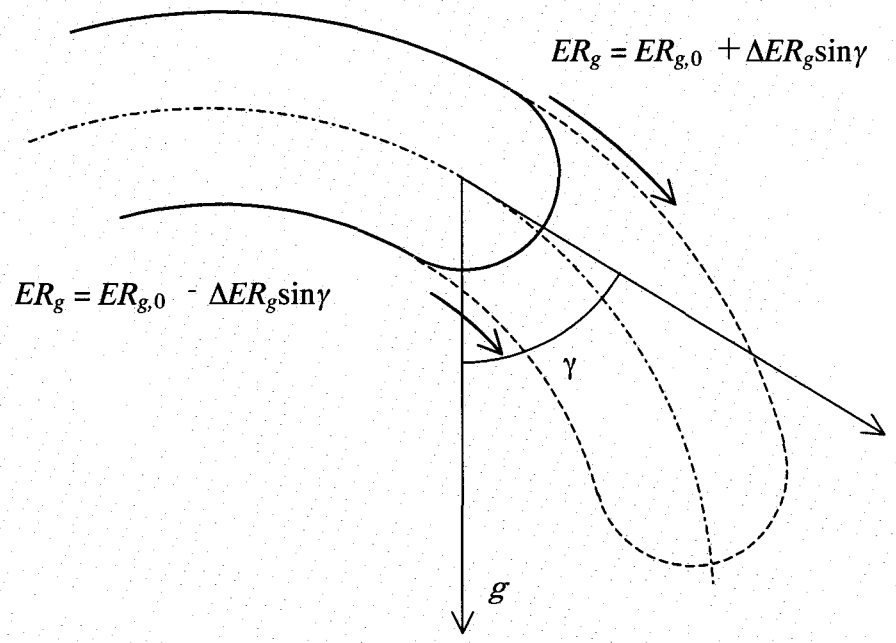

Figure 3.5 Schematic figure of gravitropic response of root, and defined elongation rate function of gravitropism.

From the results of the studies on hydrotropism (Takahashi and Scott, 1993; Takano et al., 1995) as we reviewed in the previous section, the elongation rate function of hydrotropism may be defined as shown in Figure 3.6,

Wet side;

$$ER_h = ER_{h,0} - k_h|q'| \tag{3. 9}$$

Dry side;

$$ER_h = ER_{h,0} + k_h|q'| \tag{3.10}$$

where, $|q'|$ [cm/s] is the magnitude of the component of water flux q [cm/s], perpendicular to the root at the root cap, $ER_{h,0}$ [cm/s] gives the value of the hydrotropic elongation rate when $|q'| = 0$, k_h [-] is the constant that determines the intensity of hydrotropism. The water flux q can be obtained by the calculation of soil water flow explained in the next section. Although it is still not clear whether the root senses the difference of water potential or the water flux, the author assumed that the root senses the water flux flowing across the root cap, in Equation (3.9) and (3.10). This assumption is due to the similar phenomenon that the skin of a human does not sense the temperature of an object but the heat flux from it when the skin touches the object.

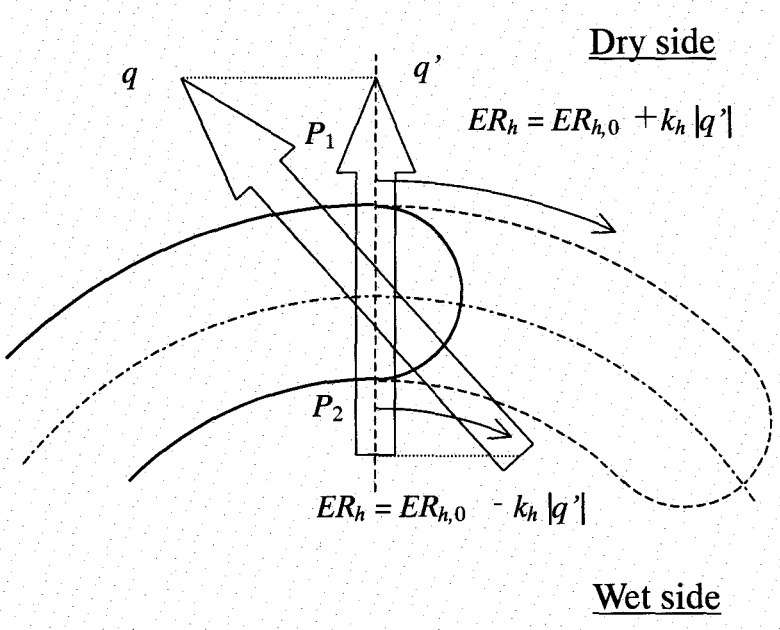

Figure 3.6 Schematic figure of hydrotropic response of root, and defined elongation rate function of hydrotropism. (The arrows of q and q' indicate the water flux and its component perpendicular to the root, respectively.)

From Equation (3.4) through (3.10), the elongation rates ER in each side of the root elongation points P_1 and P_2 are obtained. Then r and α from Equation (3.1) and (3.2) are calculated. Also ER_c from Equation (3.3) through (3.10) is obtained,

$$ER_c = ER_{g,0} + ER_{h,0} \tag{3.11}$$

According to Equation (3.11), the elongation rate of the root center does not change

according to gravitropism and hydrotropism. In the simulations, the value for ER_c is given, instead of $ER_{g,0}$ and $ER_{h,0}$ being given as independent values.

3.3.3 Conventional Root Elongation Model (Pages' Model)

To make the effects of hydrotropism on root system development clear, the behavior of the proposed model with that of one of the widely used models proposed by Pages (1989) which does not employ the hydrotropism are compared.

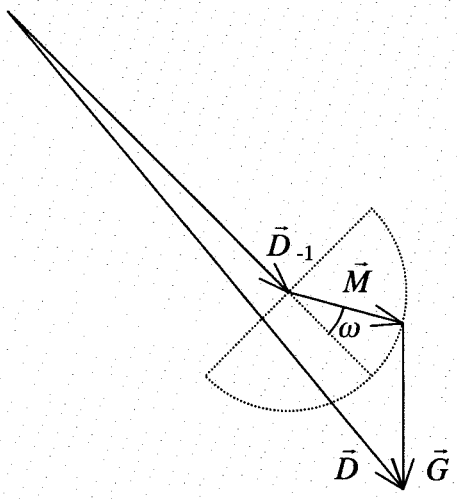

Figure 3.7 Principle for root elongation in the conventional model according to Pages (Pages et al., 1989).

The growth direction $\vec{D}$ is computed by adding three directional components represented by mathematical vectors (Figure 3.7),

$$\vec{D} = \vec{D}_{-1} + \vec{G} + \vec{M} \tag{3.12}$$

where, $\vec{D}_{-1}$ is the initial direction of the root at the previous time step whose length is equal to 1, $\vec{G}$ is a vertical vector representing geotropism (gravitropism) whose relative length to $|\vec{D}_{-1}|$ is equal to a parameter G, and $\vec{M}$ is a vector representing the mechanical constraints whose relative length to $|\vec{D}_{-1}|$ is equal to a parameter M. Mechanical constraints $\vec{M}$ may be considered as isotropic (random vector) in some

parts of the environment, whereas in other parts they may be pointing in a specific direction and represented by a fixed vector. When the vector $\vec{M}$ is considered as isotropic, $\vec{M}$ is calculated as follows,

$$\vec{M} = M\begin{bmatrix}\cos\omega & -\sin\omega \\ \sin\omega & \cos\omega\end{bmatrix}\vec{D}_{-1} \tag{3.13}$$

where, ω [degree] represent the angle between the vector $\vec{D}_{-1}$ and $\vec{M}$. From the growth direction vector $\vec{D}$ and the predetermined elongation rate [cm/sec], the location of the root apex is computed.

The notable differences between the conventional model and the proposed model are the methods describing root elongation, i.e. the former uses the addition of vectors and the later uses differential growth to describe the root elongations.

3.3.4 Method of Model Calculation

3.3.4.1 Scenario for simulations

Root system developments in Japanese red pine and soil water flow are simulated by both the proposed and Pages' models using the same environmental conditions as shown below. The assumed soil domains are as shown in Figure 3.8, for plane and slope conditions. The total size of the domain is 70×140 cm, and the interval of the nodes for finite element calculation is 3.5cm for both x and z directions. Values of soil water potential at the beginning of the calculation ψ_{int} [cm] were given to each node, so that the hydraulic potential ϕ_{int} [cm] should become -100 cm throughout the calculation area, for the plane condition. The same values of ψ_{int} as used under the plane condition were given for the slope condition. For both the sides (x = 0, W cm), and the bottom (z = 0 cm) of the calculation domain, a no-flux boundary condition was imposed.

For the boundary at the top of the domain (z = D cm), the evaporation [cm^2/hr] and the water supply [cm^2/hr] are gaven as functions of time [hr]. The root system extracts the soil water according to the transpiration rate [cm^2/hr]. The assumed changing patterns of transpiration, evaporation, and the amount of water supply throughout the calculation period are shown in Figure 3.9. As shown in Figure 3.9a, transpiration did not occur in the first 30 days after germination. The daily transpiration gradually increased from 31 to 90 days, became constant from 91 to 150 days, and gradually decreased to 0 from 150 days to the end of calculation (i.e. 210 days). The daily evaporation did not change throughout the simulation period. Figure 3.9b shows the assumed diurnal changes of the transpiration, evaporation and water

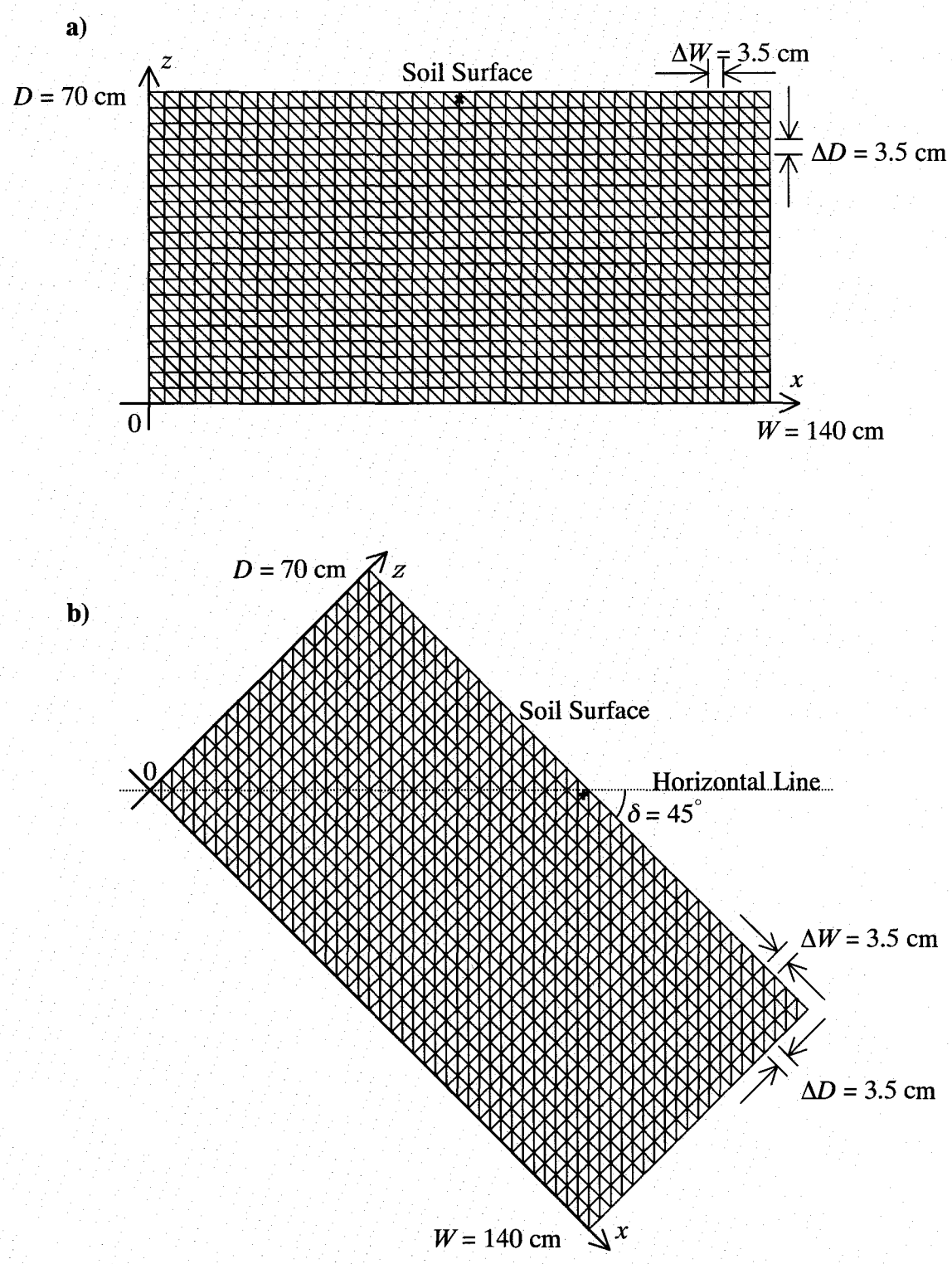

Figure 3.8 The calculation domain for the simulation, a) plane, b) slope $\delta = 45^{\circ}$ (**x** marks indicate the starting points of main root).

supply. The changes of transpiration and evaporation in the daytime were expressed by sine curves. In the nighttime, transpiration became 0 and evaporation remained constant. The water was supplied to the soil surface once a week (7 days) from 0:00 midnight to 6:00 AM. The amount of water supply was equal to the total loss of water by evaporation and transpiration for the previous 7 days.

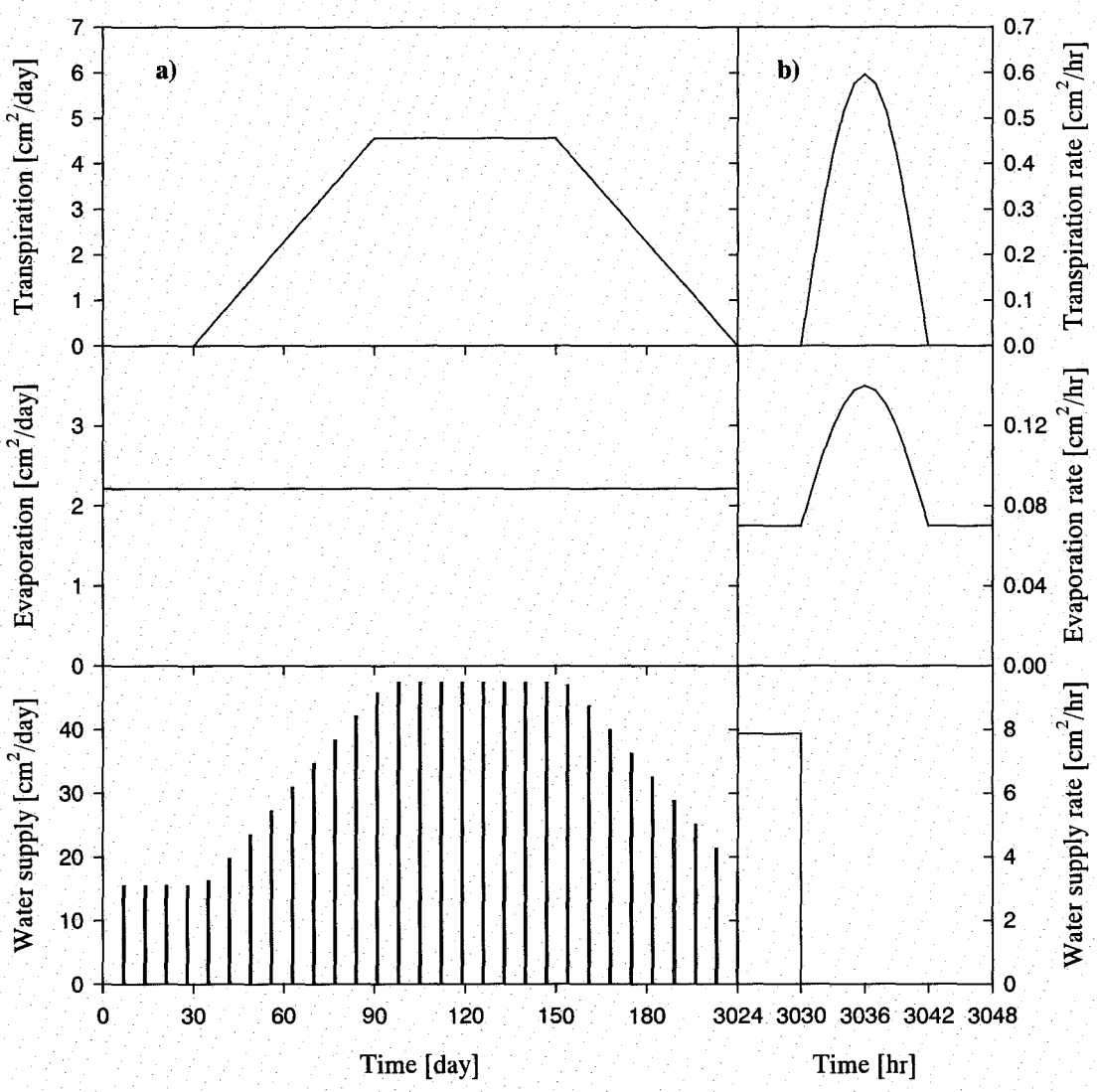

Figure 3.9 Defined pattern of transpiration, evaporation and water supply, a) throughout the calculation period [cm^2/day], b) in one-day duration [cm^2/hr].

3.3.4.2 Soil water flow and root water extraction

The soil water flow was calculated according to the following equation.

$$C_p(\psi)\frac{\partial\psi}{\partial t} = \frac{\partial}{\partial x}\left\{K(\psi)\left(\frac{\partial\psi}{\partial x} - \sin\delta\right)\right\} + \frac{\partial}{\partial z}\left\{K(\psi)\left(\frac{\partial\psi}{\partial z} + \cos\delta\right)\right\} - S \quad (3.14)$$

Equation (3.14) is the two-dimensional Richards' equation based upon water potential ψ [cm], where, z [cm] is positive upward, t [s] is the time, δ [rad] is the slope angle, $C_p(\psi)$ [cm^{-1}] is the soil water capacity and $K(\psi)$ [cm/s] is the hydraulic conductivity. Equation (3.14) was solved numerically by the partially implicit finite element method (Istoke, 1989; Zienkiewicz, 1971) using a constant time step (3600 s) and triangular elements of the same size as shown in Figure 3.8.

To represent $C_p(\psi)$ and $K(\psi)$,the lognormal model proposed by Kosugi (1996) was employed;

$$C_p(\psi) = \frac{d\theta}{d\psi} = \frac{\theta_s - \theta_r}{\sqrt{2\pi}\sigma(-\psi)}\exp\left\{-\frac{[\ln(\psi/\psi_m)]^2}{2\sigma^2}\right\} \quad (3.15)$$

$$K(\psi) = K_s\left[Q\left(\frac{\ln(\psi/\psi_m)}{\sigma}\right)\right]^{1/2}\left[Q\left(\frac{\ln(\psi/\psi_m)}{\sigma} + \sigma\right)\right]^2 \quad (3.16)$$

where, θ_s [m^3/m^3] is the saturated soil water content, θ_r [m^3/m^3] is the residual soil water content, ψ_m [cm] is the soil water potential corresponding to the median soil pore radius, σ [-] is a dimensionless parameter relating to the width of the pore-size distribution and K_s [cm/s] is the saturated hydraulic conductivity. The function Q represents the residual normal distribution and is represented as

$$Q(x) = \int_x^\infty \frac{1}{\sqrt{2\pi}}\exp\left(-\frac{u^2}{2}\right)du. \quad (3.17)$$

The parameters in Equation (3.15) were determined based upon an observed retention curve for a sandy soil sampled at the Kamigamo Experimental Forest of Kyoto Univ., and K_s in Equation (3.16) was computed from the model by Kosugi (1996), (Figure 3.10).

Water extraction intensity for the element n, S_n [s^{-1}], was determined according to the model of Herkelrath (Herkelrath et al., 1977; Kanda and Hino, 1990);

$$S_n = -\left(\frac{\theta - \theta_r}{\theta_s}\right)^b \rho\Delta\psi L \quad (3.18)$$

$$\Delta\psi = \psi_c + (R_c + 1)l - \psi \quad (3.19)$$

where, θ [cm^2/cm^2] is the soil water content at the root surface, ρ [s^{-1}] is the water penetration coefficient of root, b [-] is a correction parameter, $\Delta\psi$ [cm] is the difference of water potential between root and soil, L [cm/cm^2] is the root length density, ψ_c [cm] is the water potential of the beginning point of the main root, l [cm] is the vertical

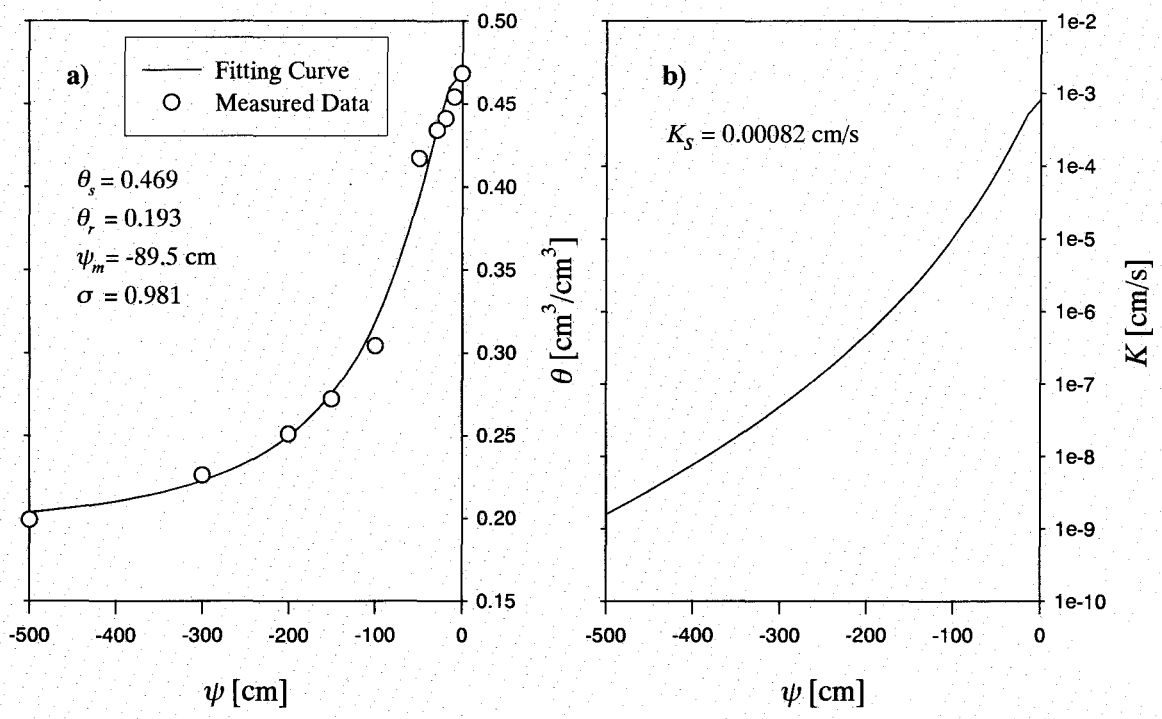

Figuer 3.10 The soil hydraulic properties, a) θ-ψ curve, b) K-ψ curve.

distance from the beginning point of the main root to the root and R_c [-] is a correction coefficient for the friction loss of water transport in the root. For the simulations, $\rho = 2 \times 10^{-10}$ s^{-1}, $b = 1$, $R_c = 0.05$ were assumed according to Herkelrath et al. (1977) and Momii et al. (1992). L was calculated as the root lengths within the element divided by the area of the element, l was calculated as the vertical distance from the beginning point of the main root to the center of the element, θ and ψ in Equation (3.18) and (3.19) were obtained by averaging the values at the 3 nodes of the element. Because roots extract water actively at the absorption zone near the root tip in actual plant root systems, the lengths of the main and first order lateral roots older than 30 days were excluded from L. The transpiration rate T [cm^2/hr] given as a function of time is related to S_n by

$$T = \sum_n A_n \cdot S_n \tag{3.20}$$

where A_n [cm^2] is the area of the element n. The substitution of Equation (3.18) and (3.19) into Equation (3.20) gives the value of ψ_c [cm]. Then, the derived ψ_c along with Equation (3.18) and (3.19) gives the value of S_n.

3.3.4.3 Parameters for root elongation

The parameters for root elongation rates ER_c, and the branching of main and each order lateral roots, L_b, L_a, I_b, were determined from the root system development

in Japanese red pine as observed by Karizumi (1979), (the final stage of the development is shown in Figure 3.2). Because the observed elongation rate of the main root decreased in the later stage of development, two elongation rate values ER_c for the main root are used (see Table 3.1). In Figure 3.2, many second order lateral roots seem to have similar lengths, although their ages were different. From this observation, it was assumed that the growth of the second order lateral roots ceased when their length reaches a certain critical value L_{cr} [cm]. Also, there seems to be two types of second order lateral root in terms of this critical length, i.e. a shorter and longer type. The critical lengths of each type were determined as the mean values of the measured length. The frequency of occurrence of the shorter and longer type second order lateral roots was 80% and 20%, respectively. Insertion angle, ϕ_i, for all lateral roots was fixed at 90 degrees. The other parameters for root system development, i.e. ΔER_g, k_h and d were determined through trial and error calculations, so that the simulation result of the root system morphology becomes similar to the actual root system developed on a plane as shown in Figure 3.2.

The parameters for the conventional Pages' model (1989) simulations are also shown in Table 3.1. These parameters are determined, so that the simulation result of root system morphology becomes similar to the actual root system developed on the plane as shown in Figure 3.2. For each time step, ω of each root was randomly decided in the range of $-90 < \omega < 90$ degrees (Figure 3.7). All the other parameters for the Pages' model simulation are exactly the same as those for the proposed model simulation shown in Table 3.1.

Table 3.1 Parameters for the model simulation

Parameters [unit]	value		
	Main	1st	more than 2nd
Common Parameters			
L_b [cm]	2.4	1.7	1.7
L_a [cm]	14.5	5.2	1.7
I_b [cm]	2.4	1.7	1.7
L_{cr} [cm]	−	−	5.2, 1.2
Elongation rate ER_c [cm/day]	0.55 (t<100day)	0.25	1.2
	0.13 (t≧100day)	−	−
Proposed Model Parameters			
d [cm]	0.040	0.020	0.013
$\Delta ER_g/ER_c$ [-]	0.0002	0.00005	0.00005
k_h [-]	200	200	200
Insertion angle ϕ_i [degree]	−	90	90
Pages' Model Parameters			
Mechanical constraint (isotropic) M [-]	0.01	0.01	0.01
Geotropism (gravitropism) G [-]	0.001	0.0002	0.0002
Insertion angle ϕ_i [degree]	−	72	45

3.4 RESULTS AND DISCCUTION

3.4.1 A Pattern of Root System Development on Plane

Figure 3.11 shows a time dependent pattern of root system development and soil water distribution based on the hydraulic potential ϕ [cm]. The right side of the figure shows the vertical profile of the root length [cm], and water extraction per unit depth [cm/hr]. In Figure 3.11, we can see that the root system develops extracting water from the soil, and the soil water distribution changes according to the developing root system. The main root grows in the direction of gravity and the lateral roots grow in the direction of higher hydraulic potential. The growth directions of first order lateral roots are deviating from the direction of gravity. These characteristics of the simulated root system development are in good agreement to those found in the actual root system in Figure 3.2. When the root systems are compared in details, the simulated root system in Figure 3.11 has more similarities to the actual root system in Figure 3.2. The angles between the main root and first order lateral roots near the soil surface are nearly perpendicular, and larger than those in the deep soil layer. The second order lateral roots orientate in directions outward from the center of the root system. These tendencies of lateral root plagiogravitropic elongation can be seen in the

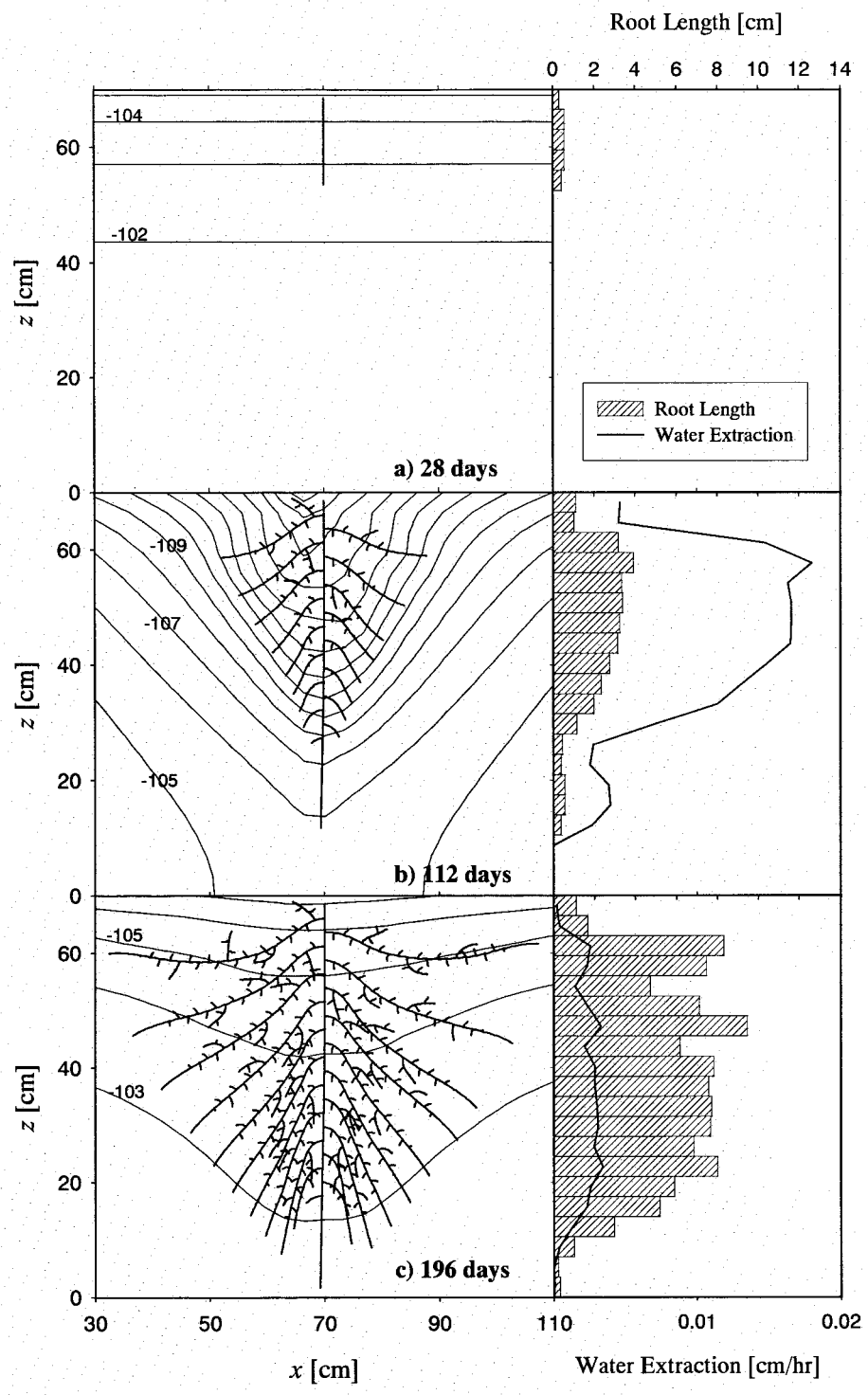

Figure 3.11 A pattern of the root system development, the soil water distribution based on hydraulic potential ϕ [cm], the root length [cm] and the water extraction per unit depth [cm/hr]. (Values in the figure are the hydraulic potential ϕ [cm].)

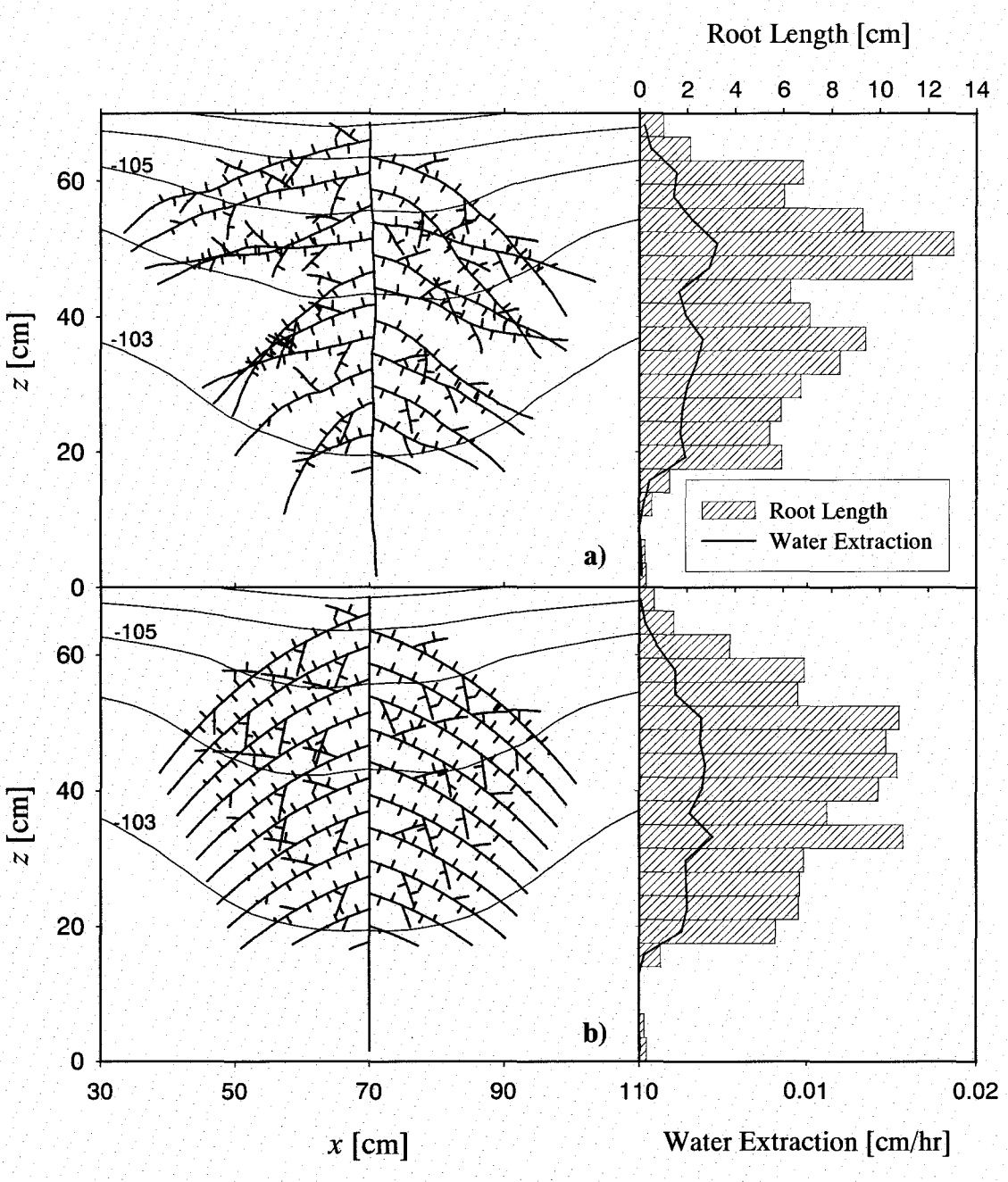

Figure 3.12 The root systems at the final stage of the simulation (196 days) by the conventional model, a) with isotropic vector (M = 0.01), b) without isotropic vector (M = 0.00).

actual root system also. On the other hand, some differences can be seen between the simulated and actual root systems. In the model simulation, the lateral roots of the same order are assumed to have uniform elongation rates. However, the elongation rates of first order lateral roots are not uniform in the actual root system, and the model simulation does not express such variations in lateral root elongations.

Figure 3.12a shows the final shape of the root systems, soil water distribution, vertical profile of the root length, and water extraction per unit depth simulated by using the conventional Pages' model (1989) with the parameters shown in Table 3.1. In this figure, the main root grows toward the direction of gravity with a winding shape, and the first order lateral roots orientate toward various directions. As a result, the simulated root system shows "natural" irregular architecture, and it seems to have relatively similar morphology to the actual root system in Figure 3.2. However, this natural irregularity in the simulated root system is due only to the random elongation factor. Therefore, the tendency of the angle between the main root and first order lateral roots becoming larger near the soil surface, as seen in Figure 3.2 and Figure 3.11, cannot be seen in Figure 3.12 a.

In order to confirm the effect of the random elongation factor on the irregular architecture of the root system, the author examines the root system developed without the random elongation factor; that is, M was fixed at 0 to derive the results seen in Figure 3.12b. In Figure 3.12b, all of the first order lateral roots on each side of the main root grow toward the same direction, and the root system shows no irregularity. From Figure 3.12a and Figure 3.12b, it is clear that the random elongation factor (isotropic vector) plays a very important role deriving the "natural" root system morphology in the conventional model. However, the random elongation factor acts as an inherent elongation factor and does not reflect the external environmental conditions. Therefore, in the conventional model, morphology of the root system is determined by gravitropism and the pre-assigned lateral root insertion angle. Various irregular factors affect the actual root elongation, e.g. the distributed soil particle size, heterogeneous soil density, and changing weather conditions. In order to understand the mechanism of actual root system development, it seems important to model each of these irregular effects reflecting the external environment as much as possible rather than to express the natural irregularity of root system development only by the inherent random elongation factor that is a mixture of all these effects. In this manner, the proposed model can simulate the root system with "natural" irregular architecture (i.e., various orientations of lateral roots and the tendency of the plagiogravitropic reaction mentioned above), without using any random elongation factors but still considering root hydrotropism, which reflects the changes of the soil water distribution depending on time and position.

3.4.2 Root System Development on a Slope

Figure 3.13a, b shows the calculated root systems on a slope by the proposed model and the conventional model respectively, where the line z = 70 cm indicates the soil surface and the arrows indicate the direction of gravity. In both simulations, an assumption that the roots that reach toward the soil surface change their direction parallel to the soil surface and do not elongate beyond the boundary was made, so that

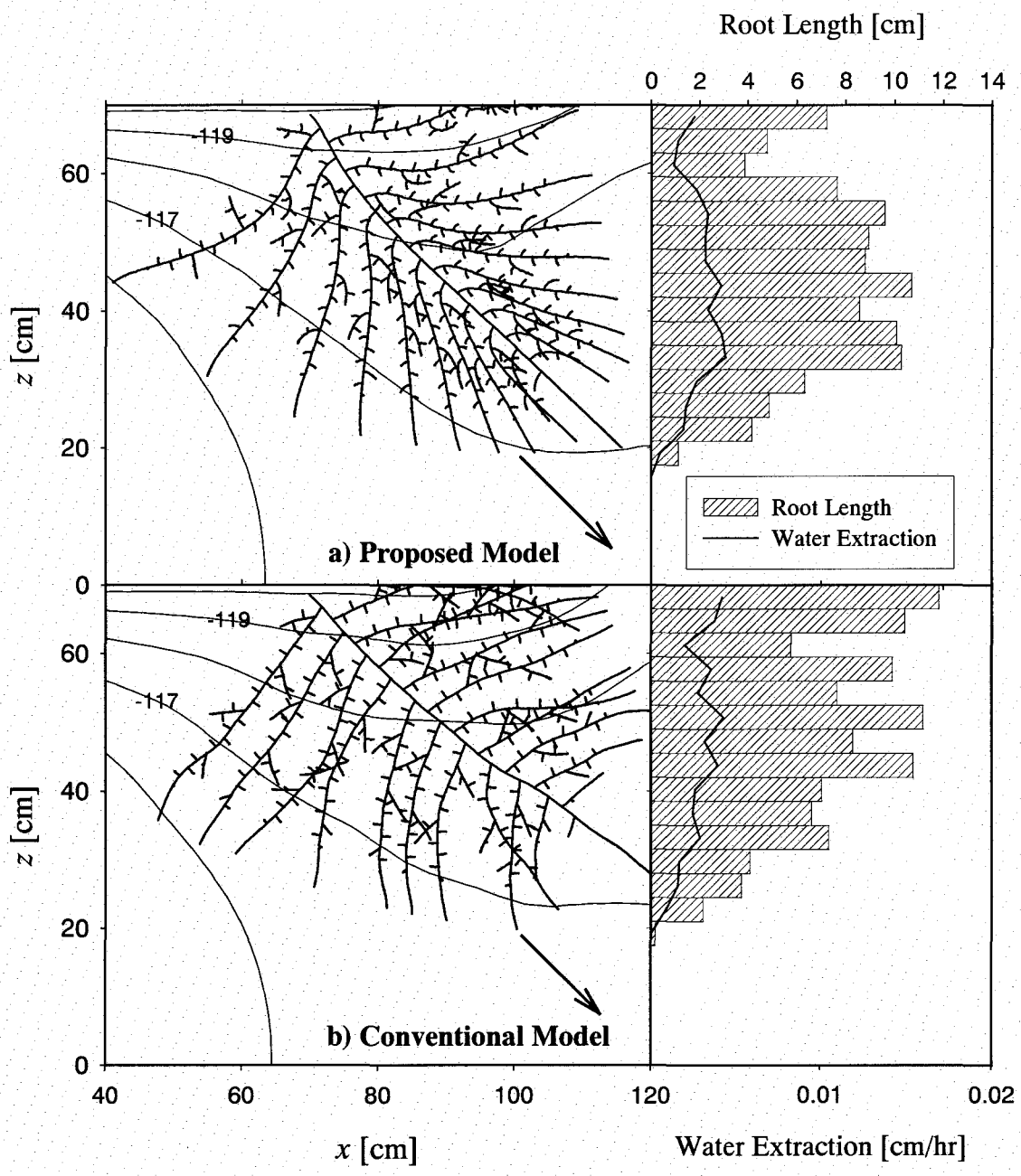

Figure 3.13 The root systems in slopes at the final stage of the simulation (196 days) simulated by a) the present model and by b) the conventional model. (Arrows in the figure indicate the direction of gravity.)

the total root length is kept equal in all the simulations. In Figure 3.13a, the main root grows nearly in the direction of gravity, and the angles between the main root and lateral roots in the up-slope direction tend to be larger than those in the down-slope direction. As a result, the root system shows an asymmetric architecture very similar to the actual root system shown in Figure 3.1b, and looks different from the symmetric root system architecture simulated on the plane, shown in Figure 3.11c. In Figure 3.13a,

it seems that the root system tries to occupy the available soil domain as much as possible, by developing its architecture asymmetrically on the slope. This asymmetry of the simulated root system is due to the interactive effect of the soil water distribution distorted by a sloped soil surface and hydrotropism. On the other hand, the root system in Figure 3.13b does not show the asymmetric architecture (except the lateral roots that reached toward the soil surface), and is almost the same as the root system calculated on the plane shown in Figure 3.12a. Because the conventional model employs no effect reflecting the slope condition on root elongation, this result seems to be a natural consequence.

According to the earlier published study (Rufelt, 1957), the plagiogravitropic response of root takes place through the combined effects of a positive geotropic (gravitropic) reaction and the negative reactions caused by various factors, i.e. pH value, composition of the nutrient, temperature, and growth substances. Because all the root growth experiments in the study of Rufelt (1957) were conducted in nutrient solutions, the hydrotropic reaction of the root was not tested. On the other hand, experimental results derived by Takahashi and Scott (1993) and Takano et al. (1995) suggest the possibility that the hydrotropism can be one of the negative gravitropic factors. In this study, the author succeeded in simulating the plagiogravitropic elongation of the lateral roots on a plane and asymmetric plagiogravitropic elongation of the lateral roots on a slope by considering root hydrotropism. Although the other factors that account for the plagiogravitropic elongation cannot be excluded, root hydrotropism may be regarded as one of the negative gravitropic reactions that contribute to the lateral root plagiogravitropic response.

3.4.3 Soil Water Extraction by Root Systems

Figure 3.14a, b shows the spatial distribution of the accumulated soil water extraction intensity, simulated by the proposed model and the conventional model (M = 0.01), on a plane. The period of accumulation is 7 days, from day 190 to 196 (See Figure 3.9). The root system distribution corresponding to Figure 3.14a and b) are shown in Figure 3.11c and Figure 3.12a. In the same way, Figure 3.15a, b shows the distribution of the accumulated soil water extraction intensity, simulated by the proposed model and the conventional model, on a slope. The root system distribution corresponding to Figure 3.15a, b is shown in Figure 3.13a, b, respectively. In all the results, the distribution of soil water extraction intensity shows good correspondence to the root system distribution, and it can be confirmed that the root systems extract the soil water depending on their morphologies. On plane, the distribution of active water extraction seems to be comparatively gentle in Figure 3.14a. On the other hand, some heavy soil water extraction intensity can be seen in Figure 3.14b. These heavy areas of soil water extraction intensity correspond to the overlaping of roots simulated by the conventional model as shown in Figure 3.12a. Because hydrotropism acts as a

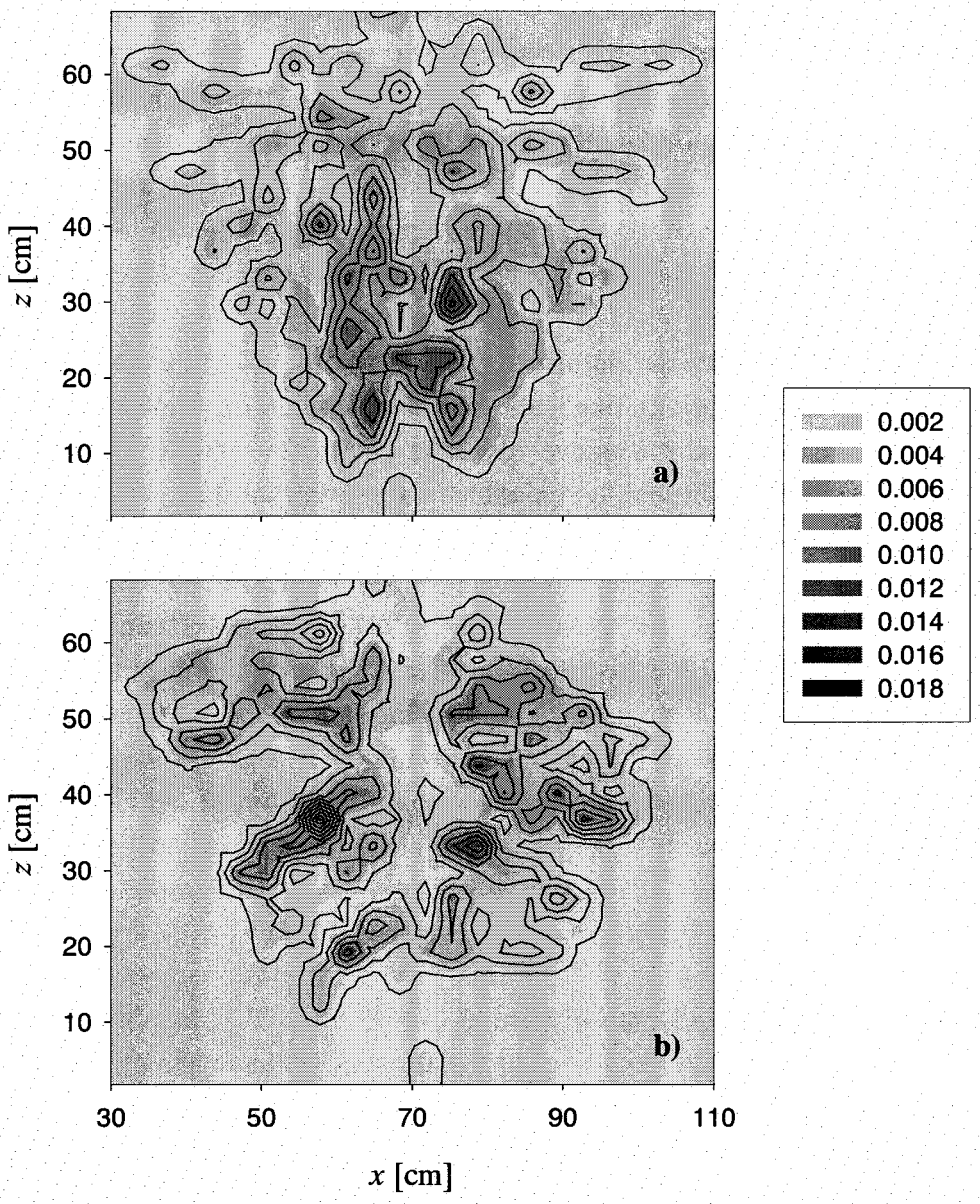

Figure 3.14 The distribution of the accumulated soil water extraction intensity [1/(7days)] at the final stage of the simulation (196 days), on a plane by a) the proposed model, and by b) the conventional model. (Interval of the contour lines is 0.002.)

repelling force between the roots, and no random elongation factor is considered in the proposed model, there were few overlapping roots in Figure 3.11c. Consequently, water extraction intensity is distributed more gently in Figure 3.14a than in Figure 3.14b. In the results on the slope, we can see a concentration of water extraction intensity in the down-slope direction, near the soil surface, in Figure 3.15b. This concentration is due to the overlapping roots, which were repelled by the soil surface

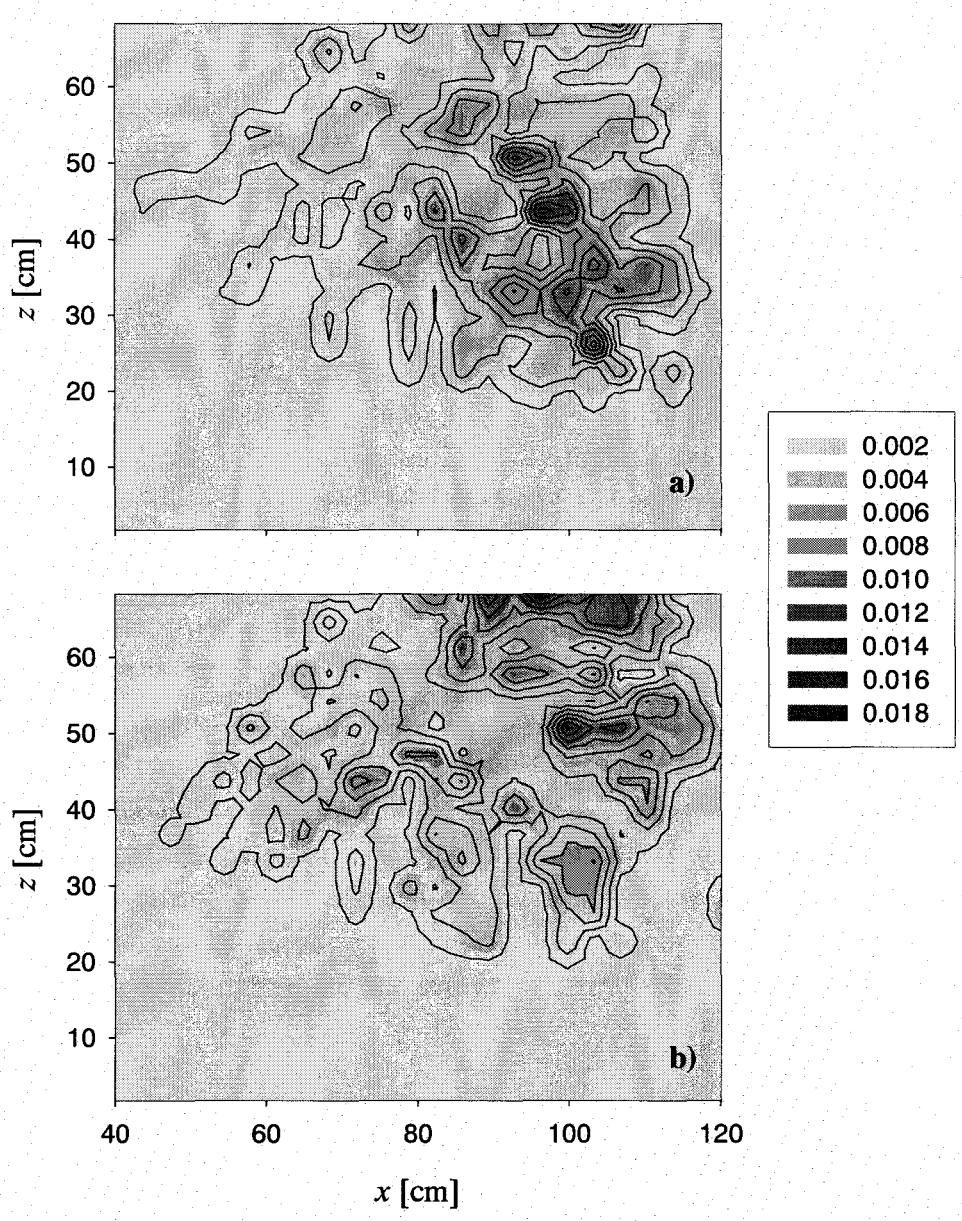

Figure 3.15 The distribution of the accumulated soil water extraction intensity [1/(7days)] at the final stage of the simulation (196 days), on a slope by a) the proposed model, and by b) the conventional model. (Interval of the contour lines is 0.002.)

(See Figure 3.13b).

To characterize the spatial distribution of the water extraction intensity, the triangular elements that were used for the simulation were classified based on water extraction intensity, and the frequency histogram as the total area of these elements was drawn (Figure 3.16). The values shown in the figures indicate the average value of

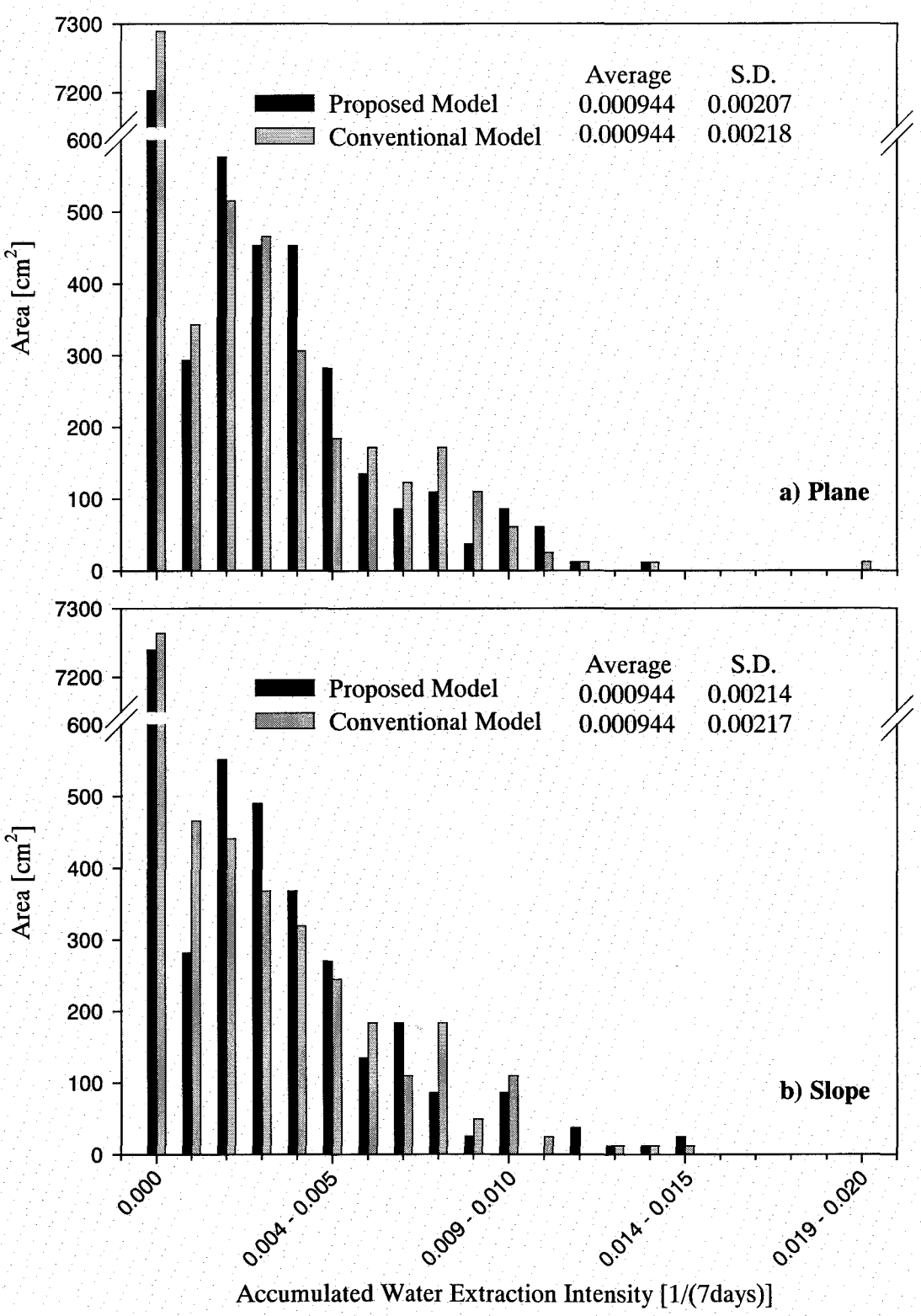

Figure 3.16 Frequency of the element classified according to the water extraction intensity [1/(7days)], simulated on a) a plane, and b) a slope.

water extraction intensity, and its standard deviation. Figure 3.16a, b show that the proposed model has a larger area with middle level water-extraction-intensity (i.e. 0.001-0.006 1/(7days)) than the convention model. The fact that the area with zero water extraction intensity is smaller in the proposed model indicates that the root systems simulated by the proposed model occupy a lager area to extract the soil water and have less overlapping of roots than those by the conventional model. The average value of water extraction intensity was the same for all the simulated results, and this came about because the total water extraction was fixed at a predetermined transpiration value. On the other hand, the standard deviations of water extraction intensity for each element were slightly different, i.e. standard deviations by the proposed model were smaller than those by the conventional model. This indicates that the distribution of soil water extraction intensity in the results by the proposed model were gentler than those in the results by the conventional model. The results shown in Figure 3.16 confirm the results shown in Figure 3.14 and Figure 3.15; the water extraction intensity tends to concentrate at some part of the soil domain in the simulated results by the conventional model, and it distributes comparatively gentle in the results of the proposed model.

As we have seen from the results of water extraction by the root systems, the difference in the root system development models causes differences in root system morphology, which affects the spatial distribution of water extraction intensity and the soil water content. In the proposed model, the soil water distribution affects the root system development by root hydrotropic response. That is, the proposed model calculates complicated feed back phenomena among root hydrotropism, root system morphology, soil water extraction, and soil water distribution.

3.5 CONCLUSION

The model proposed in this paper is designed to generate a two-dimensional root system whose elongation is controlled by both gravitropism and hydrotropism, and display the soil water extraction by the root system. The model can simulate the root system development and soil water flow both on a plane and slopes. Notably, the model succeeded in simulating the asymmetric architecture of the root systems developed on a slope, without the introduction of any random elongation factors.

The proposed model is potentially useful for investigating how the various conditions of soil water affect root system development and soil water extraction. For example, the model can simulate root system development and soil water extraction under moist or drought conditions, which may produce important information on the efficiency of various irrigation methods.

Because of the complexity of the calculation for hydrotropism, the model was constructed as two-dimensional to avoid further complexity. The simulation results of

the two-dimensional model can easily display and directly compares the actual root systems developed in small spaces such as root boxes that can be regarded as approximately two-dimensional. However, it is necessary to extent the proposed model to a three-dimensional form in order to analyze root system development and soil water extraction under actual field condition.

REFERENCES

Clausnitzer V. and Hopmans J.W. 1994 Simultaneous modeling of transient three-dimensional root growth and soil water flow. Plant and Soil 164, 299-314

Darwin C. 1880 The power of Movement in Plants. John Murray, London

Diggle A.J. 1988 ROOTMAP- a model in three-dimensional coordinates of the growth and structure of fibrous root systems. Plant and Soil 105, 169-178

Doussan C., Pages L. and Vercambre G. 1998 Modeling of the hydraulic architecture of root systems: An integrated approach to water absorption – model description. Annals of Botany 81, 213-223

Feddes R.A., Kowalik P.J. and Zaradny H. 1978 Simulation of field water use and crop yield. Simulation Monographs, Pudoc, Wageningen, The Netherlands.

Gardner W.R. 1964 Relation of root distribution to water uptake and availability. Agron. J. 56, 41-45

Greenway D.R. 1987 Vegetation and slope stability, In Slope Stability, edited by Anderson M. F. and Richards K. S. New York, Wiley, 187-230

Herkelrath W.N., Miller E.E. and Gardner W.R. 1977a Water uptake by Plants: I. Divided root experiments. Soil sci. soc. Am. J. 41, 1033-1038

Herkelrath W.N., Miller E.E. and Gardner W.R. 1977b Water uptake by Plants: II. The root contact model. Soil sci. soc. Am. J. 41, 1039-1043

Hooker H.D.Jr. 1915 Hydrotropism in roots of *Lupinus albus*. Ann. Bot. 29, 265-283

Ishikawa H., Hasenstein K.H. and Evans M.L. 1991 Computer-based video digitizer analysis of surface extension in maize roots. Planta 183, 381-390

Istoke J. 1989 Grandwater modeling by the finite element method. American Geophysical Union, Washington, DC, USA

Jourdan C. and Rey H. 1997 Modeling and simulation of the architecture and development of the oil-palm (*Elaeis guineensis* Jacq.) root system *I. The model*. Plant and Soil 190, 217-233

Kanda M. and Hino M. 1990 Numerical simulation of soil-plant-air system (1) modeling of plant system. J. Japan Soc. Hydrology and water Resources 3, 37-46 (In Japanese, with English summery)

Karizumi N. 1979 Illustrations of tree roots. Seibundo Shinkosha, Tokyo, Japan (In Japanese)

Kosugi K. 1996 Lognormal distribution model for unsaturated soil hydraulic properties. Water Resour. Res.32, 2697-2703

Lungley D.R. 1973 The growth of root systems – A numerical computer simulation model. Plant and Soil 38, 145-159

Lynch J.P., Nielsen K.L., Davis R.D. and Jablokow A.G. 1997 SimRoot: Modelling and visualization of root systems. Plant and Soil 188, 139-151

Momii K., Nozaka J. and Yano T. 1992 Comparison of root water uptake models. J. Japan Soc. Hydrol & Water Resour. 5(3), 13-21 (In Japanese, with English summary)

Pages L., Jordan M.O. and Picard D. 1989 A simulation model of the three-dimensional architecture of the maize root system. Plant and Soil 119, 147-154

Rufelt H. 1957a The course of the geotropic reaction of wheat roots. Physiol. Plant. 10, 231-247

Rufelt H. 1957b Influence of the composition of the nutrient solution on the geotropic reactions of wheat roots. Physiol. Plant. 10, 373-396

Rufelt H. 1957c Influence of temperature on the geotropic reaction of wheat roots. Physiol. Plant. 10, 485-499

Rufelt H. 1957d Influence of growth substances on the geotropic reaction of wheat roots. Physiol. Plant. 10, 500-520

Scippa G.S., Baraldi A., Urciouli D. and Chiatante D. 2001 Root response to slope condition. Which are the factors involved? Analysis at biochemical and molecular level. Proceedings of the 6th symposium of the international society of root research, 128-129

Somma F., Hopmans J.W. and Clausnitzer V. 1998 Transient three-dimensional modeling of soil water and solute transport with simultaneous root growth, root water and nutrient uptake. Plant and Soil 202,281-293

Takahashi H. 1994 Hydrotropism and its interaction with gravitropism in roots. Plant and Soil 165, 301-308

Takahashi H. and Scott T.K. 1993 Intensity of hydrostimulation for the induction of root hydrotropism and its sensing by the root cap. Plant Cell Environ 16, 99-103

Takano M., Takahashi H., Hirasawa T. and Suge H. 1995 Hydrotropism in roots: sensing of a gradient in water potential by the root cap. Planta 197, 410-413

Watson A., Phillips C. and Marden M. 1999 Root strength, growth, and rates of decay: root reinforcement changes of two tree species and their contribution to slope stability. Plant and Soil 217, 39-47

Yamadera Y. 1990 Experimental study for improving the revegetation technique on steep hillside slopes., Tokyo, Japan (In Japanese)

Zienkiewicz O.C. 1971 The finite element method in engineering science. McGraw-Hill, Berkshire, England.

CHAPTER 4

EFFECT OF HYDROTROPISM ON ROOT SYSTEM DEVELOPMENT IN SOYBEAN (*GLYCINE MAX*) - ROOT GROWTH EXPERIMENT WITH SOIL WATER MEASUREMENT IN A ROOT BOX -

4.1 INTRODUCTION

Root hydrotropism, that is root elongation bending toward moisture according to a water gradient, was recently confirmed and accepted as a genuine plant tropism by experimental studies (Takahashi, 1994; Takahashi and Scott, 1993; Takano et al., 1995). Together with other root tropisms, i.e. gravitropism, thigmotropism, thermotropism, etc., root hydrotropism may ultimately contribute to the establishment of a root system, by which roots avoid environmental risks such as drought conditions and support the growth and development of the whole plant. However, in all the experiments on root hydrotropism, only the elongation of an individual root has been investigated. There seems to have been no studies investigating the effect of hydrotropism on the entire plant root system development. Although the effect of soil moisture conditions or drip irrigation on entire root system development and its morphological architecture in various crop plants (Galamay et al., 1992; Kono et al., 1987) or vegetables (Morita and Toyoda, 1998) were investigated, root hydrotropism and soil water flow were not considered sufficiently.

One of the most useful experimental methods investigating actual plant root system development may be the root box experiment. By using the root box, it is possible to grow the root system in an approximately two-dimensional soil domain that is previously fixed by the users, and to remove the soils easily from the root system without disturbing its morphological architecture. It is possible also to observe the developing root system by using a transparent material for the root box. Thinking that many experimental studies using root boxes have been carried out and their results have been reported (e.g. Galamay et al., 1992; Iijima and Kono, 1991; Momii et al., 1992; Sassa, 1985), the root box experiment may be said an established experimental method useful for observing root system architecture.

In order to investigate the effect of soil water flow on root system development, high-resolution measurement of the soil water distribution is necessary. The most widely used method measuring the soil water concentration may be the soil water potential measurement by tensiometers. However, this method is not suitable for

soil water measurements of water uptake by plant root system, because (1) tensiometer cannot measure water potential lower than –1000 cm, and (2) roots contacting the porous cup absorb the water contained in the tensiometer. On the other hand, time domain reflectmetory (TDR) has been used extensively, and is now becoming the main method in measuring soil water content. The principle of the TDR method is to estimate the soil water content according to the waveform of the returned electromagnetic wave that is generated by TDR equipment and travels through the soil along the wires of the TDR probe. In this simple principle, the measuring procedure is brief and the measuring time very short. Also the TDR method does not have such problems as previously mentioned with the tensiometer. Therefore, the TDR is the most suitable method for measuring with high-resolution the distribution of soil water content in the root box.

An experiment in which the root systems of soybean plants were grown under a reduced effect of gravity in root boxes with 25 coil-type probes installed for TDR measurement was carried out. The two-dimensional root system architectures that developed with water supplies from different positions were observed, and the two-dimensional distribution of the soil water content change along with the root system development were measured. The objectives of this experiment was (1) to establish an experimental system combining the root box and TDR method for measuring the root system morphological architecture and the distribution of soil water content quantitatively, and (2) to investigate the effect of the soil water conditions on root system development, through quantitative measurements of root system morphological architecture and distribution of soil water content. In this chapter, the detailed methods and the results of experiment are reported.

4.2 MATERIALS AND METHOD

4.2.1 Plant

Soybean plants (*Glycine max*), which have been widely used in many experimental studies (e.g. Kono et al., 1987; Lynch and van Beem, 1993; Raper and Barber, 1970), were used in the experiment. The root system of the soybean is generally classified as a basal root system, which is similar to a main root system, and shows relatively simple morphology when compared to the fibrous root system, typically seen in cereal plants such as wheat, corn or rice.

4.2.2 Root Box

Four root boxes (30 cm in width and length, 2 cm in thickness) were made according to Kono et al. (1987). The TDR probes were installed to two of them, root box No.1 and No.2. The front and side views of the root box are shown in Figure 4.1. Gray circles in Figure 4.1 indicate the points where the TDR probes described below were installed (Root box No.1 and No.2). White circles indicate the points where

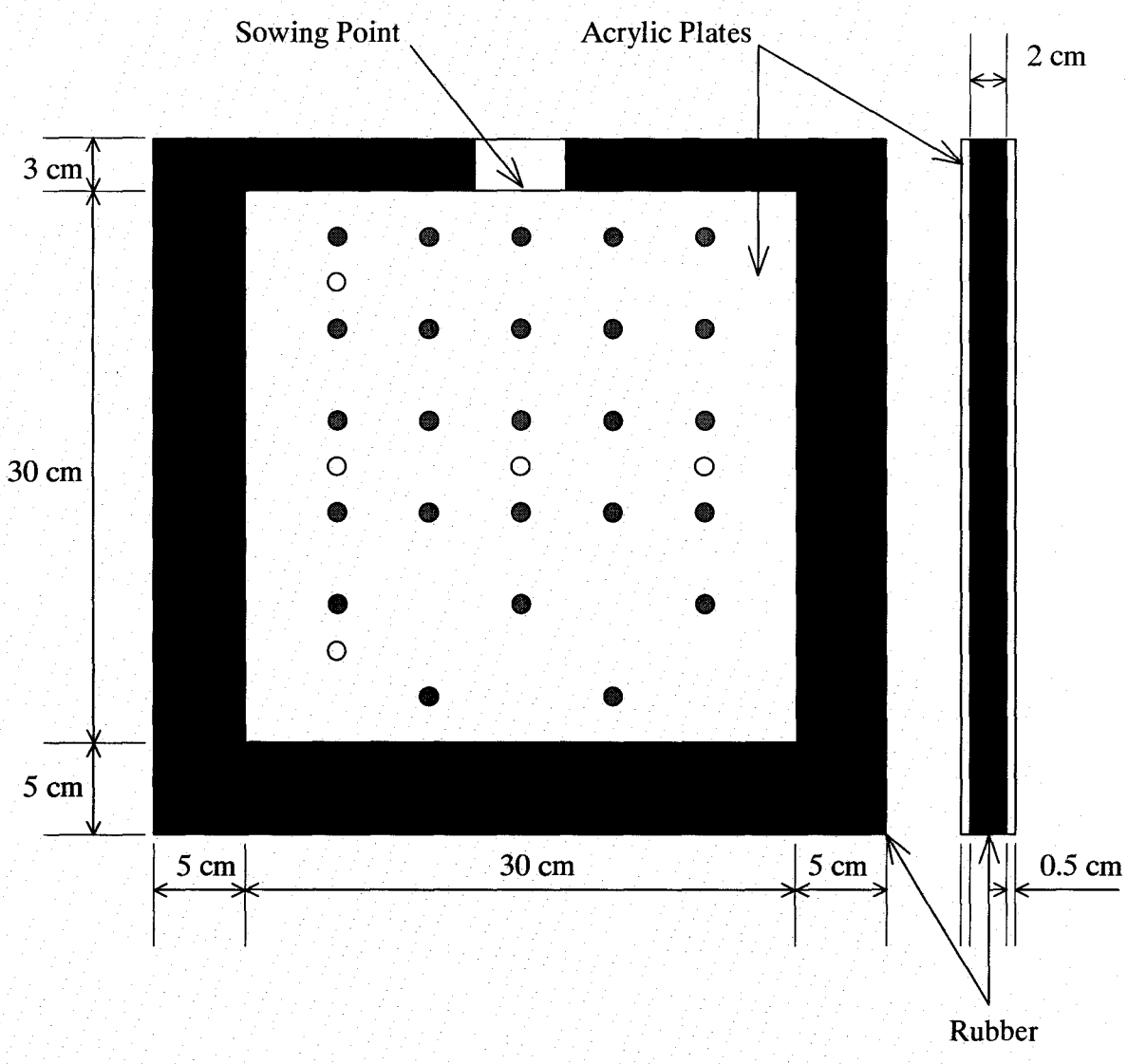

Figure 4.1 Front view and side view of the root box.
(● ; TDR probes, ○; porous cups)

porous cups were installed (horizontal 3 circles in the middle for root box No.1 and No.3, and vertical 3 circles on the left for root box No.2 and No.4). We used the porous ceramic cups that are usually used as tensiometers. Figure 4.2 shows a sectional view of a porous cup that is installed to the root box. The water supply system to the root boxes is shown in Figure 4.3. The porous cups were connected to the water tanks by tubes, and the water was continuously supplied from these porous cups. The water tanks were placed 25 cm lower than the root boxes, so that the water potential inside the porous cups was controlled to be –25 cm. The rate of water supply changes according to the differences in the water potential between the porous cups and soil, and the hydraulic conductivity of porous material. Using root boxes for root growth

experiments is profitable in preserving the root system for observation without any impairment or disturbance of its structure (Kono et al., 1987).

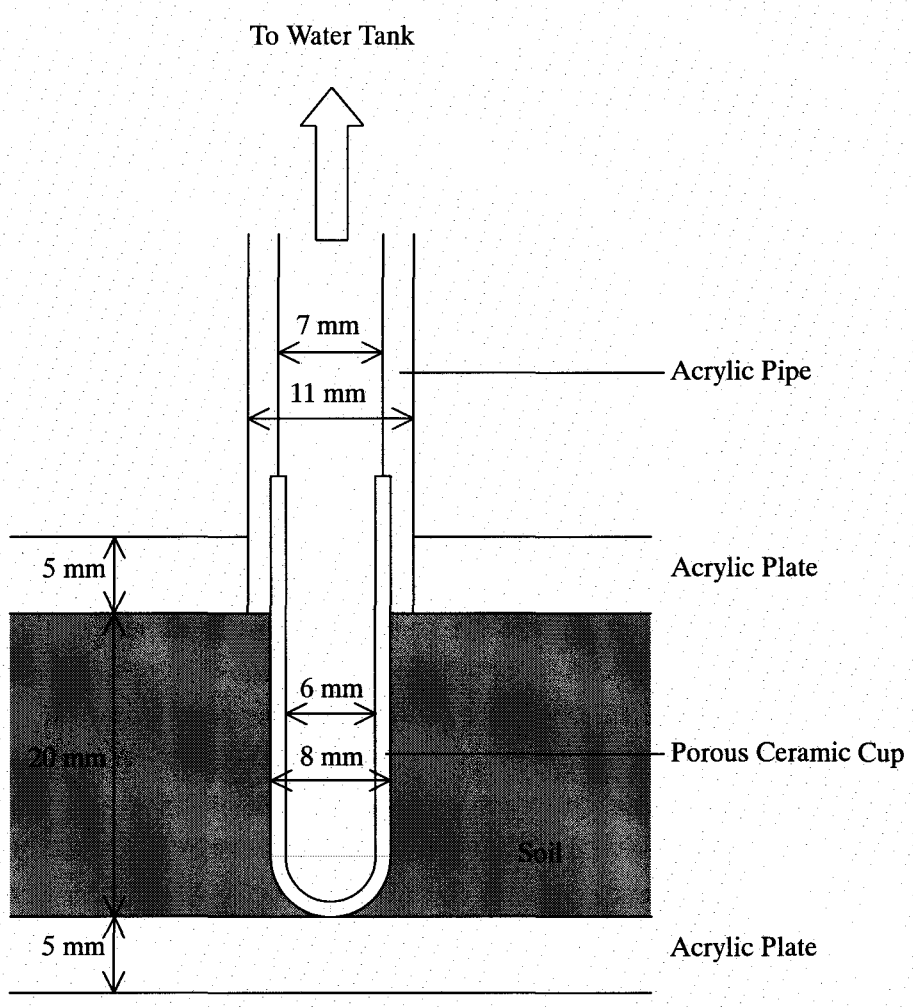

Figure 4.2 Sectional view of porous cup, and its installation to the root box.

4.2.3 TDR Probe

In order to maintain precision in the measurement of the soil water content by TDR method, it is necessary to keep the length of the probe wires (which is the sensor of the TDR measurement system) longer than 10 cm (Dalton and van Genuchten, 1986). Therefore, the soil water content measured by the rod type probe is an average value of soil domain that has the same length as the probe wires. Recently, various types of TDR probes that have shapes different from the rod type probe have been developed. The coil type probe, which is one of these newly developed probes is proposed by Nissen et al. (1998) and Vaz and Hopmans (2001). Because it is possible to keep the wire length longer than 10 cm and to make the coil length shorter by using a coil type probe, the measuring volume can be reduced while still maintaining the precision of the measurement of the soil water content. Therefore, the coil type probes

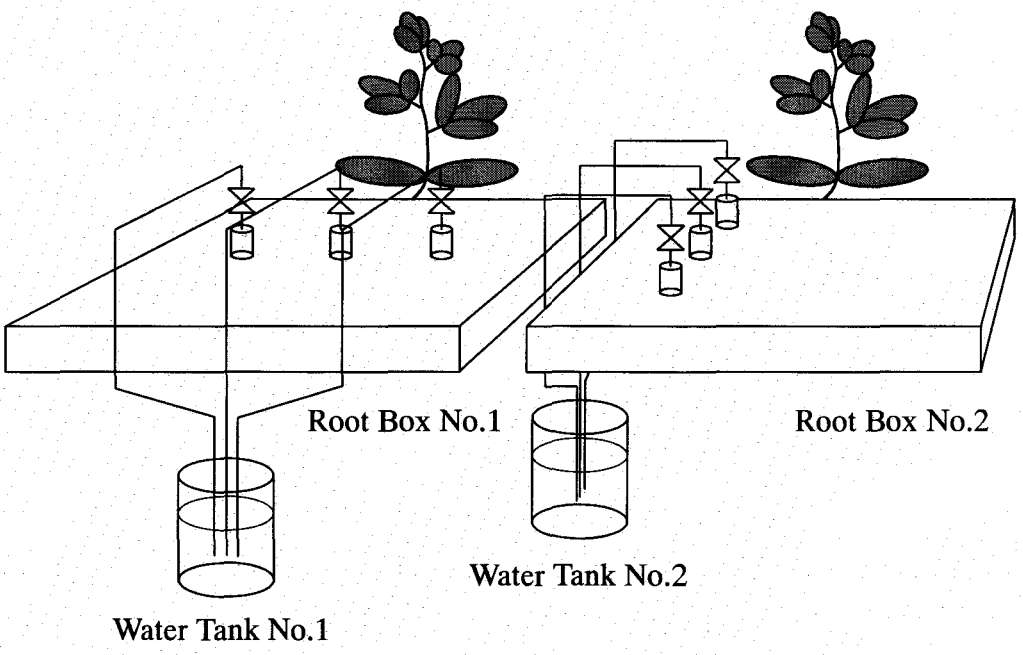

Figure 4.3 A water supply system to the root boxes; root boxes, porous cups, tubes and water tanks. (The water tanks were set 25cm lower than the root boxes, so that the water potential inside of the porous cups was controlled to be –25 cm. The root boxes were set horizontally, after the germination, 7th day after sowing.)

are suitable for two-dimensional, high-resolution measurement of soil water content in the root box, and they were employed for this experiment.

25 coil type TDR probes were installed in each root box (see Figure 4.1), so that the two-dimensional distribution of soil water content could be measured during root growth. The details of the coil type TDR probe are shown in Figure 4.4. The probes were designed to fit the root box, and manufactured in accordance with recent studies (Nissen et al., 1998; Vaz and Hopmans, 2001). For the probe material, two stainless steel wires were employed and they were coiled around an acrylic pipe. The coil length was controlled to be less than 2.0 cm, so that it fit within the depth of the root box. Therefore, the interval of the coil was about 1.7 mm. The stainless steel wires were connected to the coaxial cable inside the acrylic pipe. Inside the pipe, the wires were sleeved by silicon tubes in order to prevent a short-circuit. Further more, silicon sealant was filled into the acrylic pipe in order to prevent soil water leaking into the pipe.

One of the major advantages of the measurement of soil water content by the TDR method is that the relationship between primary output of TDR L_a/L [-] and the soil water content θ [cm^3/cm^3] is independent of temperature, type, or the void ratio of the soil under investigation. In general, an empirical equation proposed by Topp et al. (1980) is used for the calculation of soil water content measured by the widely used

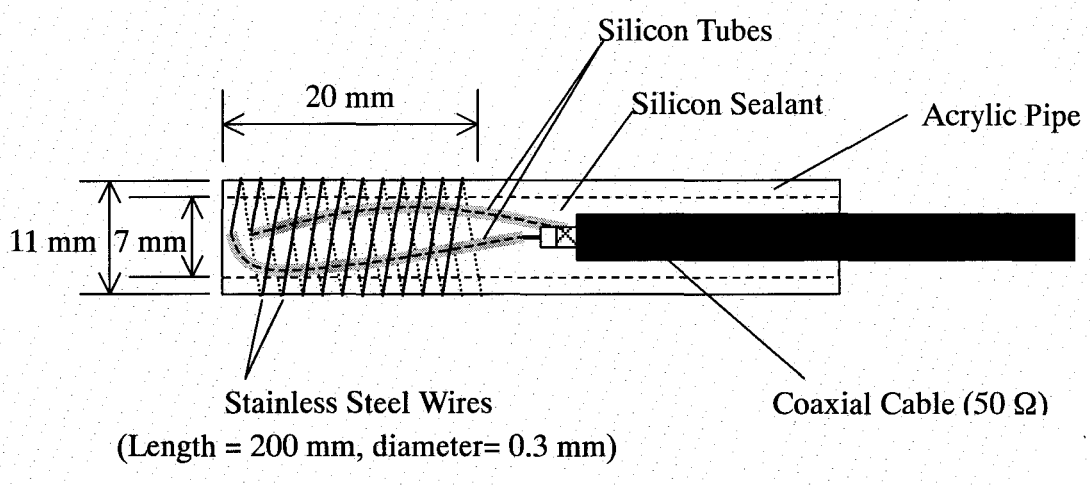

Figure 4.4 Detail of a coil type TDR probe. (The stainless steel wires were coiled around the acrylic pipe, and connected to the coaxial cable inside the pipe.)

rod type TDR probes. However, because the TDR probe used in the experiment is the coil type and its structure is much different from the rod type probe, it is necessary to fix the relationship between primary output L_a/L of the TDR and the soil water content θ as peculiar to the coil type probes used. This calibration procedure in fixing the relationship was carried out prior to the plant growth experiment measuring the soil water content in the root boxes. The probes were installed in the root boxes and soil of the same density ($0.87 g/cm^3$) as the root growth experiment was filled into the root boxes. The root boxes were set horizontally, with the back acrylic plates detached. Water was sprayed evenly onto the soil surface, until the soil became saturated. Just after soil saturation, the total weight of the root boxes and the primary outputs of TDR L_a/L for each probe were measured. For the TDR measurement, the TDR100 equipment (Campbell Scientific Inc, Utah, USA) was used. The root boxes were then left undisturbed, so that the water could evaporate from the soil surface. After some of the water evaporated, the total weight of the root boxes and the primary outputs of TDR L_a/L for each probe were measured. This procedure was repeated until the soil became air-dry. Through the measured total weight of the root boxes, together with the weight of the root boxes without the soil, the volume of the root boxes, and the void ratio of the soil as measured previously, the volumetric soil water contents were calculated. Through these measurements, we obtained 7 different relationships between the soil water content θ and primary outputs L_a/L. These relationships were approximated by curves, which were used for obtaining the soil water content in the root boxes of the root growth experiment. Detailed consideration of the approximated curves will be made in the next section, "Results and discussion".

4.2.4 Soil

A sandy soil taken from the Kamigamo Experimental Forest of Kyoto University (Kyoto City, Japan) and an organic soil were mixed (50:50 vol.%) for the experiment. The soil was fertilized with 3.0 g of granular fertilizer (N, 6%; P, 40%; K, 6%; Mg, 15%) per 1kg of the soil. The initial soil water content θ [cm^3/cm^3] was controlled previously (θ= 0.20 cm^3/cm^3), then the soil was filled into the root boxes at a controlled bulk density of 0.87 g/cm^3. The observed retention curve of the soil is shown in Figure 4.4, together with the soil hydraulic conductivity as represented by the lognormal model proposed by Kosugi (1996). The parameters for the lognormal model were determined based upon the observed retention curve, and are shown in Figure 4.5.

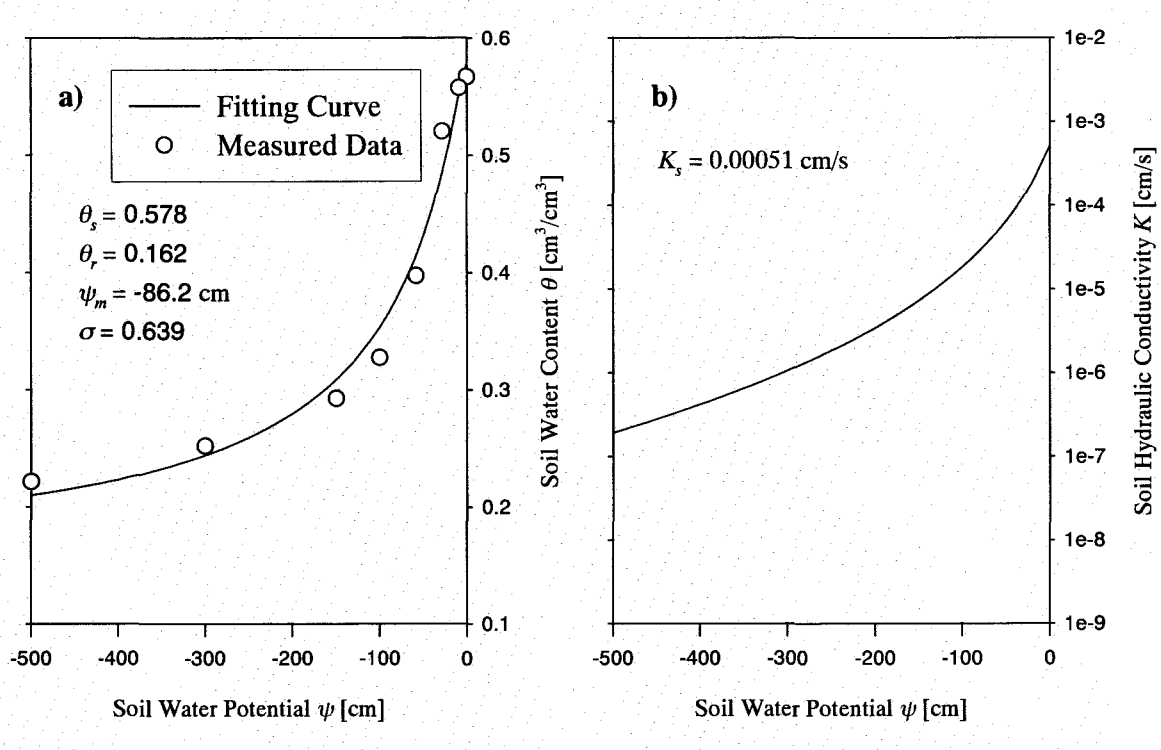

Figure 4.5 Hydraulic properties of soil, a) θ - ψ, b) K - ψ curve.

4.2.5 Experimental Procedure

The root growth experiment was carried out in a green house at the Experimental Forest of Kyoto University (Kyoto City, Japan) from April 27th to May 28th in 2002. The highest, lowest and average temperatures in the green house during the experiment were 42.9, 10.2 and 22.3 ℃, respectively. Figure 4.6 shows the changes of temperature at the green house, a) the daily maximum, minimum, and average temperature outside of the green house, and b) the temperature inside the green

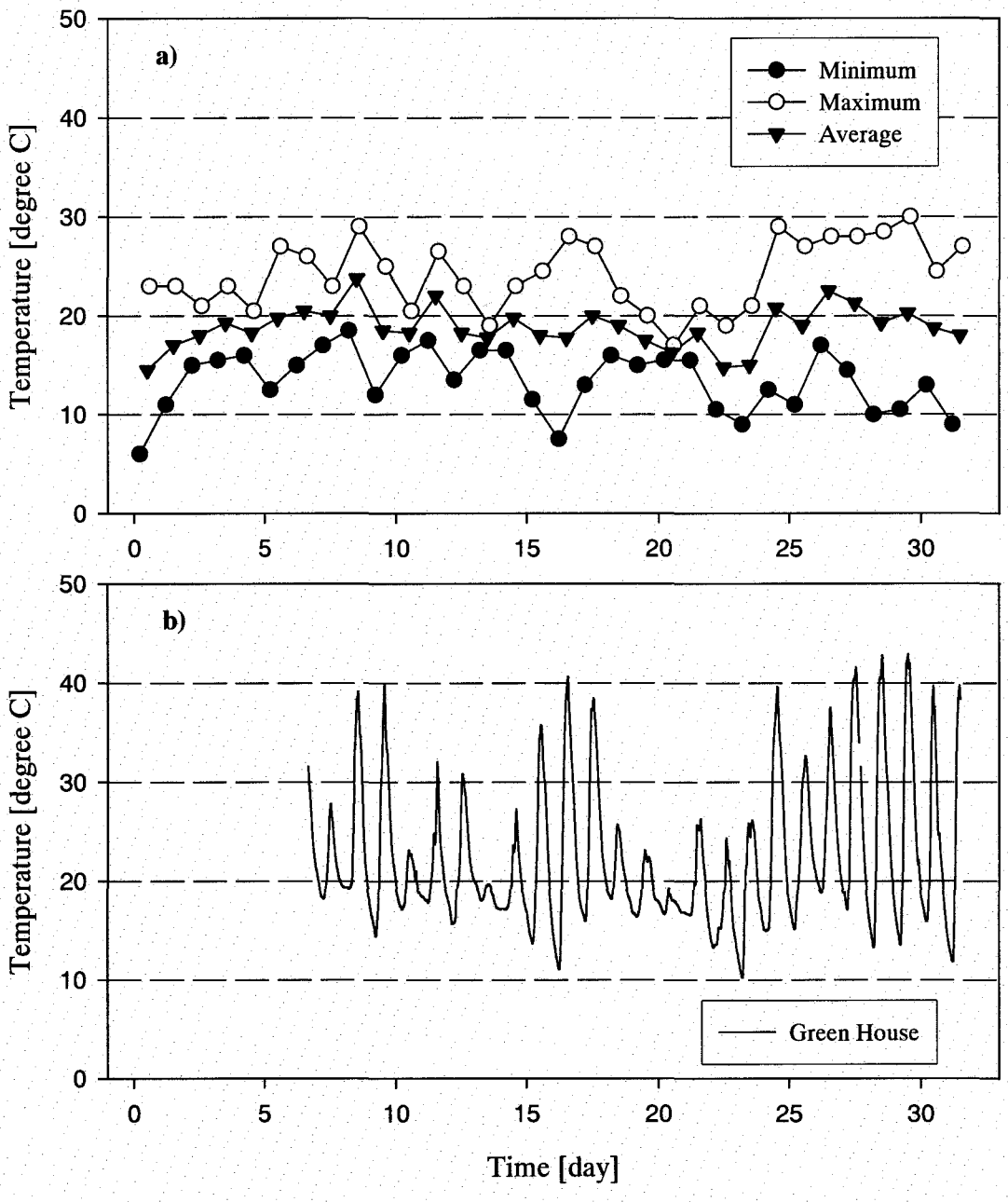

Figure 4.6 Changes of the temperature a) inside, and b) outside of the green house.

house. Figure 4.6 indicates that the temperature inside the green house is a few degrees higher than the temperature outside of the green house. At the beginning of the experiment, seeds were sown on the top of each root box. The root boxes were set vertically until the germination (7^{th} day after sowing), then were set horizontally after the germination, so that the effects of gravity both on root elongation and on soil water

flow could be reduced (See Figure 4.3). The TDR measurement and water supply were started after the germination. The interval of the TDR measurements was every 10 minuets, and the water was continuously supplied from the porous cups. By covering the soil surface, evaporation was prevented. During the experiment, the amount of supplied water and the total weight of the root boxes were measured once a day at 18:00, so that amount of daily transpiration could be obtained. At the end of the experiment, the root boxes were broken apart and the soil was removed carefully not to disturb the root systems. Photographs were then taken to record the architecture of the root systems. The characteristics of the root architecture (i.e. branching interval, root length, maximum branching order) were measured, so that they could be used in the model simulations.

4.3 RESULTS AND DISCUSSION

4.3.1 Calibration for TDR Probes

The calibration curves of the TDR probe in each root box are shown in Figure 4.7. The circles in Figure 4.7 indicate the average values of the 25 probes in each root box, and the error bars indicate the standard deviations. The fitting curves and their parameters are shown in Figure 4.7. In Figure 4.7, the relationship between the primary output L_a/L and soil water content θ in root boxes No.1 and No.2 shows similar tendencies. Value of the TDR output L_a/L for the 25 probes is distributed relatively wider in high water content level, and is closer in the low water content level. It seems that the distributed value of L_a/L is due to the difference in the contact between the probe and the soil, or the small variations in the shapes of the probes. The output of the TDR measurement L_a/L varies depending on dielectric constant of the soil κ [-]. The relationship between them can be represented by following equation (Baker and Allmaras, 1990),

$$L_a / L = \sqrt{\kappa} \tag{4.1}$$

Because soil is composed of soil particles, air and water, the value of the dielectric constant of the soil κ is determined by their volumetric compositions and each value of the dielectric constant of the soil particle κ_s, air κ_a and water κ_w. Ordinal values of the dielectric constant are κ_s =3-4, κ_a =1, and κ_w =80. Because the dielectric constant of water κ_w is much larger than those of other components κ_s and κ_a, the dielectric constant of the soil κ is largely affected by the water content. Due to the principles of the TDR measurement process, when water content level is low, the main components of the soil are soil particles and air, which have similar dielectric constants. The difference in the contact between probe and soil or the variation of the shapes of probes has little effect on the apparent values of the dielectric constant of soil κ. Whereas, when the water content level is high, the main components of the soil are soil particles and water which have much different dielectric constants, the difference in the contact

between probe and soil or the variation of shapes of the probes has great effect on the apparent values of the dielectric constant of soil κ. These reasons may accounts for the value of TDR output L_a/L being distributed widely in high water content level, and being closer in low water content level, as shown in Figure 4.7. However, from the results of the calibrations, which were carried out several times (data not shown), any particular tendencies for individual probes cannot be found. Therefore, it is supposed that the distributed value of the dielectric constant is mainly due to the difference in the contact between the probe and the soil. Because the root growth experiment was carried out after the TDR probe calibration and root boxes refilled with new soil, the contact between each probe and the soil changed after the calibration. Therefore, instead of determining and using fitting curves for each probe, a fitting curve for an average value of the 25 probes in the root box was used to calculate the soil water content. The function of the calibration curve of the probes is shown as following equation,

$$\theta = a(L_a / L - b)^d + c \tag{4.2}$$

where a, b, c, and d are the fitting parameters, and their values are shown in Figure 4.7.

In the remaining part of this subsection, the relationship between TDR outputs L_a/L and soil water content θ will be discussed, from the viewpoint of theoretical considerations. According to the mixing law (Nissen et al., 1998; Roth et al., 1990), the dielectric constant of the soil κ_{soil} [-] can be represented as the volumetric average dielectric constant value of each component, i.e. soil particles κ_s, air κ_a, and water κ_w as follows,

$$\kappa_{soil} = \left[(\phi_v - \theta)\cdot \kappa_a{}^n + (1-\phi_v)\cdot \kappa_s{}^n + \theta \cdot \kappa_w{}^n \right]^{1/n} \tag{4.3}$$

where, ϕ_v is the void ratio. The exponent n summarizes the geometry of the soil in relation to the applied electric field and varies between –1 in the case where the electric field is perpendicular and 1 in the case where the electric field is parallel to the layers of dielectrics (Roth et al., 1990). Because the wires of the coil type probe that was used in the experiment are in contact with the soil and the acrylic pipe, the mixing law is applied again, as follows,

$$\kappa_{coil} = \left[(1-w)\cdot \kappa_{soil}{}^{n_c} + w \cdot \kappa_p{}^{n_c} \right]^{1/n_c} \tag{4.4}$$

where, κ_{coil} is the dielectric constant which is obtained by the coil type probe measurement, κ_p is the dielectric constant of the acrylic pipe, and w, (1-w) represents the weighting factors for the probe material and the soil, and n_c is a factor similar to n in Equation (4.3). Substituting Equation (4.3) into (4.4), we obtain (4.5).

$$\kappa_{coil} = \left\{(1-w)\cdot\left[(\phi_v - \theta)\cdot \kappa_a{}^n + (1-\phi_v)\cdot \kappa_s{}^n + \theta \cdot \kappa_w{}^n \right]^{n_c/n} + w \cdot \kappa_p{}^{n_c} \right\}^{1/n_c} \tag{4.5}$$

By substituting the values of ϕ_v = 0.567 measured previously, κ_a = 1.0, κ_s = 3.9, κ_w =

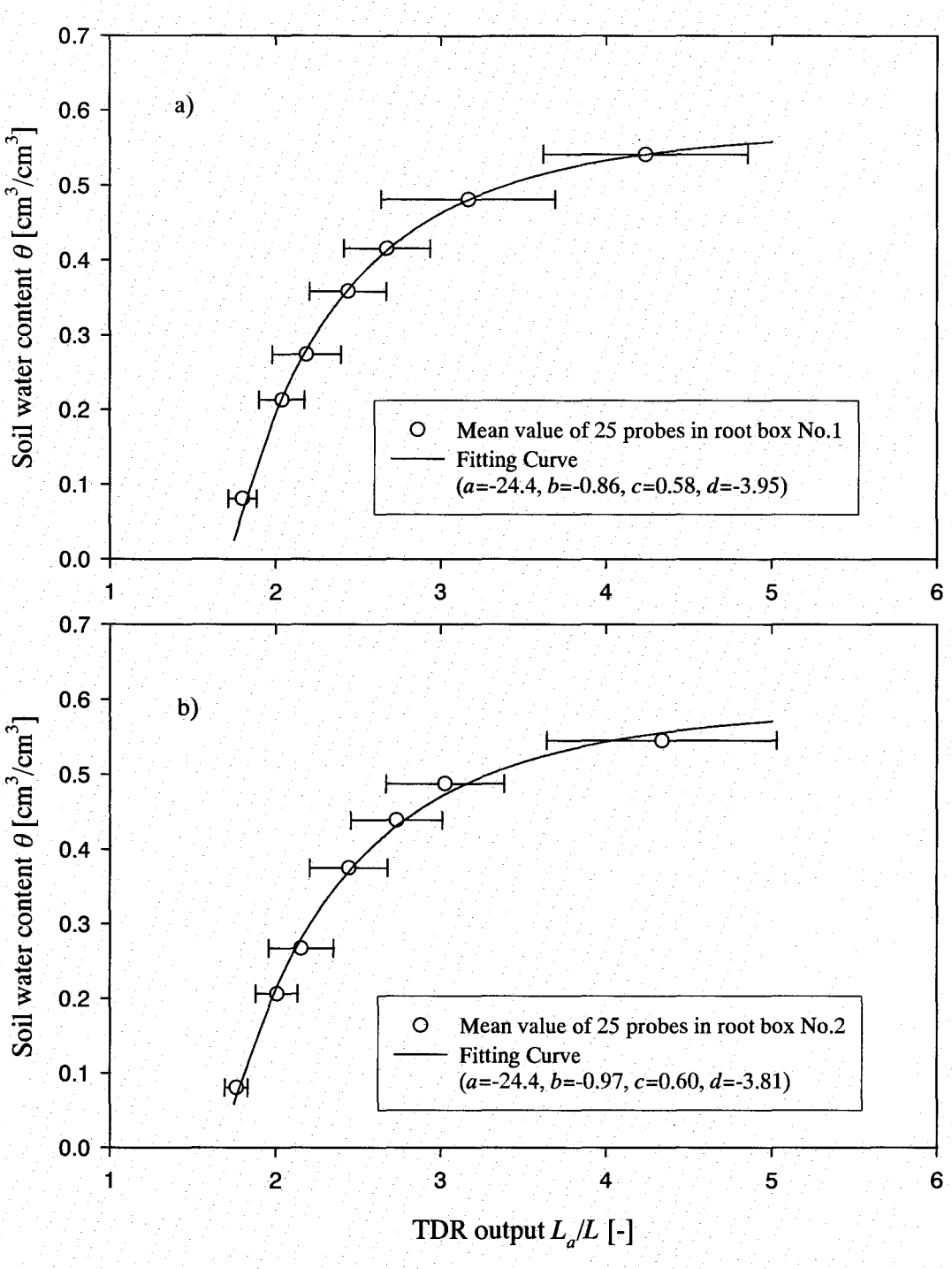

Figure 4.7 Measured calibration values of TDR probes in root box a) No.1 and b) No.2, and their fitting curves. (Fitting parameters are shown in the figures.

80 (Vaz and Hopmans, 2001), κ_p = 2.63 (Chemical handbook, 1993) as the particular value for each component, and n = 0.4 (Roth et al., 1990), n_c = –0.1, w = 0.51 (Nissen et al., 1998) according to previous studies, into Equation (4.5), we obtain the

relationship between L_a/L and θ from the theoretical mixing law, shown as the solid line in Figure 4.8. In Figure 4.8, the measured and theoretical relationship between L_a/L and θ shows relatively good agreement in low water content level. However, in high water content level, their values differ and the tendencies are also different, i.e. measured relationship between L_a/L and θ shows a tendency to the horizontal direction, whereas the theoretical relationship shows a tendency upward. Due to this disagreement, it is impossible to theoretically account for the calibration curve used for the experiment by the mixing law. It seemed that the disagreement was due to the difference in the structures of the probes that Nissen et al. (1998) used and those which were used in this study, so the author tried to fit the curve by changing the values of n_c and w. However, the disagreement improved little. Baker and Lascano (1989) reported that the spatial sensing range of a rod type TDR probe (rod diameter was 3.175mm, distance between rods was 5cm) varies according to the medium under investigation. In the case of water that has a large dielectric constant, the sensing range was large (20 $\times$65mm around the rods). And in the case of air that has small dielectric constant, the sensing range was small (20mm circles around each rod). These results suggest that the spatial sensing range of the soil by the TDR probe varies according to the soil water content. If this dependency of the sensing range on soil water content is included into the mixing law, w have to be defined not as a constant but as a function of soil water content θ, because the contribution of the sensing range of the acrylic pipe for the measured dielectric constant does not vary, while the contribution of the sensing range of soil increases depending on the increased soil water contentθ. Therefore the function of w is re-defined as follows,

$$\frac{w_1 - w}{w_1 - w_2} = \left(\frac{\phi_v - \theta}{\phi_v} \right)^{n_w} \tag{4.6}$$

where, w_1, w_2 are constants which range from 0.0 to 1.0, and n_w is a constant that ranges from –1.0 to 1.0 and is similar to the parameter n. If $w_1 > w_2$, w is an increasing function of θ, and if $w_1 < w_2$, w is a decreasing function of θ. The relationship between L_a/L and θ considering the spatial sensing range variations according to the soil water content θ was determined and are as shown in Figure 4.8 as dotted lines. The values of w_1, w_2, n_w by which Equation (4.5) approximates the measured relationship most closely are also shown in Figure 4.8. In Figure 4.8, the measured and theoretical relationship as a dotted line shows excellent agreement through all range of soil water content. Moreover, the relationship of $w_1 < w_2$ indicates that the w is a decreasing function of θ, and this implies that 1- w is a increasing function of θ. This result agrees well with the idea that the contribution of the sensing range of the soil increases depending on the increasing soil water content, as was mentioned previously. It may be concluded that the measured relationship between L_a/L and θ can be explained by the mixing law with the newly proposed function of w as shown in Equation (4.6)

theoretically, and the calibration curves are available for the calculation of soil water content.

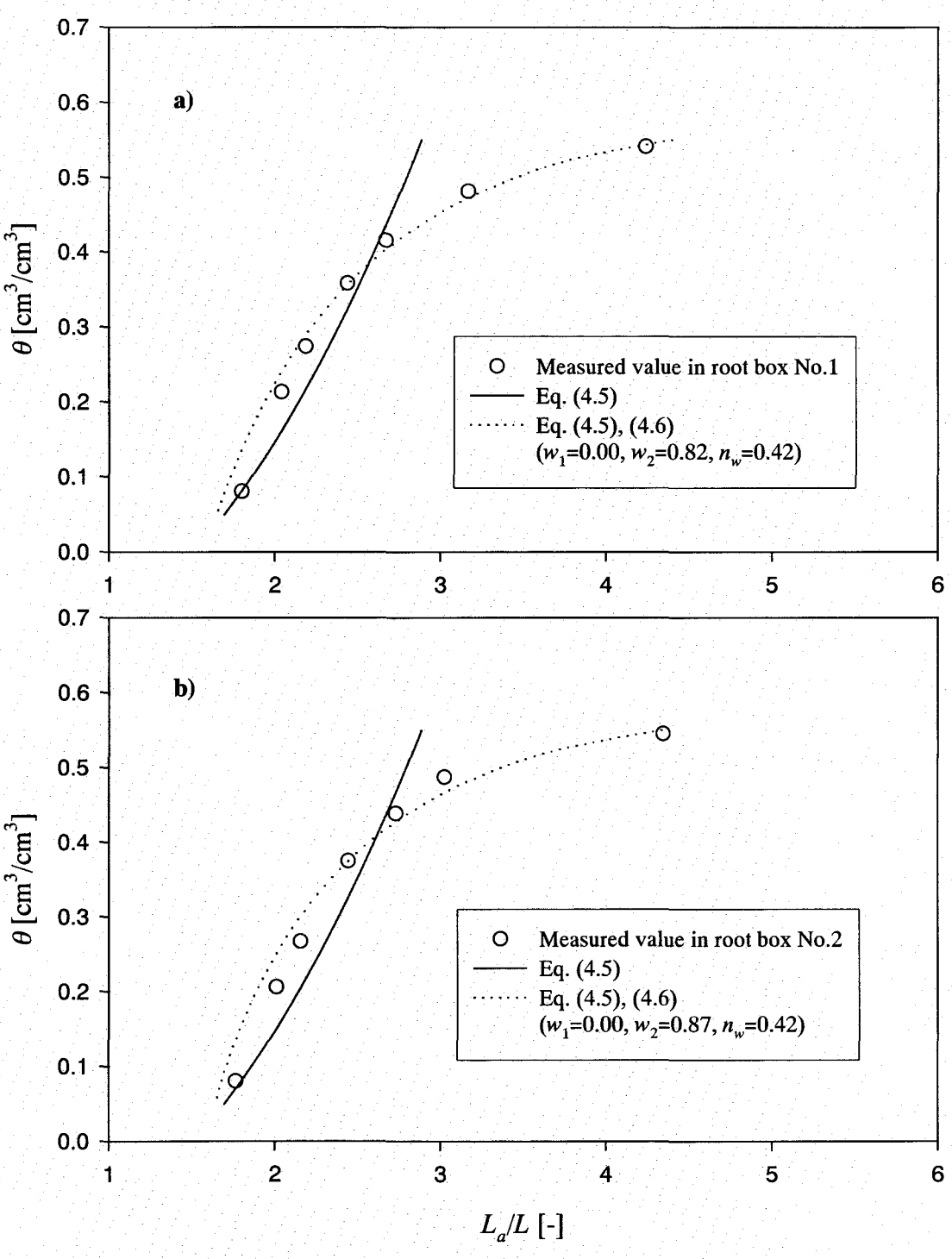

Figure 4.8 Theoretical relationships between L_a/L-θ, according to the mixing law.

4.3.2 Water Supply and Daily Transpiration

Figure 4.9a shows the amount of water that was supplied to the root boxes from the porous cups, and Figure 4.9b shows the amount of daily transpiration. Figure 4.10 shows the distribution of soil water content θ [cm^3/cm^3] at 15:00 in root box No.1 and No.2, obtained by the TDR measurements. Until the 7th day after sowing, the amount of supplied water was zero because the porous cups were not connected to the water tanks. Just after the porous cups were connected to the water tanks (the 8th day after sowing), a large amount of water was supplied to the root boxes because the soil water conditions were relatively dry (average water content θ_{av} = 0.20 cm^3/cm^3), and the water supply rapidly decreased because the soil then became relatively moist (θ_{av} = 0.25 cm^3/cm^3 in the root No.1 and θ_{av} = 0.28 cm^3/cm^3 in the root No.2, see Figure 4.10a). From the water supply, the soil near the porous cups became moist (see Figure 4.10a). At this stage of the experiment, transpiration did not occur, because the plants had not grown sufficiently (Figure 4.9b). From the 13th day after sowing, transpiration began, and a roughly constant amount of water was supplied from the 12th through the 24th day after sowing. From the 24th day after sowing, transpiration increased along with plant growth, and the amount of water supply increased from the 25th day after sowing. The increase in transpiration caused drought areas to form in the root box soil (see Figure 4.10b). From 18:00 on the 29th day after sowing until 21:00 on the 30th day after sowing, the supplied water to the root boxes was stopped in order to measure the soil water distribution in the case of zero water supply. Due to this condition, the soil became drier and the drought areas increased (see Figure 4.9b). The transpiration and the amount of water supply decreased during the last few days. Comparing the amount of supplied water and transpiration between root boxes, the difference was little. On the other hand, the distribution of soil water content was different between the root boxes, due to the differences in root system distributions and the position of the water supply.

Transpiration is affected by weather conditions, especially the radiation, temperature and humidity. In general, the temperature in the green house becomes high when the weather is fine, then the amount of transpiration may increase. The transpiration in Figure 4.9b changes, obviously depending on the temperatures shown in Figure 4.6.

4.3.3 Changes of Soil Water Volume in the Root Box

Figure 4.11 shows the changes of soil water volume in the root boxes. Dots indicate the changes of soil water volume, obtained from the measured values of the total weight of the root boxes subtracted by empty weight of the root boxes and previously obtained dry weight of the soil. On the other hand, Solid lines indicate the continuous changes in soil water volume calculated from the soil water content obtained by the TDR measurement. In the calculation, the soil in root boxes was

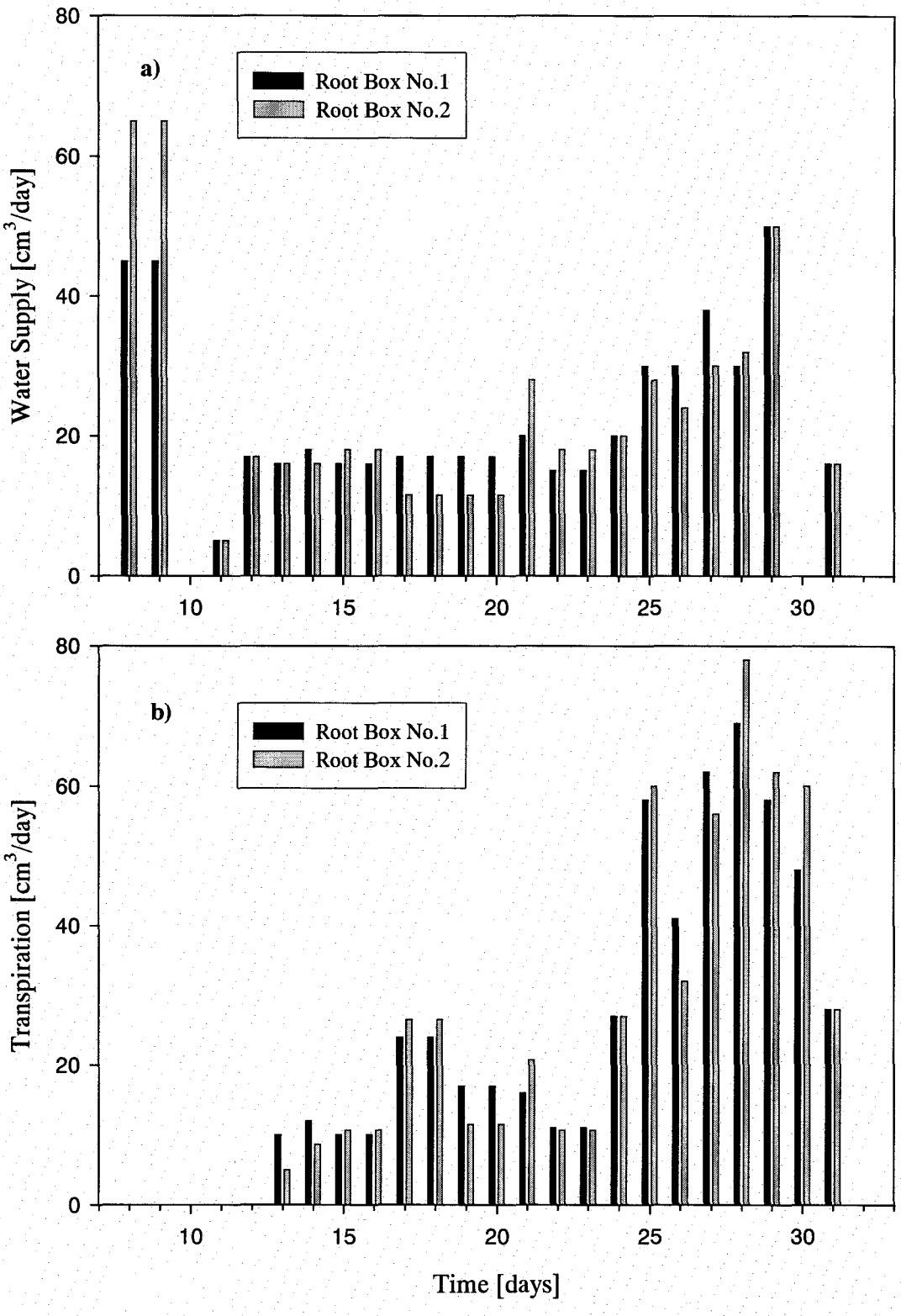

Figure 4.9 Changes of a) water supplied to the root boxes, and b) daily transpiration rate.

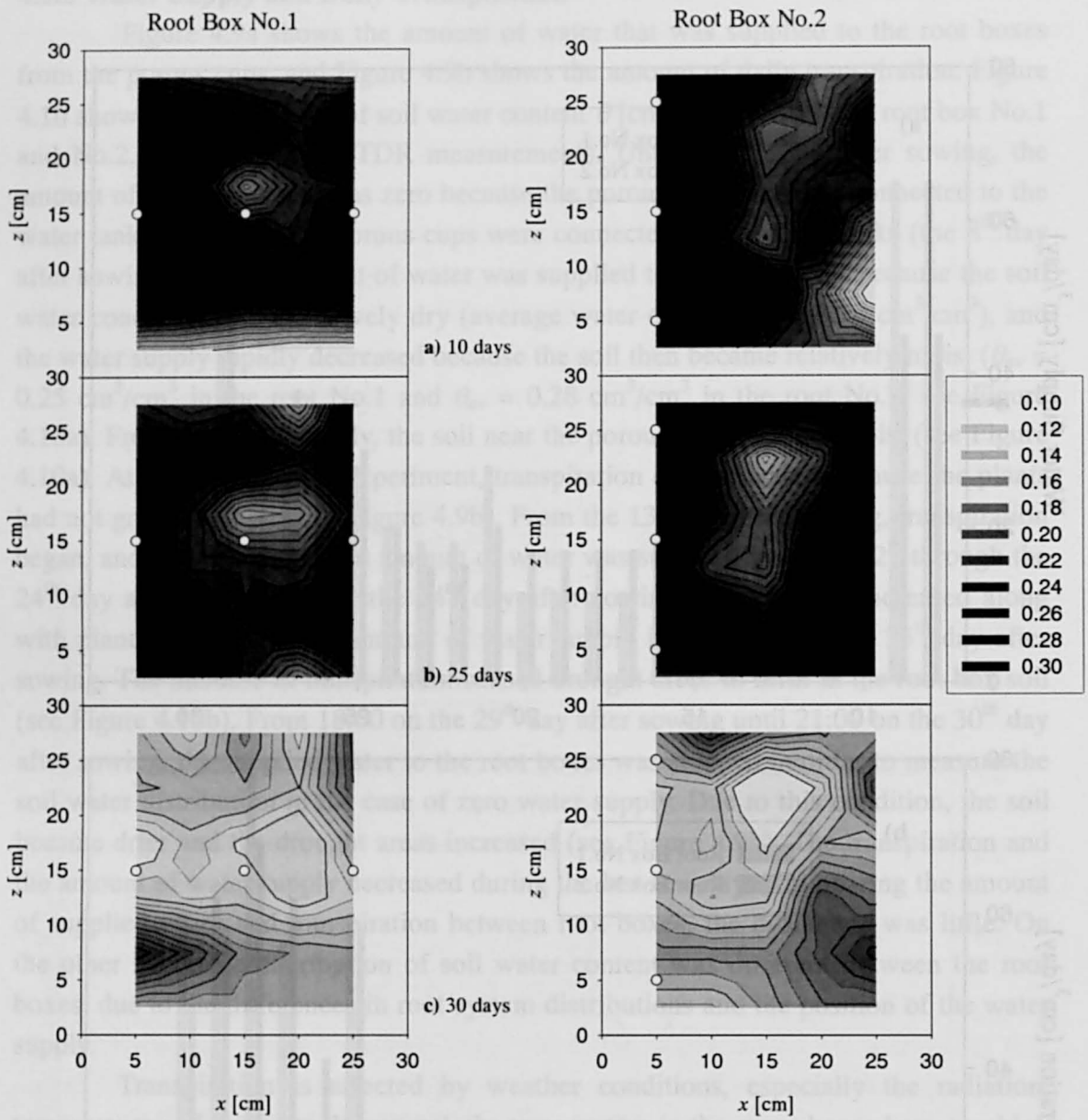

Figure 4.10 Changes of the distribution of soil water content θ [cm^3/cm^3] in the root boxes No.1 and No.2, measured by TDR method. (White circles indicate the points of water supply.)

divided into 25 rectangular shaped domains, and in each of these domain one TDR probe was included. Then, it was assumed that the value of soil water content measured by the probe represented the average value of the domain in which the probe was included. Hence the soil water volume was calculated as the sum of the volume of water in each domain, which is the soil water content multiplied by the volume of the domain.

The volume of water obtained by weight in each root box was stable until the 7th day after sowing, then increased when the water supplies started. From the 12th through the 24th day after sowing, the increase and decrease repeated, and remained relatively high level, possibly due to water supply and transpiration. From the 25th day after sowing, it decreased until the end of the experiment. These changes in soil water volume are due to the changes of supplied water and the daily transpiration as shown in the previous subsection.

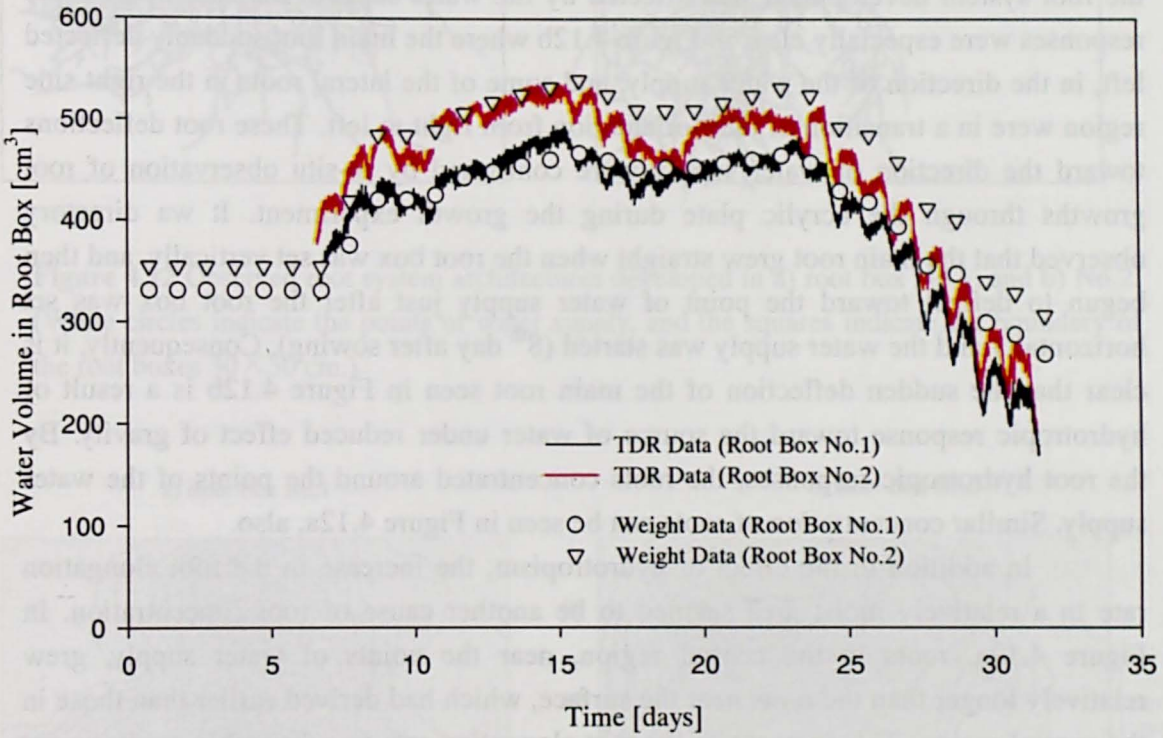

Figure 4.11 Changing soil water volume in the root boxes obtained from measured weight of root boxes and TDR data.

The volume of water calculated from the TDR measurements changed in good agreement with the volume of water obtained by weight in each root box. Also, it reflects the daily changes, i.e. in the daytime the water volume decreased because the transpiration was larger than the water supply, and in the nighttime the water volume increased because of the water supply. From the 24th day after sowing, the volume of water calculated from the TDR measurements became slightly lower than the volume of water obtained by weight. This difference may be due to the accuracy of the TDR probe calibrations. However, the total changes in water volume as calculated from the TDR measurements well represent the actual changes in water volume in the root boxes, and their difference may be permissible. Therefore, it may be concluded that the TDR measurements by coil type probes are reliable enough to obtain the distribution of

soil water content in the root boxes, and to analyze their effect on root system development.

4.3.4 Observed Root System Architecture

Figure 4.12a, b shows the observed root system architectures that developed in root boxes No.1 and No.2. Squares indicate the boundaries of the root boxes, and the white circles indicate the position of the porous cups from which water was supplied. In Figure 4.12a, b, two root systems show different morphology and it is obvious that the root system development was affected by the water supply. The root hydrotropic responses were especially clear in Figure 4.12b where the main root suddenly deflected left, in the direction of the water supply, and some of the lateral roots in the right side region were in a transition of their orientation from right to left. These root deflections toward the direction of water supply were confirmed by in-situ observation of root growths through the acrylic plate during the growth experiment. It wa directory observed that the main root grew straight when the root box was set vertically, and then begun to deflect toward the point of water supply just after the root box was set horizontally and the water supply was started (8^{th} day after sowing). Consequently, it is clear that the sudden deflection of the main root seen in Figure 4.12b is a result of hydrotropic response toward the source of water under reduced effect of gravity. By the root hydrotropic responses, the roots concentrated around the points of the water supply. Similar concentration of roots can be seen in Figure 4.12a, also.

In addition to the effect of hydrotropism, the increase in the root elongation rate in a relatively moist area seemed to be another cause of root concentration. In Figure 4.12a, roots in the central region, near the points of water supply, grew relatively longer than the roots near the surface, which had derived earlier than those in the central region. This increase in the root elongation rate in a favorable environment is called "compensatory growth", and was reported in an earlier published study (Crossett et al., 1975). As a result, it may be concluded that root system development and its related morphological architecture as shown in Figure 4.12a, b were affected by both root hydrotropism and the compensatory growth.

In order to quantitatively estimate the root morphological architecture, especially the concentration of roots, the each square (30×30 cm) shown in Figure 4.12a, b were divided into 144 sub-squares (2.5×2.5 cm) by lines parallel to the x and y axis, then the root length in each sub-square was measured by using an image analyzing software (Scion Image, Scion Co., U.S.A.). The root length density [cm/cm^2] was obtained by dividing the measured root length by the area of the sub-square. Figure 4.13 shows the distribution of root length density [cm/cm^2], in root boxes No.1 and No.2. We can see that Figure 4.13 accurately reflects the actual root system architectures and the concentration of roots shown in Figure 4.12. By collating the distribution of root length density as shown in Figure 4.13 and the distribution of soil

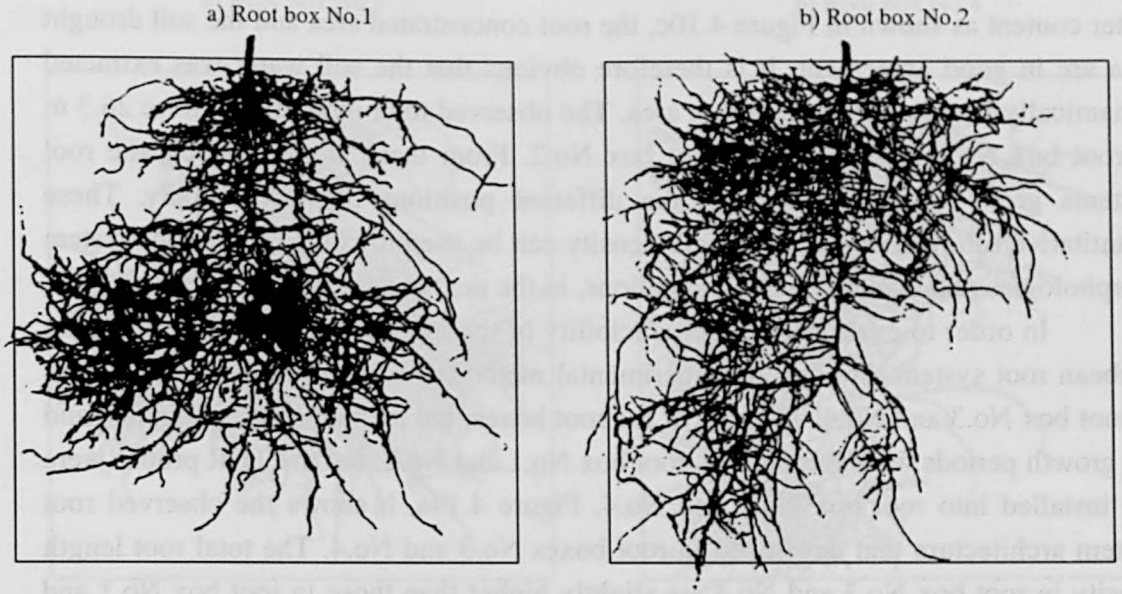

Figure 4.12 Observed root system architectures developed in a) root box No.1, and b) No.2. (White circles indicate the points of water supply, and the squares indicate the boundary of the root boxes 30×30 cm.)

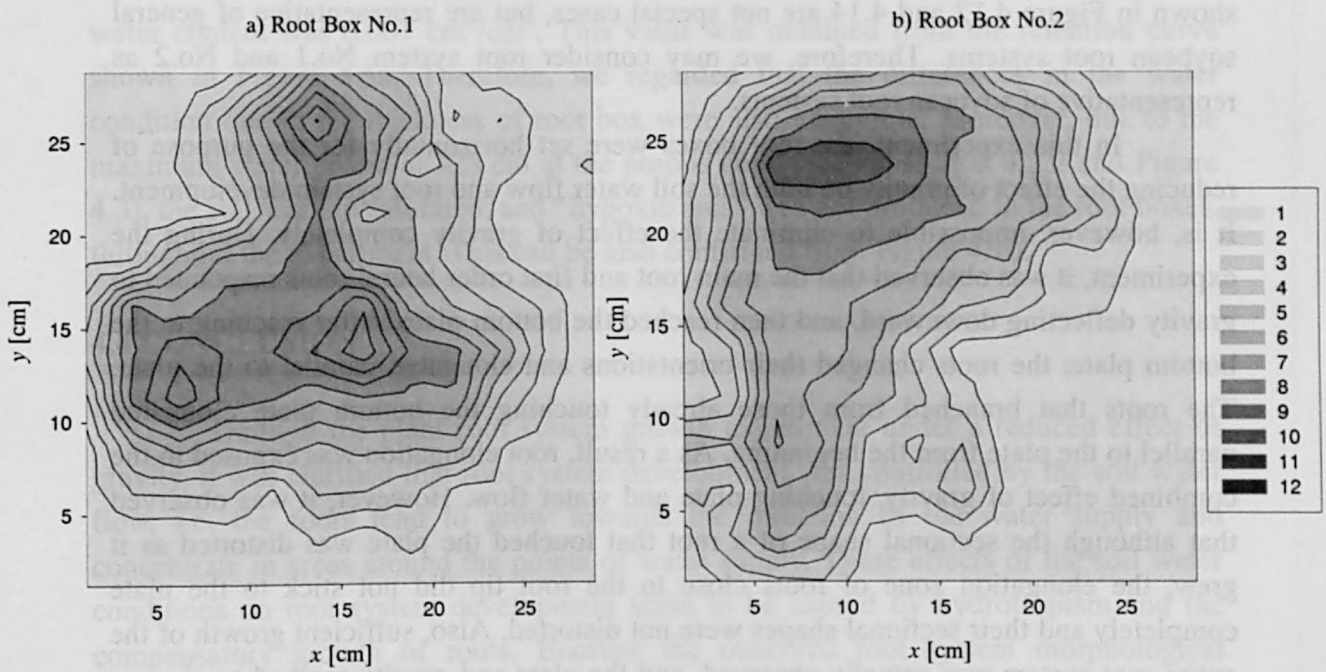

Figure 4.13 Distribution of the root length density [cm/cm^2] in a) root box No.1, and b) No.2, measured by image analyzing software. The concentration of the root length can be seen. (The figures are corresponding to the root systems shown in Figure 4.12.)

water content as shown in Figure 4.10c, the root concentrated area and the soil drought area are in good agreement. It is therefore obvious that the soil water was extracted dynamically in the concentrated root area. The observed total root lengths were 26.3 m in root box No.1 and 26.0 m in root box No.2. From these similar values, the root systems grew equally in spite of the different positions of water supply. These quantitative estimations of root length density can be used to compare the root system morphologies obtained by model simulations, in the next chapter.

In order to examine the reproducibility of the morphological architecture of a soybean root system through the experimental methods, we grew two more soybeans in root box No.3 and No.4. The size of the root boxes, the method of water supply, and the growth periods were the same as root box No.1 and No.2, but the TDR probes were not installed into root box No.3 and No.4. Figure 4.14a, b shows the observed root system architecture that developed in root boxes No.3 and No.4. The total root length density in root box No.3 and No.4 are slightly higher than those in root box No.1 and No.2. Each individual root elongation is also different from the other. However, the morphological architectures of the root systems developed in root box No.3 and No.4; i.e., root concentration, and the root deflection toward the point of water supply, are very similar to those in root box No.1 and No.2. By comparing these two sets of root systems, it can be said that the root system architecture affected by the water supply shown in Figure 4.12 and 4.14 are not special cases, but are representative of general soybean root systems. Therefore, we may consider root system No.1 and No.2 as representative of soybean root systems.

In this experiment, the root boxes were set horizontally for the purpose of reducing the effect of gravity on both the soil water flow and root system development. It is, however, impossible to eliminate the effect of gravity completely. During the experiment, it was observed that the main root and first order lateral roots responded to gravity deflecting downward, and then reached the bottom plate. After reaching to the bottom plate, the roots changed their orientations and elongated parallel to the plate. The roots that branched from those already touching the bottom plate elongated parallel to the plate from the beginning. As a result, root elongation was exposed to the combined effect of gravity, touching plate and water flow. However, it was observed that although the sectional shape of a root that touched the plate was distorted as it grew, the elongation zone of roots close to the root tip did not stick to the plate completely and their sectional shapes were not distorted. Also, sufficient growth of the entire root system was actually observed, and the plate and gravity seemed to give no harmful effect on the root elongation. Therefore, we regarded that the effect of touching the plate, "thigmotropism", might cancel out the effect of gravity "gravitropipsm", and that it is not necessary to consider this reduced effect of gravity on root system development. On the other hand, the difference of water potential between soil on the upper and lower plate was 2 cm, and the maximum difference of

a) Root box No.3 b) Root box No.4

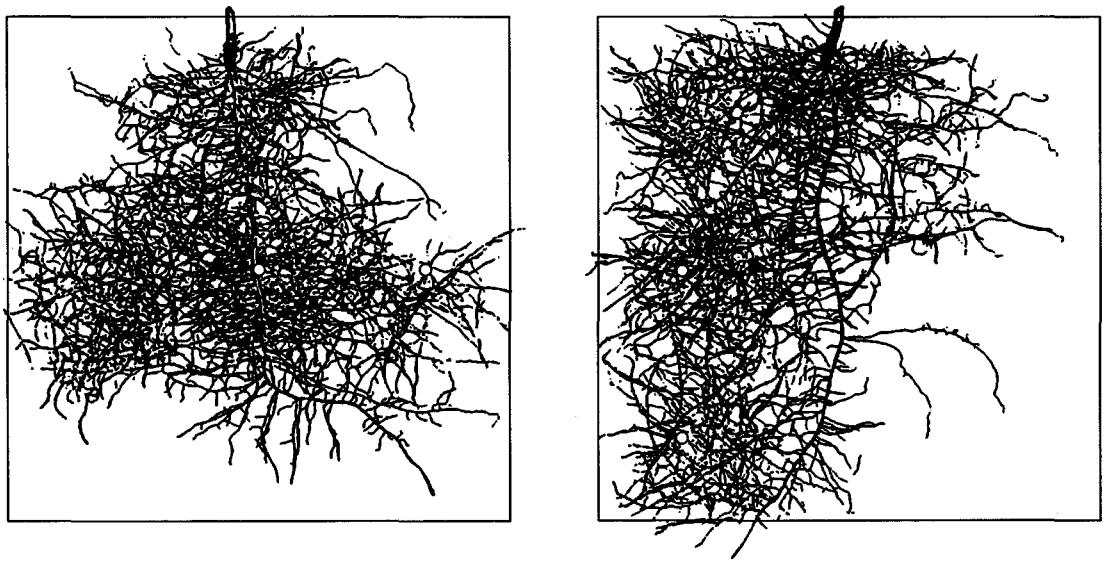

Figure 4.14 Observed root system architectures developed in a) root box No.3, and b) No.4, without the TDR measurement. (White circles indicate the points of water supply, and the squares indicate the boundary of the root boxes 30×30 cm.)

water content was 0.007 cm^3/cm^3. This value was obtained from the retention curve shown in Figure 4.5a. Therefore, we regarded that the differences in the water condition due to the thickness of root box were also negligible. Moreover, due to the maximum water potential –25 cm at the porous cups (See subsection 4.2.2 and Figure 4.3), the soil was not saturated, and "hypoxic area" was not produced in the root boxes, throughout the experiment. This can be also confirmed from Figure 4.10.

4.4 CONCLUSION

Through the plant root system growth experiment under a reduced effect of gravity, it was clarified that root system development was controlled by the soil water flow, i.e. the roots tend to grow towards the direction of the water supply and concentrate in areas around the points of water supply. These effects of the soil water conditions on root system development seem to be caused by hydrotropism and the compensatory growth of roots. Because the observed root system morphological architectures were obviously affected by the positions of water supply and the changes of distribution of soil water content as obtained by TDR measurements, the hypothesis that root hydrotropism is the dominant factor in root system development in the case of reduced effect of gravity, was confirmed. Also, the importance of root compensatory growth in root system development was suggested by the observations of the root

system development in the root boxes.

In the next chapter, the root system development and soil water flow obtained in the experiment will be simulated by a two-dimensional root system development model considering hydrotropism, so that the hypothesis that root hydrotropism is one of the most important factor in root system development will be demonstrated.

REFERENCES

Baker J.M. and Allmaras R.R. 1990 System for automating and multiplexing soil moisture measurement by time-domain reflectometry. Soil Sci. Soc. Am. J. 54, 1-6

Baker J.M. and Lascano R.J 1989 The spatial sensitivity of time-domain reflectometry. Soil Sci. 147, 378-384

Chem. Soc. Jpn. 1993 Handbook of chemistry, basic edition. Maruzen, Tokyo, Japan. II-503

Crossett R.N., Campbell D.J. and Stewart H.E. 1975 Compensatory growth in cereal root systems. Plant and Soil 42, 673-683.

Dalton F.N. and van Genuchten M.Th. 1986 The time-domain reflectometry method for measuring soil water content and salinity. Geoderma. 38, 237-250

Darwin C. 1880 The power of movement in plants. London. John Murray.

Durtochet H. 1824 Physiologische Untrsuchungen uber die Beweglichkeit der Pflanzen. Ubersetzt von Nathansohn. Ostwald's Klassiker der exacten Wissenschaften, 144 Cited by von Sachs (1887).

Galamay T.O., Yamauchi A., Nonoyama T. and Kono Y. 1992 Acropetal lignification in protective tissues of cereal nodal root axes as affected by different soil moisture conditions. Jpn. J. Crop Sci. 61(3), 511-517

Hooker H.D.Jr. 1915. Hydrotropism in roots of Lupinus albus. Ann. Bot. 29: 265-283.

Iijima M. and Kono Y. 1991 Interspecific differences of the root system structures of four cereal species affected by soil compaction. Jpn. J. Crop. Sci. 60(1), 130-138

Keith P. 1815 On the development of the seminal germ. Trans. Linn. Soc. 11, 252-269.

Kono Y., Yamauchi A., Nonoyama T., Tatsumi J. and Kawamura N. 1987 A revised experimental system of root-soil interaction for laboratory work. Environ. Control in Biol. 25(4), 141-151

Kosugi K. 1996 Lognormal distribution model for unsaturated soil hydraulic properties. Water Resour. Res.32, 2697-2703

Lynch J and van Been J.J. 1993 Growth and architecture of seedling roots of common bean genotypes. Crop Sci. 33, 1253-1257

Momii K., Nozaka J., and Yano T. 1992 Comparison of root water uptake models. J. Jpn. Soc. Hydrol. Water Res. 5(3), 13-21 (in Japanese with English summery)

Morita S. and Toyota M. 1998 Root system morphology of pepper and melon at harvest stage grown with drip irrigation under desert conditions. Jpn. J. Crop Sci. 67(3), 353-357 (in Japanese with English summery)

Nissen H.H., Moldrup P. and Henriksen K. 1998 High-resolution time demain reflectometry coil probe for measuring soil water content. Soil Sci. Soc. Am. J. 62, 1203-1211

Raper C.D. Jr. and Barber S.A. 1970 Rooting system of soybeans. I. Difference in root morphology among varieties. Agron. J. 62, 581-584

Roth K., Schulin R., Fluhler H. and Attinger W. 1990 Calibration of time domain reflectometry for water content measurement using a composite dielectric approach. Water Resour. Res. 26(10), 2267-273

Sassa T. 1985 Weekly variation of shoot extension, needle development, root elongation and root ramification, and the correlations among them, in Japanese red pine seedlings (Pinus densiflora). – A consideration from physiological aspect, under different thermal conditions – Bull. For. For. Prod. Res. Inst. 332, 21-37 (in Japanese

with English summery)
Takahashi H. 1994 Hydrotropism and its interaction with gravitropism in roots. Plant and Soil 165, 301-308
Takahashi H. and Scott T.K. 1993 Intensity of hydrostimulation for the induction of root hydrotropism and its sensing by the root cap. Plant Cell Environ 16, 99-103
Takano M., Takahashi H., Hirasawa T. and Suge H. 1995 Hydrotropism in roots: sensing of a gradient in water potential by the root cap. Planta 197, 410-413
Topp G.C., Davis J.L. and Annan A.P. 1980 Electromagnetic determination of soil water content: Measurements in coaxial transmission lines. Water Resour. Res. 16, 574-582
Vaz C.P.M. and Hopmans J.W. 2001 Simultaneous Measurement of soil penetration resistance and water content with a combined penetrometer-TDR moisture probe. Soil Sci. Soc. Am. J. 65, 4-12

CHAPTER 5

APPLICATION OF A TWO-DIMENSIONAL ROOT SYSTEM DEVELOPMENT MODEL TO A ROOT GROWTH EXPERIMENT IN ROOT BOXES

5.1 INTRODUCTION

Numerical simulation using a root system development model is one of the available methods for theoretical consideration of the mechanisms of root system development. Root system development models, in which root elongation factors (i.e. elongation rate, growth orientation, and branching) are described mathematically, can simulate the root system development under the ground, and have been used to predict the root system architecture in various kinds of plant. The root system development models are also used for inspecting the appropriateness of the hypothesis employed in the model, by comparing the simulated and actually observed root system morphologies. Furthermore, root system development models, combined with water or nutrient uptake models, are used for simulating the synchronized root system development and its soil water uptake or nutrient uptake behavior. Diggle (1988) and Pages et al. (1989) separately proposed fundamental models that simulate the three-dimensional growth and architecture of a root system. On the other hand, Clausnizter and Hopmans (1994) proposed a model that combined root system development and soil water uptake. Farther more, Somma et al. (1998) proposed a model that combined root system development and nutrient uptake. They all succeeded in simulating the three-dimensional root system development and soil water or nutrient uptake behavior. Many models have been proposed to simulate the root system development in various plant species (e.g. Lynch et al., 1997; Jourdan and Rey, 1997; Shibusawa, 1994). Although gravitropic response in root elongation was considered in all the models, the hydrotropic response of roots was not considered in almost all models. Only in the model by Clausnitzer and Hopmans (1994), the root hydrotropic effect is considered implicitly; they assumed that roots respond to the soil strength gradient that is defined as a function of the soil moisture content. In Chapter 3, a two-dimensional root system development model considering hydrotropism explicitly, which was combined with a soil water uptake model, was proposed. The model simulated root system development of Japanese red pine (*Pinus densiflora*) and soil water flow due to water extraction. The simulation results demonstrated plagiogravitropic elongation of lateral roots and the asymmetric architecture of the root

systems on slopes (Tsutsumi et al., 2001, 2003). However, because the comparison between simulated and actually observed root systems was not sufficient in previous studies, the effect of hydrotropism on root system development was not confirmed clearly.

In Chapter 4, the method and the result of an experiment, in which Soybean plants were grown and their root system architectures observed together with the quantitative measurement of soil water content in the root boxes, were reported. In this chapter, the root system development and the soil water flow that were obtained in the experiment were simulated by using a model that considers hydrotropism (Tsutsumi et al., 2003), and clarified the role of hydrotropism in root system development by comparing the actually observed and the simulated root systems. The concept of root compensatory growth was also employed into the model, and the effect of compensatory growth on root system development was investigated.

5.2 ROOT SYSTEM DEVELOPMENT MODEL

5.2.1 Root Elongation

A combined model of the two-dimensional root system development and soil water flow (Tsutsumi et al., 2003) was previously proposed, and reported on it in Chapter 3. In the proposed model, root hydrotropism was considered specifically as well as gravitropism, and root elongation was expressed by the differential growth, which is regarded as a mechanism of actual root elongation (Ishikawa et al., 1991; Takahashi, 1994). The same principle was employed in the model to simulate the results of the experiment that was reported in Chapter 4. Figure 5.1a, b, and c show the mechanism of root differential growth, gravitropic response of a root and hydrotropic response of a root. The function of hydrotropic elongation rate was defined as (see Figure 5.1c),

Wet side;

$$ER_h = ER_{h,0} - k_h|q'| \tag{3. 9}$$

Dry side;

$$ER_h = ER_{h,0} + k_h|q'| \tag{3.10}$$

where, $|q'|$ [cm/s] is the magnitude of the component of water flux q [cm/s], perpendicular to the root at the root cap and $ER_{h,0}$ [cm/s] gives the value of the hydrotropic elongation rate when $|q'|= 0$. In the previously proposed model (Tsutsumi et al., 2003) reported in Chapter 3, k_h was assumed to be a constant. In this chapter, in order to simulate the root system morphology obtained by the experiment, k_h was assumed to be a decreasing function of the soil water potential ψ [cm] at the root tip. The function k_h was defined as follows,

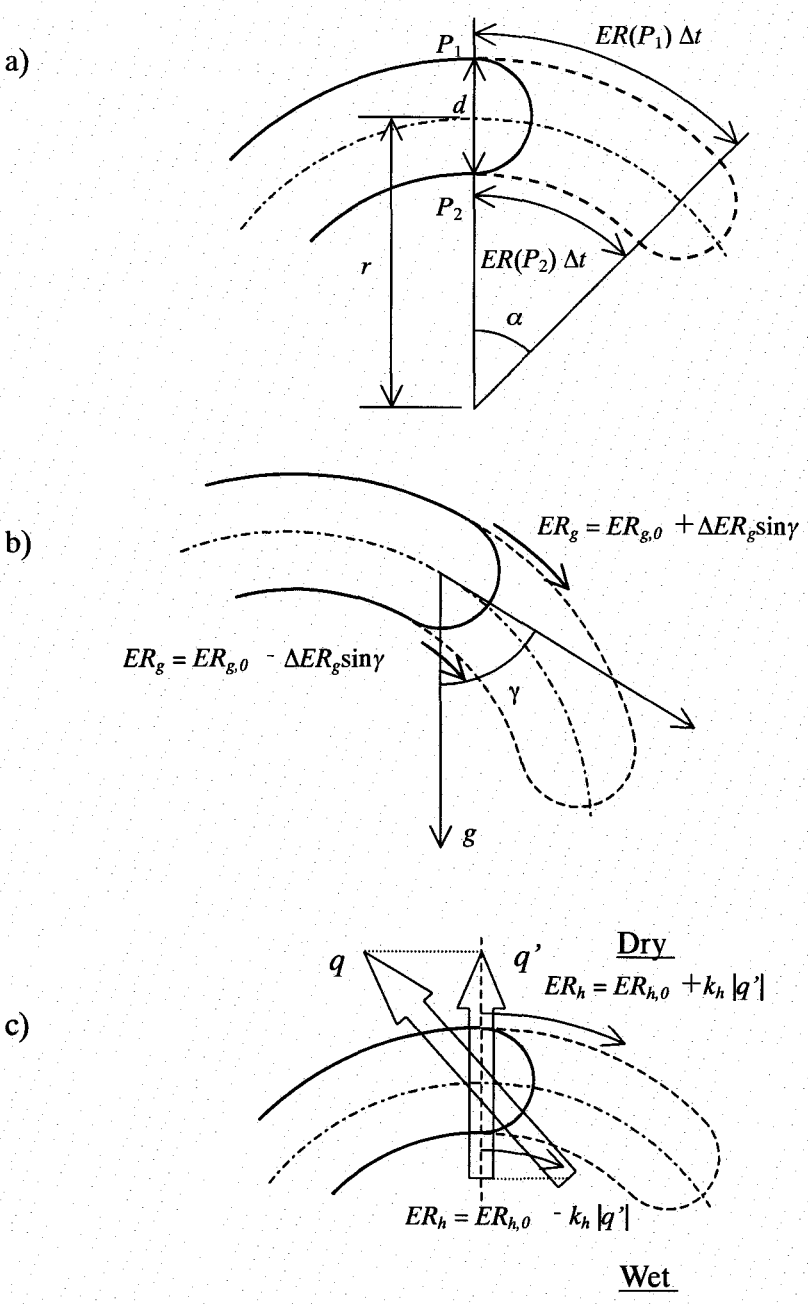

Figure 5.1 Model principles of the root elongation. a) mechanism of differential growth, b) gravitropic response, and c) hydrotropic response of root.

$$k_h = a_h(\psi - \psi_h) \qquad \psi < \psi_h \tag{5.1}$$

$$k_h = 0 \qquad \psi_h \leqq \psi \tag{5.2}$$

where, a_h [cm^{-1}] and ψ_h [cm], are constants which have negative values. By this

definition, the root hydrotropic response becomes stronger under drought condition, and the root does not show hydrotropism under moist condition where ψ is greater than ψ_h. From the physiological point of view, it seems to be quite natural that the root responds hydrotropically stronger under drought conditions than under a moist condition where the root can easily extract water.

To take into account the compensatory growth of the root system that was observed in the actual root system, a new function, root elongation activity A_e [-], is introduced as follows,

$$A_e = 0 \qquad \psi \leqq \psi_e \tag{5.3}$$

$$A_e = a_e(\psi - \psi_e) \qquad \psi_e < \psi \tag{5.4}$$

where, a_e [-] is a constant which has a positive value, and ψ_e [cm] is a constant which has a negative value. By multiplying A_e to the elongation rare ER_c, the root grows faster in moist area and stops growing in area where the soil water potential ψ is less than ψ_e. To keep the total root length independent from the root elongation activity A_e, the root elongation rate considering the root elongation activity, ER_c' [cm/hr], is defined as follows,

$$ER_c' = \frac{\sum_n ER_c}{\sum_n A_e ER_c} A_e ER_c \tag{5.5}$$

where, n [-] is the root number. By this definition, the total root length will be preserved in each simulation. Instead of ER_c, ER_c' was used for obtaining ER in equation (3.4).

5.2.2 Root Branching

Root branching is as important as root elongation, in root system development. From the observation of actual root systems in the experiment presented in Chapter 4, we confirmed main root growth as obvious and first order lateral root branching from the main root at a roughly constant interval. More than third order lateral root is negligible. We therefore assumed the soybean root system to be a main root system, and dealt with the main root and less than second order lateral roots. For simplicity, a constant branching interval is assumed. The details of the branching parameters are in accordance with the model proposed by Pages (Pages et al., 1989), and described in Chapter 3.

5.2.3 Soil Water Flow

The soil water flow was calculated according to the two-dimensional Richards' equation based upon water potential. The soil water capacity and hydraulic

conductivity in the Richards' equation were represented according to the lognormal model proposed by Kosugi (1996), (See Figure 4.5). In the simulations, the Richards' equation assuming an x-z coordinate were employed, and root gravitropism were considered until the 7th day after sowing. From the 8th day after sowing, the Richards' equation assuming an x-y coordinate were employed, and root gravitropism was not considered. Water extraction by the root system was determined according to the model of Herkelrath (Herkelrath et al., 1977; Kanda and Hino, 1990) as follows;

$$S = -\left(\frac{\theta - \theta_r}{\theta_s}\right)^b \rho \Delta \psi L \tag{3.18}$$

$$\Delta \psi = \psi_c + R_c l - \psi \tag{5.6}$$

where, S [s^{-1}] is the water extraction intensity, θ [cm^3/cm^3] is the soil water content at the root surface, ρ [s^{-1}] is the water penetration coefficient of the root, b [-] is a correction parameter, $\Delta\psi$ [cm] is the difference of the water potential between root and soil, L [cm/cm^2] is the root length density, ψ_c [cm] is the water potential of the beginning point of the main root, l [cm] is the distance from the beginning point of the main root to the root and R_c [-] is a correction coefficient for the friction loss of the water transport in the root. The length of the root whose age does not exceed 10 days was assumed to be counted in L, and contributes to soil water extraction. The equations for soil water flow were solved numerically by the partially implicit finite element method (Istoke, 1989; Zienkiewicz, 1971). The detailed methods were reported in Chapter 3. In order to simulate root system development and soil water flow in the root box experiment, the observed data for the actual daily amount of water supply and transpiration were used (The data is shown in Chapter 4). In the model calculation, the transpiration rate was assumed to be changing according to a sine curve during daytime similar to the assumption found in Chapter 3, and the water was supplied equally to three porous cups at a constant rate during a day.

5.2.4 Taking Experimental Results into Model Simulation

All the parameters used for the model simulation are shown in Table 5.1. From the observations and measurements of the root systems shown in Chapter 4, the root elongation rates were obtained. Then, first order lateral roots were classified into two types, i.e. long type and short type, and the different elongation rates for each type were given (see Table 5.1). The frequency of the long type and the short type first order lateral root were 33% and 67%, respectively. Based on the observation that the elongation rate of the main root changed during the experiment, the elongation rate of the main root was defined as a function of time (see Table 5.1). ΔER_g, a_h, ψ_h, a_e and ψ_e were determined by trial and error calculations, so that the model would simulate root systems similar to the actual root system. Branching parameters, i.e., apical

non-branching zone [cm], basal non-branched zone [cm], branching interval [cm] and insertion angle [degree] (see Chapter 3) were obtained by measurement of the actual root system. Parameters for water extraction i.e., b, ρ and R_c were determined according to Herkelrath et al. (1977) and Kanda and Hino (1990).

Table 5.1 Parameters for the model simulation

Parameters [unit]			
	Main root	1st order lateral root	2nd order lateral root
ER_c [cm/day]	$2.77(1\text{-}t/t_{max})^{1.345}$	0.59 (long type) 0.17 (short type)	0.34
$\Delta ER_g/ER_c$ [-]	0.0004	0.0001	0.0001
a_h [-]	-2.5	-2.5	-2.5
ψ_h [-]	-60	-60	-60
a_e [-]	4.0	4.0	4.0
ψ_e [-]	-250	-250	-250
Apical non branching zone [cm]	5.25	3.55	—
Basal non branching zone [cm]	0.245	0.370	—
Branching interval [cm]	—	0.245	0.370
Insertion angle [degree]	—	90	90
b* [-]	1	1	1
ρ* [s^{-1}]	$1.0*10^{-9}$	$1.0*10^{-9}$	$1.0*10^{-9}$
R_c* [-]	0.05	0.05	0.05

* According to Herkelrath et al. (1977), Kanda and Hino (1990)

5.3 RESULTS AND DISCCUTION

5.3.1 Simulated Root System and Distribution of Soil Water Content

Figure 5.2 shows the simulated root system development and distribution of soil water content θ [cm^3/cm^3] in root boxes No.1 and No.2 at 15:00, at each of three different stages of the simulations, corresponding in time to those shown in Figure 4.10. On the 10th day after sowing, the main root grew straight in root box No.1. On the other hand, the main root began to deflect toward the direction of the water supply in root box No.2. This deflection was similarly observed in the actual root system development in root box No.2, as mentioned in Chapter 4. The distribution of soil water content caused by the water supply can be seen in both root boxes. On the 25th day after sowing, root systems grew larger and many lateral roots elongated toward the porous cups. Because of the soil water extraction by the roots, drought areas appeared in both root boxes. On the 30th day after sowing, the soil became drier and their areas corresponded to root distributions. The concentrations of the roots to the points of

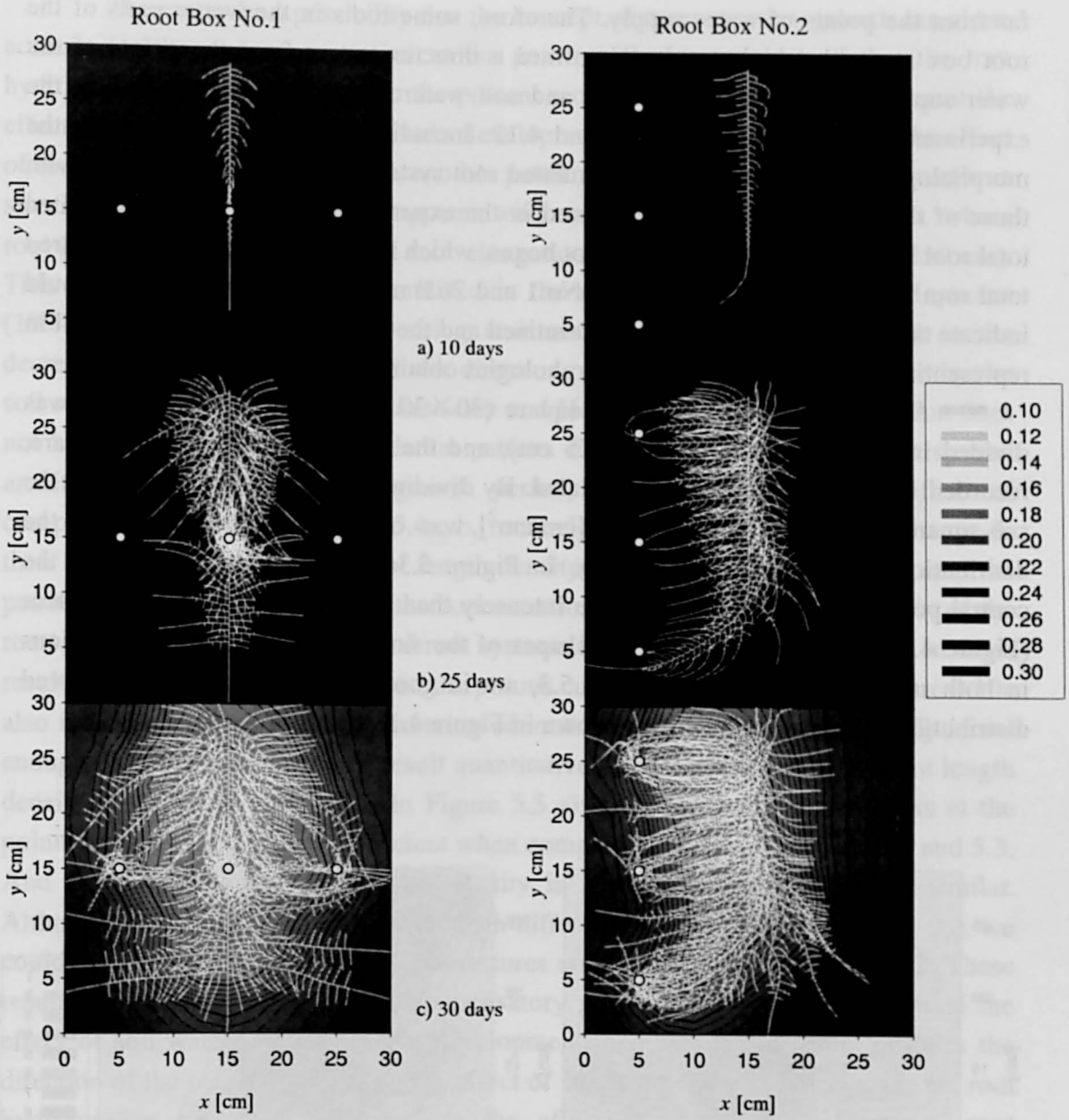

Figure 5.2 Simulated root system development and distributions of soil water content in the root boxes. (White circles indicate the points of water supply.)

water supply can be seen in both root boxes, similar to the actual root systems (see Figure 4.12). In both root systems, not all roots elongated toward the points of water supply. There were some roots elongating in a direction away from the points of water supply (e.g., lower part in root box No.1, and right lower part in root box No.2). This elongation may be explained as follows. At the later stage of the growth period, the soil area corresponding to the root system became drier due to transpiration, and the

moisture content was not evenly distributed. As a result, there appeared wetter areas far from the points of water supply. Therefore, some roots in the wetter parts of the root box responded hydrotropically toward a direction away from the points of the water supply. Similar root elongation and soil water distribution can be seen in the experimental results in Figure 4.10 and 4.12. Including these roots elongations, the morphological architectures of the simulated root systems are in good agreement with those of the actual root systems observed in the experiment. Moreover, the simulated total root length was 24.6 m in both root boxes, which is close to the actually measured total root lengths (26.3 m in root box No.1 and 26.0 m in root box No.2). This would indicate that ER_c was appropriately determined and the model simulations successful in representing the actual root system morphologies obtained by the experiment.

Similar to Figure 4.13, each square (30×30 cm) shown in Figure 5.2c was divided into 144 sub-squares (2.5×2.5 cm), and the root length in each sub-square, recorded in the simulation, was calculated. By dividing the root length by area of the sub-square, the root length density [cm/cm^2] was obtained. Figure 5.3 shows the distribution of the root length density. In Figure 5.3a, the roots concentrated at the central point of the water supply more intensely than the observed actual root system (Figure 4.13a). However, the overall shapes of the simulated root length distributions in both root boxes, shown in Figure 5.3, are in good agreement with the observed distributions of root length density, shown in Figure 4.13.

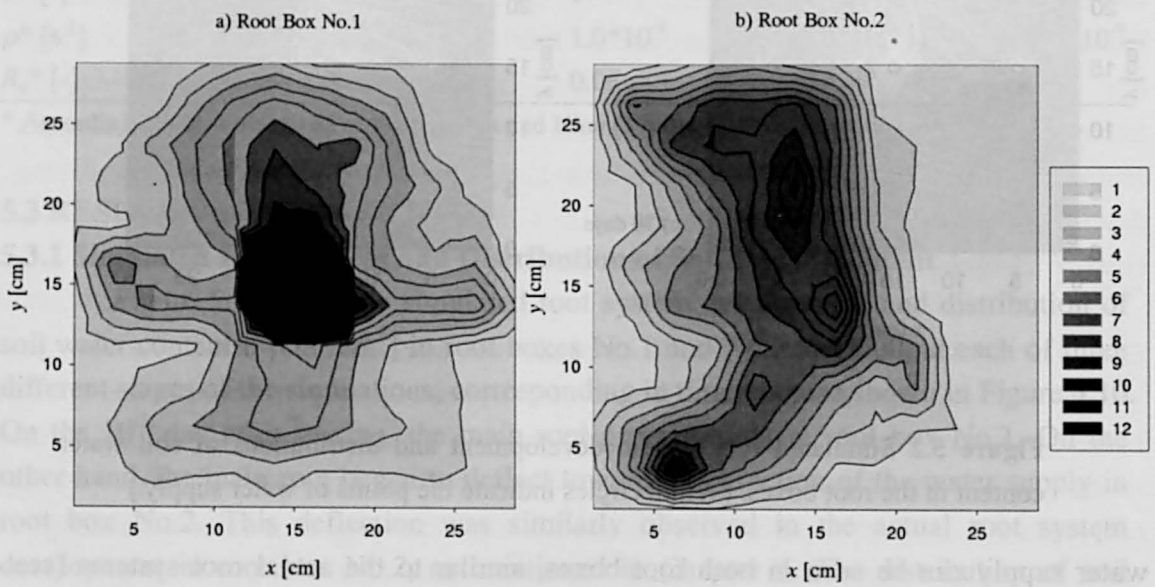

Figure 5.3 Simulated distribution of root length density [cm/cm^2] in the root box a) No.1 and b) No.2.

5.3.2 Simulated Root System Morphologies without Hydrotropism

There may be a possibility that the concept of compensatory growth can alone account for the root concentration to the points of water supply, and that the root hydrotropic response employed in the present model is not necessary to represent the effect of soil water flow on root system development. In order to demonstrate the effect of root hydrotropism in the model, another pattern of the root system development was simulated, i.e. root system development with only the compensatory growth, where root hydrotropism does not affect root elongation (k_h = 0.0, a_e = 40, ψ_e = -250 cm). This pattern is similar to that simulated in the model by Clausnitzer and Hopmans (1994), in a sense that the increasing resistance of root elongation is due to the decreasing soil moisture. Although the direction of root elongation was affected by the soil resistance in the model by Clausnitzer and Hopmans (1994), root orientation does not however change in this simulation pattern. Figure 5.4a, b shows the root system architecture at the end of the growth period, simulated only with the effect of compensatory growth. In Figure 5.4a, b, roots elongate straight and do not change in their direction of growth. The root length density seems to be slightly higher near the points of water supply. However, the concentrations to the point of water supply of the roots, which were seen in the actual root systems in root boxes, cannot be seen in these results. Higher water content around the porous cups in Figure 5.4 than in Figure 4.10c also indicates that the root concentration of roots to the points of water supply is not enough. In order to confirm this result quantitatively, the distribution of the root length density is shown in Figure 5.5. In Figure 5.5 also, the concentration of roots at the points of water supply is not sufficient when compared to those in Figure 4.13 and 5.3. And the distribution of root length density in Figure 5.5a and b is quite similar. Although we repeated the simulations with different values of parameters (a_e, ψ_e), we could not obtain the root system architectures similar to those in Figure 4.12. These results indicate that the effect of compensatory growth only cannot demonstrate the effect of soil water on root system development, and that a factor that changes the direction of the root growth due to the effect of soil water is necessary. Therefore, root hydrotropism, which is employed as the effect changing the direction of root elongation in the model, is an irreplaceable factor for representing the effect of soil water flow on root system development. Because the root branching interval was assumed to be constant in the model, there still remains the possibility that the compensatory growth with changing branching interval represents the root concentration to the points of water supply. In any event, however, without an effect such as hydrotropism changing the direction of root elongation, the model cannot simulate root deflection toward the point of water supply or elongation away from the point of water supply, as described previously.

As we have seen, the simulated root system architectures (Figure 5.2c) are in good agreement with the observed actual root system architectures (Figure 4.12), and

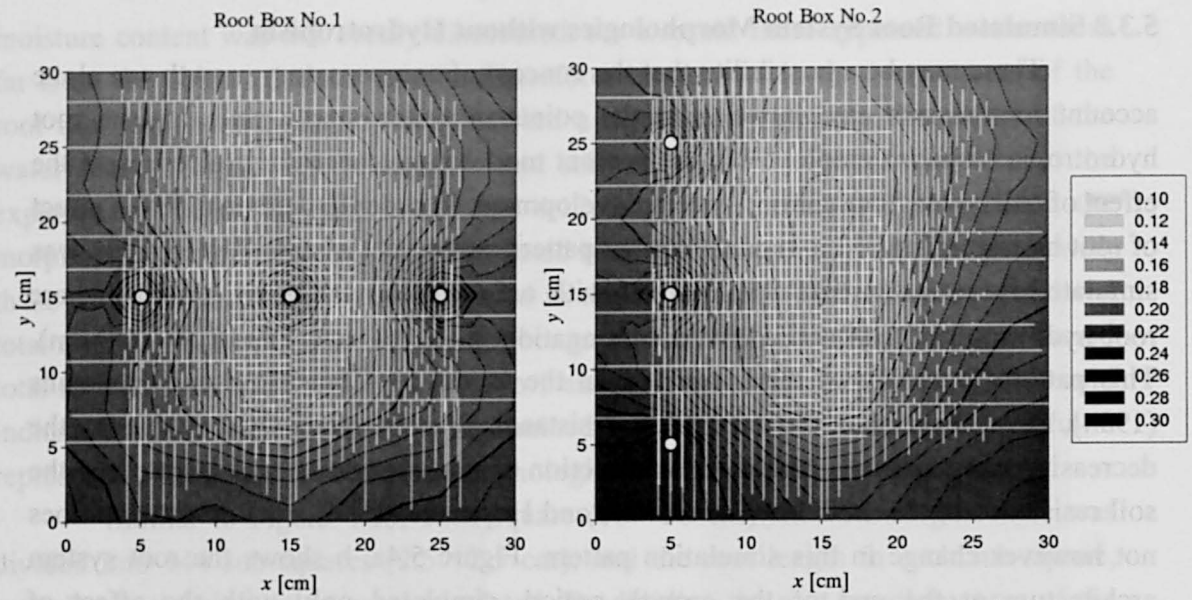

Figure 5.4 Root system architectures and distributions of soil water content in the root box a) No.1, and b) No.2, simulated without the effect of hydrotropism.

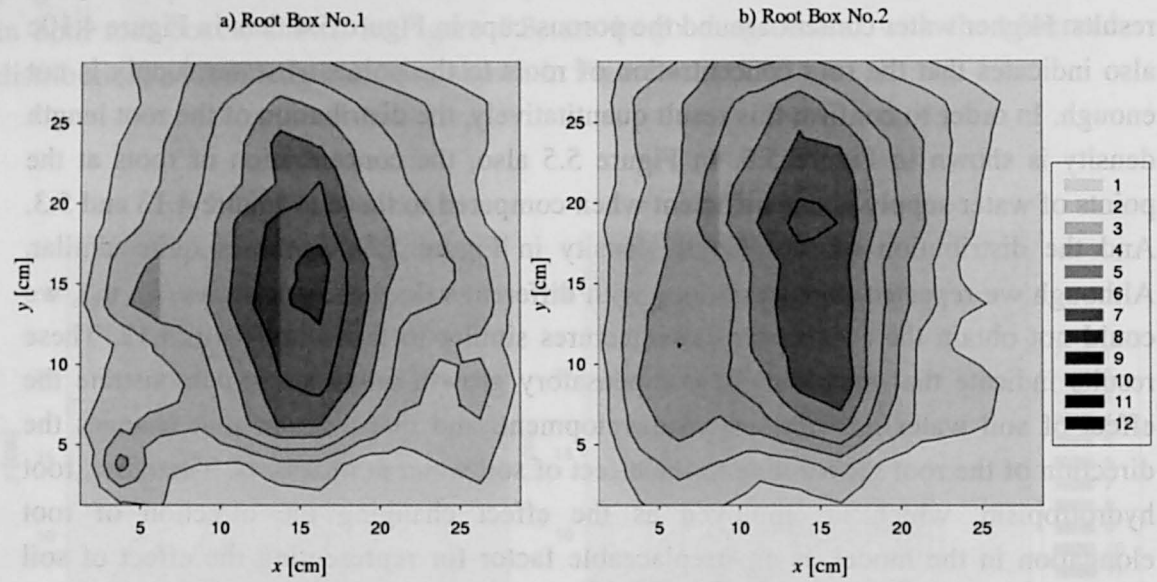

Figure 5.5 Distributions of root length density [cm/cm^2] in the root box a) No.1 and b) No.2, simulated without the effect of hydrotropism.

the changes in distribution of the soil water content (Figure 5.2) are also in good agreement with those obtained by TDR measurements in the experiment (Figure 4.10). These results confirm that the combined model of root system development and soil water flow used in this study successfully simulated root system development under different environmental soil water conditions, and that hydrotropism and the

compensatory growth of roots are the dominant factors in root system development under a reduced effect of gravity.

5.4 CONCLUSION

In the previous chapter, it was clarified that root system development was controlled by the soil water flow, through the plant root system growth experiment under a reduced effect of gravity, i.e. the roots tend to grow towards the direction of the water supply and concentrate in areas around the points of water supply. These effects of the soil water conditions on root system development seem to be caused by hydrotropism and the compensatory growth of roots. In this chapter, the two-dimensional model considering both root hydrotropism and the compensatory growth successfully simulated the root system development and soil water flow. Because the observed and simulated root system morphological architectures, and the measured and simulated changes of the distribution of soil water content were in good agreements quantitatively, the hypothesis that root hydrotropism is the dominant factor in root system development in the case of reduced effect of gravity, was confirmed. Also, the importance of root compensatory growth in root system development was suggested by the observations and simulations of the root system development in the root boxes. It was confirmed that compensatory growth alone, however, cannot account for the root concentration to the points of water supply seen in the experiment.

The combined model of root system development and soil water flow considering root hydrotropism and compensatory growth used in this study can simulate and predict the root system development under various soil water conditions. The model can be applied to design and control root system architecture under the influence of drip irrigation. Furthermore, the model can provide important information on how to control root system development under no gravity conditions, i.e. plant growth in a space station.

In this chapter, a two-dimensional model was used to simulate the root system development and soil water flow, because the root box experiment may be regarded as two-dimensional. However, it is necessary to extend the model into a three-dimensional form, in order to simulate practical root system development under field conditions. In the next chapter, a three-dimensional root system development model considering root hydrotropism will be developed.

REFERENCES

Clausnitzer V. and Hopmans J.W. 1994 Simultaneous modeling of transient three-dimensional root growth and soil water flow. Plant and Soil 164, 299-314

Diggle A. J. 1988 ROOTMAP －a model in three-dimensional coordinates of the growth and structure of fibrous root systems. Plant and Soil 105, 169-178

Herkelrath W.N., Miller E.E. and Gardner W.R. 1977a Water uptake by Plants: I. Divided root experiments. Soil sci. soc. Am. J. 41, 1033-1038

Herkelrath W.N., Miller E.E. and Gardner W.R. 1977b Water uptake by Plants: II. The root contact model. Soil sci. soc. Am. J. 41, 1039-1043

Ishikawa H., Hasenstein K.H. and Evans M.L. 1991 Computer-based video digitizer analysis of surface extension in maize roots. Planta 183, 381-390

Istoke J. 1989 Grandwater modeling by the finite element method. American Geophysical Union, Washington, DC, USA

Jourdan C. and Rey H. 1997 Modeling and simulation of the architecture and development of the oil-palm (Elaeis guineensis Jacq.) root system I. The model. Plant and Soil 190, 217-233

Kanda M. and Hino M. 1990 Numerical simulation of soil-plant-air system (1) modeling of plant system. J. Jpn Soc. Hydrology and water Resources 3, 37-46

Kosugi K. 1996 Lognormal distribution model for unsaturated soil hydraulic properties. Water Resour. Res.32, 2697-2703

Lynch J.P., Nielsen K.L., Davis R.D. and Jablokow A.G. 1997 SimRoot: Modelling and visualization of root systems. Plant and Soil 188, 139-151

Pages L., Jordan M.O. and Picard D. 1989 A simulation model of the three-dimensional architecture of the maize root system. Plant and Soil 119, 147-154

Shibusawa S. 1994 Modelling the Branching Growth Fractal Pattern of the Maize Root System Plant and Soil 165, 339-347

Somma F., Hopmans J.W. and Clausnitzer V. 1998 Transient three-dimensional modeling of soil water and solute transport with simultaneous root growth, root water and nutrient uptake. Plant and Soil 202, 281-293

Takahashi H. 1994 Hydrotropism and its interaction with gravitropism in roots. Plant and Soil 165, 301-308

Tsutsumi D., Kosugi K. and Mizuyama T. 2001 Application of root system development model assuming the tropisms for seedling in Japanese red pine (Pinus densiflora) J. Jpn. Soc. Reveget. Tech. 26(4), 309-319 (in Japanese with English summery)

Tsutsumi D., Kosugi K. and Mizuyama T. 2003 Root system development and water extraction model considering hydrotropism. Soil Sci. Soc. Am. J. (in press)

Zienkiewicz O.C. 1971 The finite element method in engineering science. McGraw-Hill, Berkshire, England.

CHAPTER 6

A THREE-DIMENSIONAL ROOT SYSTEM DEVELOPMENT MODEL CONSIDERING HYDROTROPISM, AND ITS APPLICATION TO ACTUAL PLANTS ON A SLOPE

6.1 INTRODUCTION

Mathematical modeling of a plant root system development is useful for understanding mechanisms of development, morphological architecture and physiological functions of root systems. In Chapter 3, a two-dimensional model for root system development and water extraction was proposed employing not only the gravitropism, but also the hydrotropism using the differential growth method, and it was reported that hydrotropism is a dominant factor in root system development both on a plane and on a slope (Tsutsumi et al., 2003). In Chapter 5, the model was applied to the results obtained by the root box experiments presented in Chapter 4, and the hypothesis that root hydrotropism is a dominant factor in establishment of a root system was confirmed (Tsutsumi et al., 2002). However, except for the special condition such as a root box experiment in which the root system development may be regarded as two-dimensional, a plant root system develops spatially in a three-dimensional soil domain. Therefore, in order to simulate the actual plant root system developments on natural slopes, it is necessary to extent the model to a three-dimensional form. As we reviewed the previously proposed root system development models in Chapter 2, almost all models were described three-dimensionally (Clausnitzer and Hopmans, 1994; Diggle, 1988; Doussan et al., 2001; Dunbabin et al., 2001; Pages et al., 1989; Somma et al., 1998; Zhenyang et al., 2000). In this chapter, the root system development model will be extended to a three-dimensional form, that can be applied to actual plant root system development and soil water flow both on a plane and slope. In this model, gravitropism, hydrotropism, and circumnutation, that is also thought to be an important factor of determining the elongating direction as well as root tropisms (Hirota, 2001; Inoue et al., 1993; Johnsson et al., 1997; Shimotashiro et al., 1998a, b), are employed as the main factors of root elongation.

Before the model simulation, actual plant root systems that grew on a natural slope were excavated and examined, in order to observe the architecture of the root system, and to obtain the morphological characteristics, i.e. elongation rate, maximum

branching order, and branching intervals. The observations were carried out in an experimental field in the southern part of China, where the weather conditions i.e. temperature and rain fall intensity, had been continuously monitored. In addition to the root system observation, soil samples were taken to measure the soil hydraulic properties, which will be used in the model simulation. The development of the observed root systems will be simulated by the model, and the outputs from the model will be compared with the observed root systems, in order to examine the model hypothesis.

Figure 6.1 View of Dahou Experimental Field, where the root systems were observed and sampled. The vegetation is relatively poor, with the dominant tree species, pine (*Pinus massoniana*).

6.2 FIELD OBSERVATION

Actual plant root systems grown on the natural fields were observed and examined to measure their morphological characteristics (i.e. branching intervals and averaged elongation rates). The measured morphological characteristics of the actual

Table 6.1 Geographical characteristics of the slopes, and the characteristics of the plant.

Slope Characteristics	[unit]		Slope No.1	Slope No.2
Slope angle	[degree]		31.0	37.0
Slope direction	[-]		southeast	east
Soil layer thickness	[cm]		25.0	53.0
Soil strength*	[mm]	(Surface)	26.1	21.4
		(Bottom)	25.5	21.5
Plant Characteristics				
Plant age	[year]		2	2
Plant height	[cm]		18.0	15.5
Shoot weight	[g]		11.7	7.3
Root weight	[g]		7.0	5.5
Total weight	[g]		18.7	12.8

* Soil strengths were measured by Yamanaka's penetrometer.

root systems were used as the model parameters. The development of the observed plant root systems are then simulated, and their morphological architectures compared to those of the observed plant root systems. Through these processes, validity of the present model and the mechanisms of root system development considered in the model are examined.

The root system observations and measurements were carried out in the Dahou Experimental Fields located in JianXi Province, China (115° 28'E, 26° 30'N). The soil type of the experimental fields is a weathered granite. The soil surface on slope is heavily eroded, and the soil layer is thin. Vegetation is relatively poor, with pine tree (*Pinus massoniana*) as the dominant species. The mean annual precipitation was in a range of 1485.9 to 1953.6 mm from 1994 to 2001. The mean air temperature was 17.5℃, with a highest monthly mean temperature of 27.8℃, and a lowest of 5.9℃. The altitude of the fields ranged from 340 to 420 m and the slope angles ranged from15 to 40° (Kimoto et al., 2000). Under such bared slope conditions, the plant root system morphologies have a meaningful effect of preventing erosion and landslides. Figure 6.1 shows the view of the Dahou Experimental Field.

Two-year-old pine trees close to the ridge of two slopes (slope No.1, and No.2) were chosen for root system observation and measurement. The root systems were excavated from the soil, and the soil around the root systems was carefully removed so as not to disturb the shape of the root systems. Photos of the bared root systems were taken to record their morphological architectures. Then the characteristics of the root architecture, i.e. branching intervals and root lengths by root branching orders, and maximum branching order, were measured. The soils were sampled at surface and bottom of the soil layer in order to obtain the hydrological

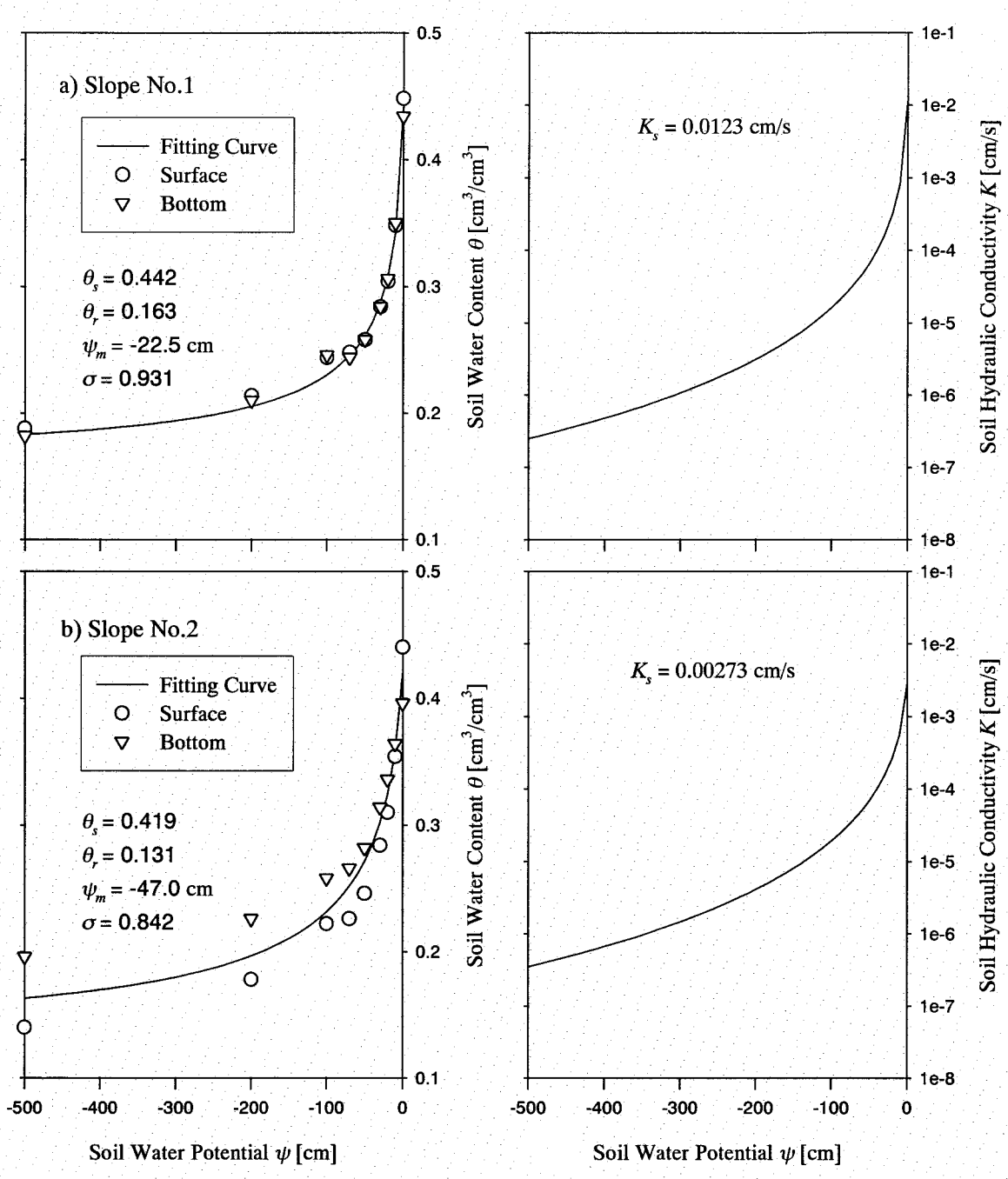

Figure 6.2 Hydraulic properties of soil; θ-ψ, K-ψ curve for the soils of slope a) No.1, and b) No.2.

characteristics of the soil. The geographical characteristics of the slopes, and the common characteristics of the plants are listed in Table 6.1. The observed retention curve of the soil is shown in Figure 6.2, together with soil hydraulic conductivity represented by the lognormal model proposed by Kosugi (1996). The parameters of the lognormal model were determined based upon the observed retention curve, and are

shown in Figure 6.2.

6.3 MODEL DESCRIPTION

The root system development model described in this chapter basically follows the two-dimensional model previously presented in Chapter 3 and 5, but was extended to a three-dimensional form. The model is outlined hereafter.

6.3.1 Root Elongation (Differential Growth Method)

Similar to the two-dimensional root elongation previously shown in Chapter 3, three-dimensional root tropism is also caused by the difference in elongation rates ER_{max}, ER_{min} [cm/s], at elongation points P_1 and P_2, which are located opposite each other (see Figure 6.3). The part of the three-dimensional root elongation model that is obviously different from that of the two-dimensional is that it is necessary to find out the points where the elongation rate has the maximum and minimum values, ER_{max}, ER_{min}, around a root sectional circle. After the points where the elongation rate ER_{max} and ER_{min} are determined, the behavior of root tropism can be obtained in the same way as the two-dimensional model. Here, the radius r [cm] and the angle α [rad] within the time Δt [s] can be obtained as follows,

$$r = \left| \frac{ER_{max} + ER_{min}}{ER_{max} - ER_{min}} \right| \frac{d}{2} \tag{6.1}$$

$$\alpha = \frac{\left| ER_{max} - ER_{min} \right|}{d} \Delta t \tag{6.2}$$

where, d [cm] is the diameter of the root at the elongation point. Also, the elongation rate at the center of the root, ER_c [cm/s], can be obtained as follows,

$$ER_c = \frac{ER_{max} + ER_{min}}{2} \tag{6.3}$$

From Figure 6.3 and Equation (6.1), (6.2), and (6.3), it is found that the behavior of the tropism is determined by the elongation rate ER at the each elongation points. To determine the tropism, it is necessary to describe the elongation rate as a function of the tropism factors. Because gravitropism, hydrotropism and circumnutation are dealt with, the elongation rate functions of gravitropism, hydrotropism and circumnutation are written as ER_g [cm/s], ER_h [cm/s] and ER_n [cm/s] respectively, and the summed elongation rate around the sectional circle across the elongation zone of root ER_s [cm/s] is written as,

$$ER_s = ER_g + ER_h + ER_n \tag{6.4}$$

For the extension of the model description into the three-dimensional form,

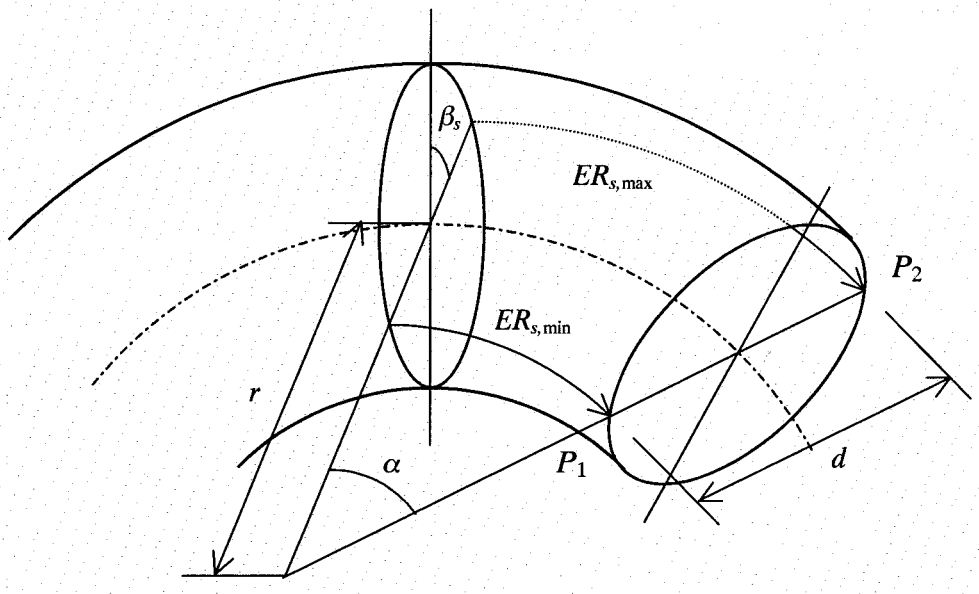

Figure6.3 Schematic figure showing the differential growth in three-dimensional root elongation. The root elongation rate has the minimum and maximum values at the point P_1 and P_2, respectively.

ER_s must be expressed as follows,

$$ER_s(\beta) = \frac{(ER_{s,\max} - ER_{s,\min})\cos(\beta - \beta_s) + ER_{s,\max} + ER_{s,\min}}{2} \tag{6.5}$$

where, $ER_{s,\max}$ and $ER_{s,\min}$ are the maximum and minimum values of ER_s, β [rad] is the angle around the root sectional circle from the top point of the circle, and when $\beta = \beta_s$, $\beta_s+\pi$, ER_s has a maximum value of $ER_{s,\max}$ and a minimum value of $ER_{s,\min}$, respectively (See Fig.6.3). The elongation rate of each factor around the sectional circle ER_i ($i = g, h, n$) is expressed by the following equation similar to Equation (6.5),

$$ER_i(\beta) = \frac{(ER_{i,\max} - ER_{i,\min})\cos(\beta - \beta_i) + ER_{i,\max} + ER_{i,\min}}{2} \tag{6.6}$$

where, $ER_{i,\max}$ and $ER_{i,\min}$ are the maximum and minimum values of ER_i. When $\beta = \beta_i$, $\beta_i+\pi$, ER_i has a maximum value of $ER_{i,\max}$ and a minimum value of $ER_{i,\min}$, respectively. From Equation (6.4) through (6.6), β_s, $ER_{s,\max}$ and $ER_{s,\min}$ are obtained as follows,

$$ER_{s,\max} = \frac{S_1 + (S_2^2 + S_3^2)^{1/2}}{2} \tag{6.7}$$

$$ER_{s,\min} = \frac{S_1 - \left(S_2{}^2 + S_3{}^2\right)^{1/2}}{2} \tag{6.8}$$

$$\beta_s = S_2\left(S_2{}^2 + S_3{}^2\right)^{-1/2} \qquad 0 \leqq S_3 \tag{6.9a}$$

$$\beta_s = 2\pi - S_2\left(S_2{}^2 + S_3{}^2\right)^{-1/2} \qquad S_3 < 0 \tag{6.9b}$$

where,

$$S_1 = \sum_i \left(ER_{i,\max} + ER_{i,\min}\right) \tag{6.10}$$

$$S_2 = \sum_i \left(ER_{i,\max} - ER_{i,\min}\right)\cos\beta_i \tag{6.11}$$

$$S_3 = \sum_i \left(ER_{i,\max} - ER_{i,\min}\right)\sin\beta_i \tag{6.12}$$

From these values of β_s, $ER_{s,\max}$ and $ER_{s,\min}$, three-dimensional trajectory of the root tip can be obtained similar to the two-dimensional. The next step is to define the elongation rate function of each factor ER_i.

Similar to Equation (3.5) to (3.8), the maximum and minimum elongation rate functions of gravitropism are defined as follows,

$$ER_{g,\max} = ER_{g,0} + \Delta ER_g \sin\gamma \qquad 0 \leqq \gamma \leqq \pi/2 \tag{6.13a}$$

$$ER_{g,\max} = ER_{g,0} + \Delta ER_g \qquad \pi/2 < \gamma \leqq \pi \tag{6.13b}$$

$$ER_{g,\min} = ER_{g,0} - \Delta ER_g \sin\gamma \qquad 0 \leqq \gamma \leqq \pi/2 \tag{6.14a}$$

$$ER_{g,\min} = ER_{g,0} - \Delta ER_g \qquad \pi/2 < \gamma \leqq \pi \tag{6.14b}$$

$$\beta_g = 0 \tag{6.15}$$

where, γ [rad] is the angle between the direction of gravity and the root's orientation, $ER_{g,0}$ [cm/s] gives the value of the gravitropic elongation rate when the root is directed towards gravity ($\gamma = 0$), and ΔER_g [cm/s] is the constant that determines the intensity of gravitropism.

Similar to Equation (3.9) and (3.10), the minimum and maximum elongation rate function of hydrotropism on the wet side and dry sides are defined as follows,

Wet side;

$$ER_{h,\min} = ER_{h,0} - k_h\left|q'\right| \tag{6.16}$$

Dry side;

$$ER_{h,\max} = ER_{h,0} + k_h|q'| \tag{6.17}$$

$$\beta_h = \beta_h(q') \tag{6.18}$$

where, $|q'|$ [cm/s] is the magnitude of the component of water flux q [cm/s], perpendicular to the root at the root cap, $ER_{h,0}$ [cm/s] gives the value of the hydrotropic elongation rate when $|q'|= 0$, condition β_h correspond to the direction of q' that across the center of the sectional circle of the root. In this chapter, k_h is assumed to be a decreasing function of the soil water potential ψ [cm] at the root tip, similar to that found in Chapter 5. Function k_h is defined as follows,

$$k_h = a_h\left[\exp(-b_h\psi)-1.0\right] \tag{6.19}$$

where, a_h (>0) [-] and b_h (>0) [cm^{-1}] are constants, which determined the intensity of root hydrotropism. In Chapter 5, k_h is defined as the liner function of soil water potential ψ in Equation (5.3) and (5.4). The function which is defined here in Equation (6.19) has a form similar to those of Equation (5.3) and (5.4), but changes continuously according to the changes of soil water potential ψ.

Circumnutation is the regular, helical growth movement of plant organs such as shoots, roots and tendrils around a preferred growth direction (Darwin, 1880). Root circumnutation was confirmed by experiments (Shimotashiro et al., 1998a, b; Hirota, 2001), and is thought to be an important factor in determining the root elongation direction as well as root tropisms (Inuoe et al., 1993). There are two main types of models describing plant circumnutation, one is the "internal oscillator model", in which gravity plays no role in the generation of circumnutations, and the other is the "gravitropic overshoot model", in which the gravitropic reactions play a central role in the generation of circumnutation (Johnsson, 1997; Lubkin, 1994). In this study, former type of model was employed, which should be able to describe patterns on a ring structure in a transverse section of the circumnutating plane as rotating wave patterns, as follows,

$$ER_{n,\max} = ER_{n,0} + \Delta ER_n \tag{6.20a}$$

$$ER_{n,\min} = ER_{n,0} - \Delta ER_n \tag{6.20b}$$

$$\beta_n = \omega_n \Delta t \tag{6.21}$$

where, $ER_{n,0}$ [cm/s] gives the value of the elongation rate of circumnutation when the intensity of circumnutation is zero, ΔER_n [cm/s] gives the intensity of circumnutation, and ω_n [rad/s] is the angular velocity of circumnutation. Through these definitions, the root shows a regular, helical growth movement. As we can see that ER_n is the functions of time only, the circumnutation is the movement independent of the surrounding

environments, even though gravitropism and hydrotropism depend on gravity and soil water flow, respectively.

From the definitions of the root elongation rate as shown above, Equation (6.3), the elongation rate at the center of the root, is redefined as follows,

$$ER_c = ER_{g,0} + ER_{h,0} + ER_{n,0} \tag{6.22}$$

According to Equation (6.22), the elongation rate at the center of the root does not vary according to the value of ΔER_g, k_h and ΔER_n. In the simulations, only the value of ER_c is given, instead of giving independent values for $ER_{g,0}$, $ER_{h,0}$ and $ER_{n,0}$.

6.3.2 Root Branching

Root branching is as important as root elongation in root system development. According to the classification of the actually observed plant root system, the root system under consideration is regarded as a main root system, a main root with less than third order lateral roots. For simplicity, a constant branching interval is assumed. It is also assumed that the branching direction is not affected by the surrounding environment, i.e. the lateral roots branch toward every direction uniformly. The details of the branching parameters are in accordance with the model proposed by Pages (Pages et al., 1989), and are described in Chapter 3.

6.4 METHOD FOR SIMULATION

6.4.1 Soil Water Flow

To combine root system development and soil water extraction by the root system, and to obtain the soil water flux in Equation (6.16) and (6.17), soil water flow in the considered soil domain is numerically calculated. The soil water flow can be calculated according to the following equation;

$$C_p(\psi)\frac{\partial \psi}{\partial t} = \frac{\partial}{\partial x}\left\{K(\psi)\left(\frac{\partial \psi}{\partial x}\right)\right\} + \frac{\partial}{\partial y}\left\{K(\psi)\left(\frac{\partial \psi}{\partial y}\right)\right\} + \frac{\partial}{\partial z}\left\{K(\psi)\left(\frac{\partial \psi}{\partial z}+1\right)\right\} - S \tag{6.23}$$

Equation (6.23) is the three-dimensional description of the Richards' equation based on water potential ψ, where z [cm] is positive upwardly, t [s] is the time, $C_p(\psi)$ [cm^{-1}] is the soil water capacity and $K(\psi)$ [cm/s] is the hydraulic conductivity. In order to represent $C_p(\psi)$ and $K(\psi)$, the lognormal model proposed by Kosugi (1996) shown as Equation (3.15), (3.16) and (3.17) in Chapter 3 was also employed. S [s^{-1}] is the water extraction intensity by the root system. Equation (6.23) was solved numerically by the partially implicit finite element method (Zienkiewicz, 1971; Istoke, 1989).

6.4.2 Evaporation, Transpiration and Rainfall

Potential rate of evapotroanspiration was estimated by an empirical method proposed by Thornthwaite (Thornthwaite, 1948), which consists of a set of equations

as follows,

$$E_t = 1.6\left(\frac{10T_i}{I}\right)^{a_t} / 30 \tag{6.24}$$

where, E_t [cm/s] is the potential rate of evapotranspiration, T_i [℃] is the monthly mean temperature, I [℃] and a_t [-] are functions represented as follows,

$$I = \sum_{i=1}^{12}\left(\frac{T_i}{5}\right)^{1.514} \tag{6.25}$$

$$a_t = \left(492390 + 17920I - 77.1I^2 + 0.675I^3\right)\cdot 10^{-6} \tag{6.26}$$

The actual measured temperatures were used for estimating potential rate of the evapotranspiration E_t from the sloped soil surface in the experimental field. The estimated value of potential evapotranspiration was divided into potential evaporation E_p [cm/day] and potential transpiration T_p [cm/day] by ratios R_E [-], 1- R_E [-]. Because the potential transpiration rate changes with plant growth, a linearly increasing function of time $r_T(t)$ [-] is multiplied, to give the potential transpiration T_p. Then they are distributed into E_p' [cm/s] and T_p' [cm/s] according to sine curves, similar to the assumption in Chapter3 and 5. E_p' and T_p' in daytime, therefore, are described as follows,

$$E_p' = \frac{E_T \cdot R_E}{24\times 3600}\sin\pi\left(\frac{t - 6\times 3600}{12\times 3600}\right) \tag{6.27}$$

$$T_p' = \frac{E_T(1-R_E)\cdot r_T(t)}{24\times 3600}\sin\pi\left(\frac{t - 6\times 3600}{12\times 3600}\right) \tag{6.28}$$

where, R_E is assumed to be 0.75 in the simulation, and

$$r_T(t) = \frac{t}{t_{\max}} \tag{6.29}$$

where, $t_{\max}$ [s] represents the plant growth period. In nighttime, E_p' and T_p' become zero.

Actual evaporation E_a [cm/s] is calculated as follows,

$$E_a = \alpha_E(\theta)E_p' \tag{6.30}$$

where, $\alpha_E(\theta)$ is a function of water content θ on the soil surface, defined as follows,

$$\alpha_E(\theta) = 1.0 \qquad \theta_1 \leqq \theta \tag{6.31a}$$

$$\alpha_E(\theta) = \frac{\theta - \theta_2}{\theta_1 - \theta_2} \qquad \theta_2 \leqq \theta < \theta_1 \tag{6.31b}$$

$$\alpha_E(\theta) = 0.0 \qquad \theta < \theta_2 \tag{6.31c}$$

where, θ_1 and θ_2 are the threshold values of the soil water content, and assumed θ_1 = 0.20 and $\theta_2 = \theta_r$. On the other hand, potential transpiration T_p' [cm/s] is divided into potential water extraction intensity S_p [s^{-1}] from each finite element according to the model of Herkelrath (Herkelrath et al., 1977a, b; Kanda and Hino, 1990) as follows,

$$S_{p,n} = -\left(\frac{\theta - \theta_r}{\theta_s}\right)^b \rho \Delta\psi L \tag{6.32}$$

$$\Delta\psi = \psi_c + (R_c + 1)l - \psi \tag{6.33}$$

where, n is the element number, θ [cm^3/cm^3] is the soil water content at the root surface, ρ [cm/s] is the water penetration coefficient of the root, b [-] is a correction parameter, $\Delta\psi$ [cm] is the difference in water potential between the root and the soil, L [cm/cm^3] is the root length density, ψ_c [cm] is the water potential at the beginning point of the main root, l [cm] is the distance from the beginning point of the main root to the root and R_c [-] is a correction coefficient for the friction loss of water transport in the root. For the simulations, $\rho = 2 \times 10^{-10}$ cm/s, $b = 1$, $R_c = 0.05$ were assumed according to Herkelrath et al. (1977a, b) and Momii et al. (1992). L was calculated as the root length within the element divided by the volume of the element, l was calculated as the distance from the beginning point of the main root to the center of the element, θ and ψ in Equation (6.32) and (6.33) were obtained by averaging the values at the 4 nodes of the element, which is shown in the following subsection. Because roots in actual plant root systems extract water actively at the absorption zone near the root tip, the lengths of the main and first order lateral roots older than 90 days were excluded from L. The potential transpiration T_p' given as a function of time is related to $S_{p,n}$ by

$$T_p' = \sum_n V_n \cdot S_{p,n} \tag{6.34}$$

where V_n [cm^3] is the volume of the element n. The substitution of Equation (6.32) and (6.33) into Equation (6.34) gives the value for ψ_c [cm]. Then, the derived ψ_c along with Equation (6.32) and (6.33) gives the value of $S_{p,n}$. In Chapter 3 and 5, where the actual transpiration is given as a function of time, the value of $S_{p,n}$ obtained from previous equations could be used as the actual water extraction intensity. In this chapter, however, the transpiration rate is given as a potential value estimated from the empirical method. Therefore, it is necessary to introduce another model estimating the actual water extraction intensity S_a [s^{-1}]. The actual water extraction intensity was

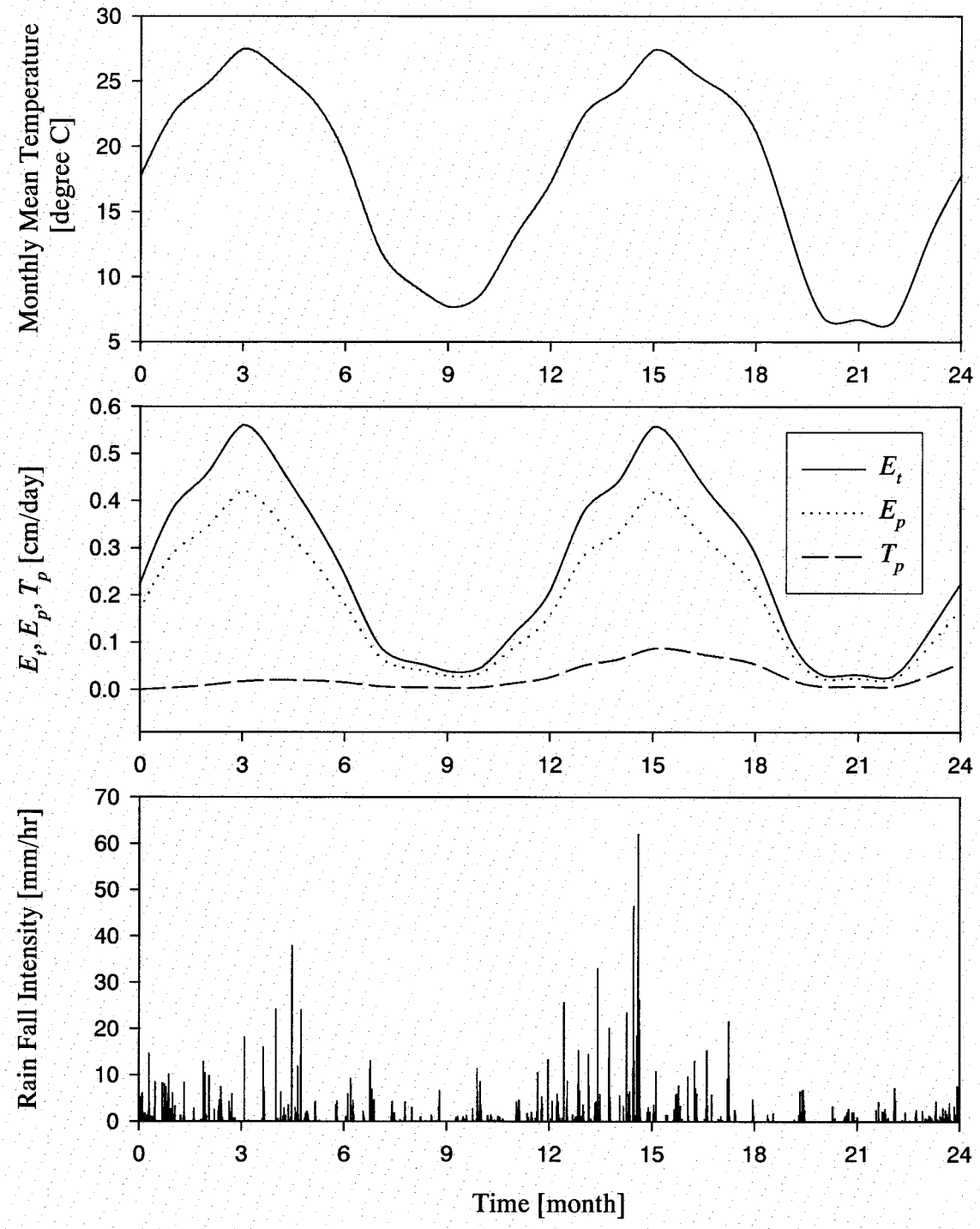

Figure6.4 Weather conditions used in the simulation.

estimated according to the model of Feddes (Feddes et al., 1978), as follows,

$$S_{a,n} = \alpha_T(\psi) S_{p,n} \tag{6.35}$$

where, ψ is the soil water potential at the root surface which is obtained by averaging the values at the 4 nodes of the element, $\alpha_T(\psi)$ is the water extraction function represented as follows,

$$\alpha_T(\psi) = \frac{\psi}{\psi_1} \qquad \psi_1 \leqq \psi < 0 \tag{6.36a}$$

$$\alpha_T(\psi) = 1.0 \qquad \psi_2 \leqq \psi < \psi_1 \tag{6.36b}$$

$$\alpha_T(\psi) = \frac{(\psi_3 - \psi)}{(\psi_3 - \psi_2)} \qquad \psi_3 \leqq \psi < \psi_2 \tag{6.36c}$$

$$\alpha_T(\psi) = 0.0 \qquad \psi < \psi_3 \tag{6.36d}$$

For the simulation, $\psi_1 = -30$, $\psi_2 = -500$, $\psi_3 = -20000$ cm are assumed according to the suggested values by Feddes et al. (1978).

For the soil surface, the rainfall intensity data, actually measured in the experimental field, were applied. Figure 6.4 shows the changes in temperature, the estimated potential evaporation E_p, potential transpiration T_p and rainfall intensity during the plant growth period, from April 2000 to March 2002.

6.4.3 Finite Element Grids of Sloped Domain, Boundary and Initial Conditions

Figure 6.5 shows a studied soil domain divided by grids for the finite element method calculations. For slope No.1 (L_x, L_y, L_z) are set (700, 50, 25) cm, and for slope No.2 (700, 50, 53) cm. Each parallelepiped domain is divided into 6 tetrahedral finite elements as shown in Figure 6.6. No-flux boundary condition for the bottom, upstream-end, and side boundaries of the sloped soil domain was imposed. The evaporation and rainfall, previously defined, are applied to the surface boundary. It was assumed that the soil water potential distributes parallel to the slope close to the downstream-end, if the slope is long enough when compared with the soil depth. Therefore, as the boundary condition on the downstream-end, the water potential values of nodes on the boundary are assumed to be equal to those of the nodes next to them in the upper direction. Simulation is carried out for three root system developments, upper, middle and lower, on the same slope, in order to examine the generality of root system development on a slope. As shown in Figure 6.5, the soil domain around the root systems is divided into small grids in x-direction, in order to obtain the detailed soil water flow around the root systems.

As an initial condition of soil water distribution, the water potential is assumed to distribute parallel to the slope. However, this condition little affects the soil water flow and the root system development, because the soil water distribution and soil water flow became identical once rainfall is applied to the soil surface.

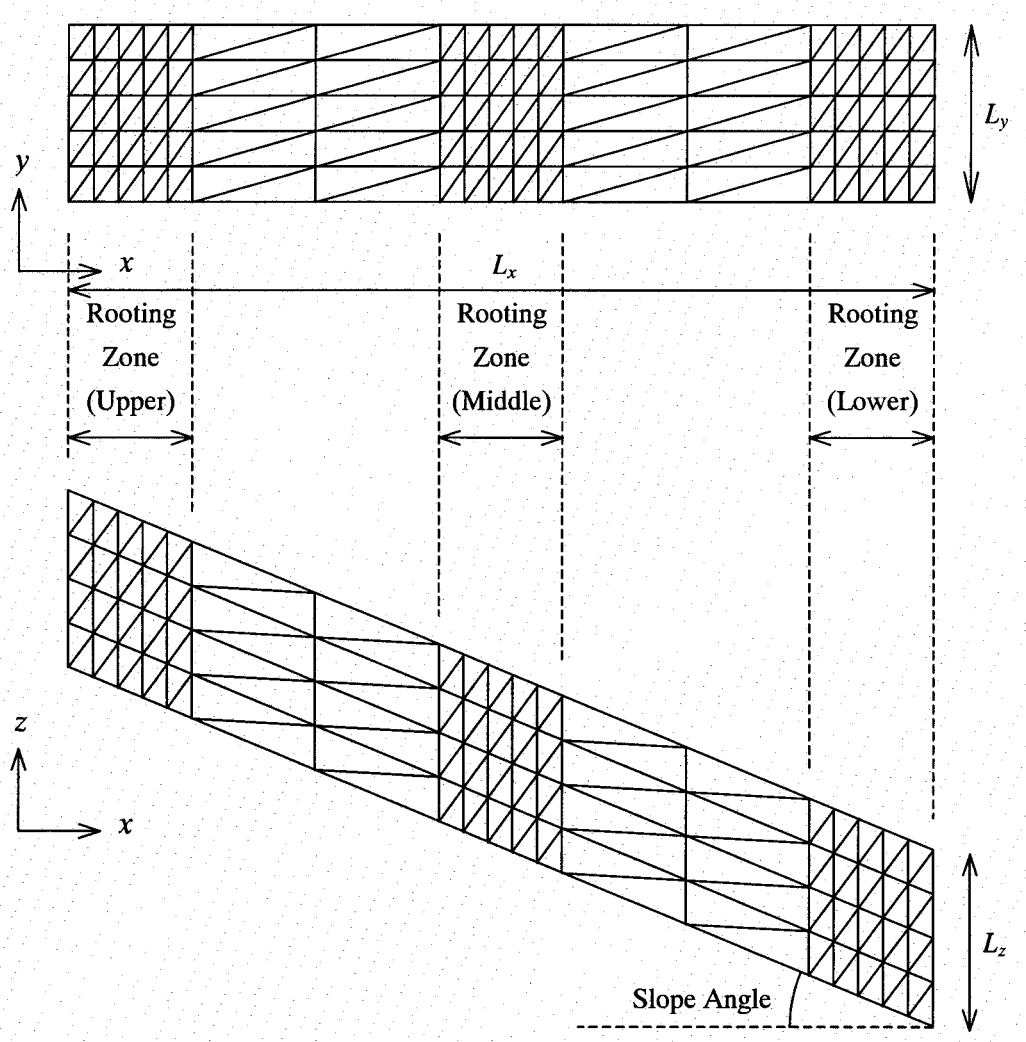

Figure 6.5 Considered soil domain, divided by the finite element grid.

6.4.4 Parameters for Simulation

In Table 6.2, the parameters of root development are listed. Based on the observation and measurement of the root systems shown in section 6.2, the root elongation rates ER_c were determined. According to the definition in Chapter 3 and 5, the elongation rate of the main root is assumed to be changing during the growth period; the elongation rate of the main root was defined as a function of time (see Table 6.2). d, ΔER_g, a_h, b_h, ΔER_n and ω_n were determined by trial and error calculations, so that the model would simulate root systems similar to actual root systems. Branching parameters, i.e., apical non-branching zone L_a [cm], basal non-branched zone L_b [cm], branching interval I_b [cm], and insertion angle ϕ_i [degree] (see Chapter 3) were obtained based on the measurement of the actual root systems.

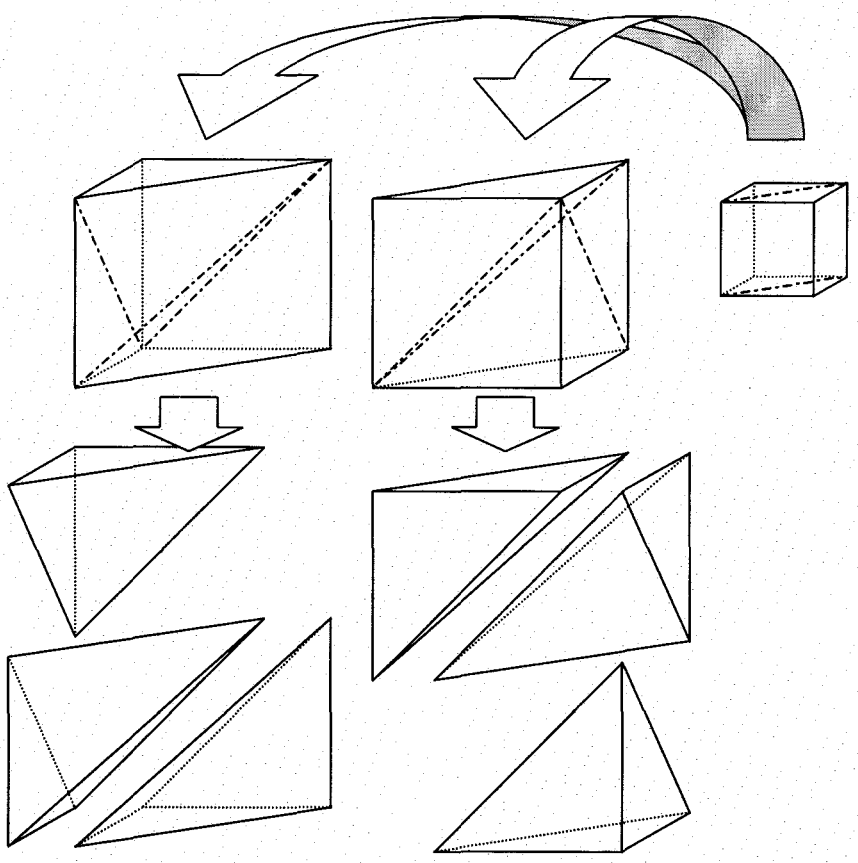

Figure 6.6 Parallelepiped domain and 6 divided tetrahedral finite elements.

6.5 RESULTS AND DISCUSSION

6.5.1 Observed Actual Plant Root Systems

The photographs of the root system architectures were transformed into binary images by using an image analyzing software (Scion Image, Scion Co., U.S.A.). In Figure 6.7 and 6.8, the observed morphological architectures of the actual plant root systems on slope No.1 and No.2 are shown. These figures show the projected architecture of root systems onto the *x-z* plane. In Figure 6.7, the roots are distributed shallowly in the thin soil layer, and the main root elongation is restrained. The lateral roots up-slope of the main root elongated toward the upper direction, and the lateral roots down-slope of the main root elongated toward the lower direction. In Figure 6.8, the main root grew longer than that found on the slope No.1, because of the deeper soil layer. However, the rest of the root system distributed shallowly. The lateral roots up-slope of the main root elongated toward the upper direction, and the lateral roots down-slope of the main root elongated toward the lower direction, similar to those found on slope No.1. In both figures, the root systems show asymmetric architectures,

Table 6.2 Parameters for the simulations.

Parameters	[unit]	main root	1st order lateral root	2nd order lateral root
Root Elongation				
d	[cm]	0.12	0.06	0.04
ER_c	[cm/day]	$C_1 \cdot ER_c(t)$*1	$5.5*10^{-2}$	$8.4*10^{-3}$
$\Delta ER_g / ER_c$	[-]	0.1	0.001	0.001
a_h	[-]	2.5	2.5	2.5
b_h	[cm^{-1}]	0.0011	0.0011	0.0011
$\Delta ER_n / ER_c$	[cm/s]	0.01	0.01	0.01
ω_n	[rad/hr]	0.01	0.01	0.01
Root Branching				
L_b	[cm]	–	2.19	1.66
L_a	[cm]	–	10*2, 30*3	1.66
I_b	[cm]	–	2.19	1.66
ϕ_i	[degree]	–	90	90

*1; $ER_c(t) = 0.01 t_{max} \cdot \exp(-0.01t)/(1.0 - \exp(-0.01 t_{max}))$

, $C_1 = 0.0416$ (Slope No.1), 0.0832 (Slope No.2)

*2; Slope No.1

*3; Slope No.2

which have been presented in Chapter 3, previously. In Figure 6.8, the notable characteristic of the root elongation is presented as a circumnutation. The main root especially shows a regular, helical trajectory of root elongation. The range of its helical movement is much larger than the size of soil particles. Therefore, it is obvious that this behavior of main root elongation was not due to the mechanical restriction of the soil particles.

6.5.2 Simulated Soil Water Flows on Slopes

In order to simulate the actual plant root system growth that was observed on the slope, two years of simulation of root system development and soil water flow, from April 2000 to March 2002, were carried out.

In Figure 6.9, 6.10, changes of the distributions of soil water potential ψ on slope No.1 and No.2 are shown, simulated by the model. The distributions in Figure 6.9a, 6.10a are in an x-z plane in the middle of the soil domain (y = 25 cm), and those in Figures 6.9b, 6.10b are in a plane parallel to the slope in the middle of the soil layer. In all figures, a few common tendencies can be seen. In spite of the greater amount of rainfall during the summer seasons (see Figure 6.4), the soil tends to be dry due to the higher evapotranspiration, and inversely tends to be wet during the winter season. The

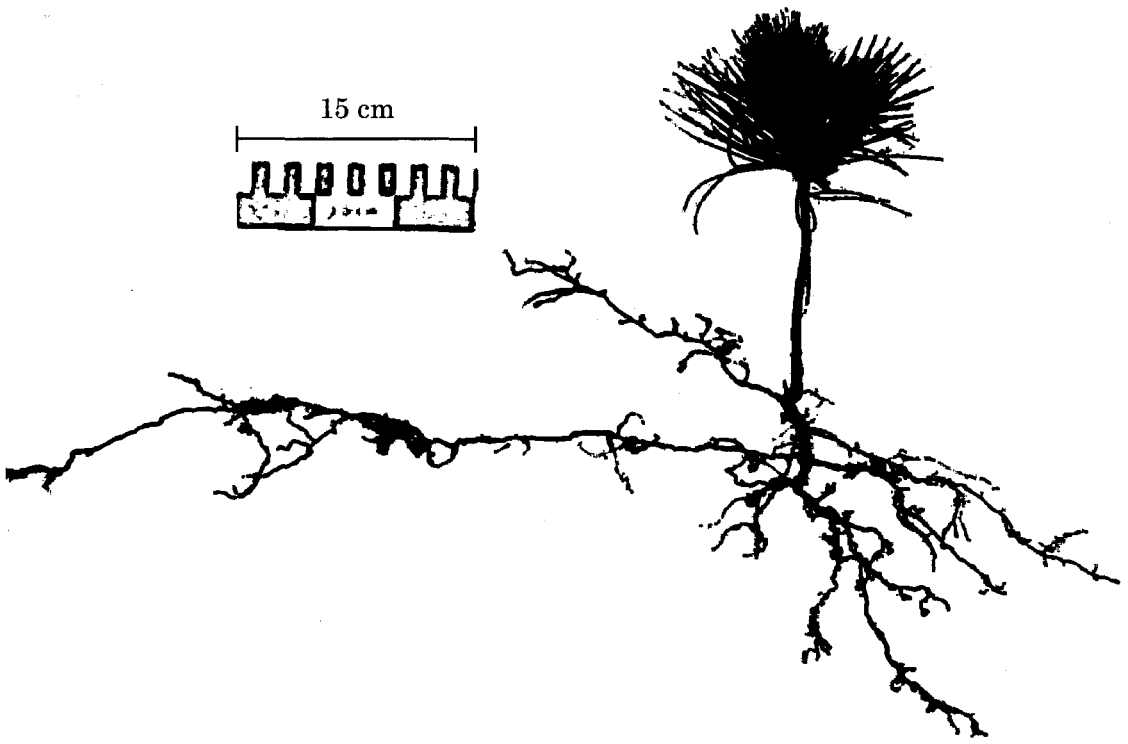

Figure 6.7 Observed architecture of actual root system of 2-year-old pine tree (*Pinus massoniana*), on slope No.1 (slope angle = 31 degrees, soil layer thickness = 25 cm).

soil water potential from the middle to the downstream-end of the slope distributed almost parallel to the slope. Close to the upstream-end of the slope, the soil is always drier than that in the lower part of the slope, due to the no-flux boundary condition on the upstream-end of the slope. All these tendencies seem to be quite natural when considering the soil water flow in actual slopes. Comparing slope No.1 and No.2, it can be seen that the soil water potential on slope No.2 tends to be lower than on slope No.1 in spite of the deeper soil layer on slope No.2. This may be due to the different hydraulic properties of the soil (see Figure 6.2), and the steeper slope gradient of slope No.2 (see Table 6.1). Moreover, the effect of transpiration on soil water distribution is more obvious on slope No.1, than on slope No.2. This may be due to the different hydraulic properties of the soil, and the different amount of the water maintained within the soil layer, which is approximately proportional to the soil layer thickness.

Figures 6.11 and 6.12 show the distribution of hydraulic potential ϕ [cm] corresponding to Figures 6.9 and 6.10, respectively. The interval of the contour lines is 100 cm. In Figures 6.11 and 6.12, contour lines are drawn nearly perpendicular to the slope, with the exception of those bending toward the upstream direction close to the soil surface during the summer seasons, and those being disturbed close to the

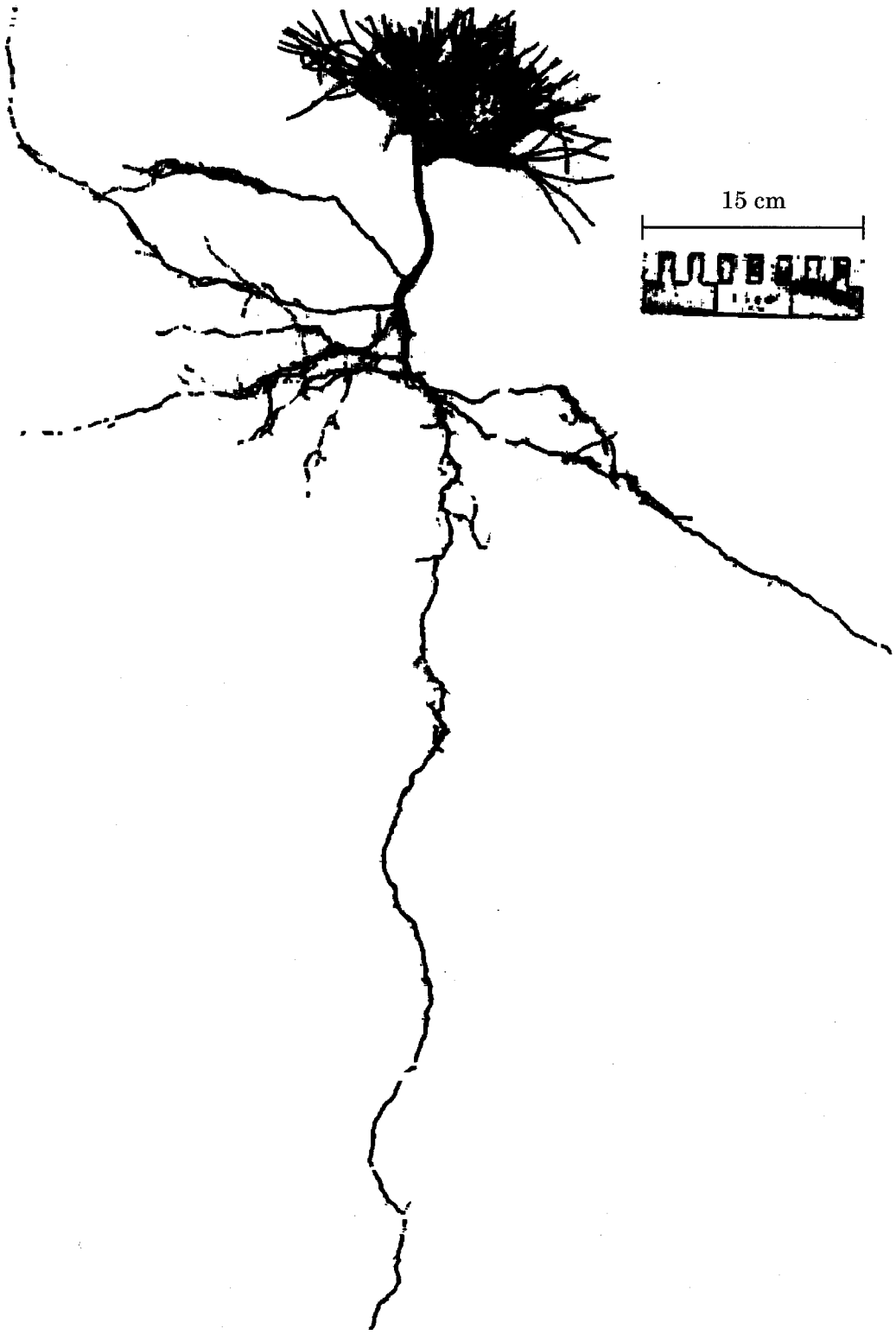

Figure 6.8 Observed architecture of actual root system of 2-year-old pine tree (*Pinus massoniana*), on slope No.2 (slope angle = 37 degrees, soil layer thickness = 53 cm).

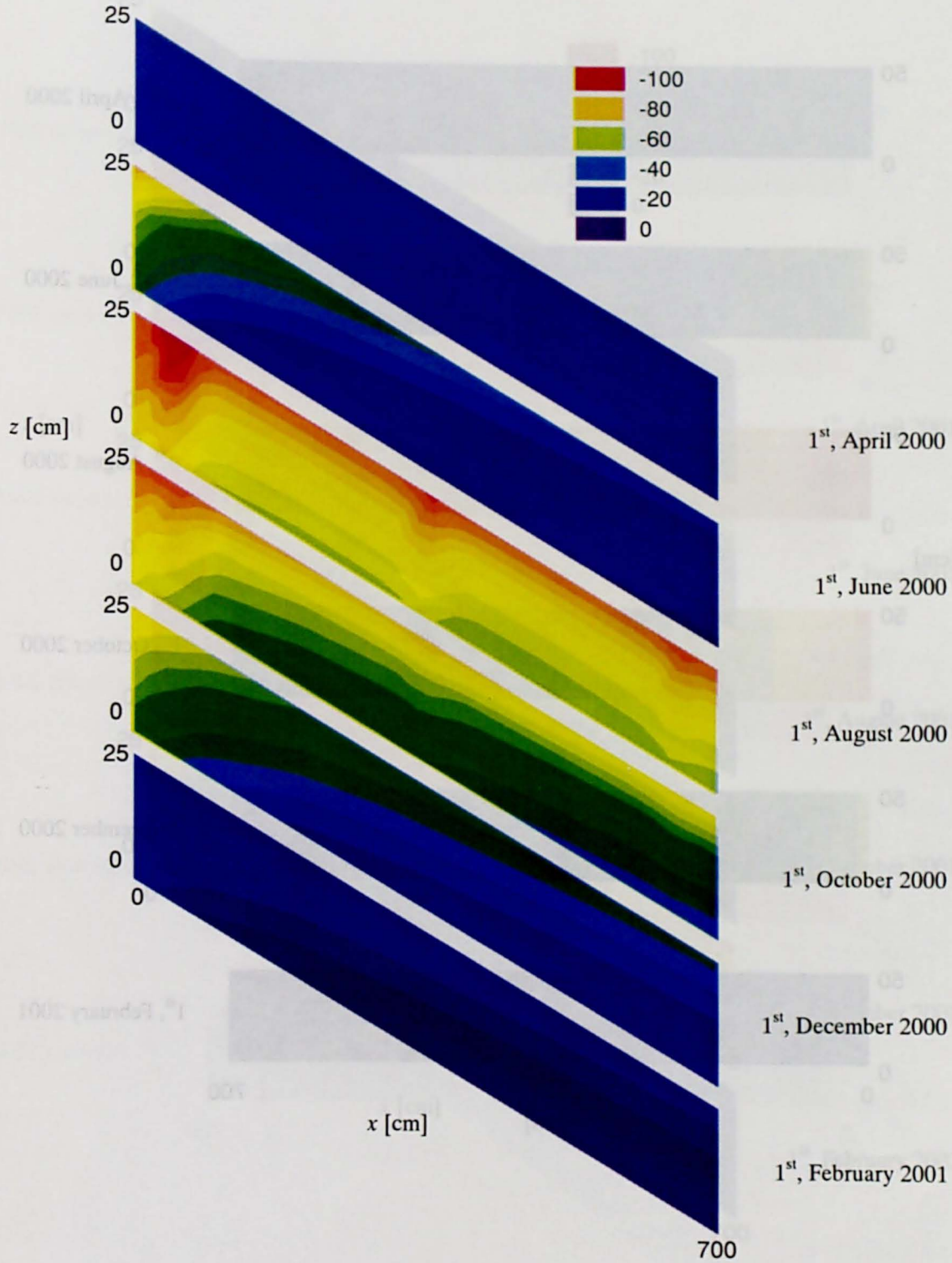

Figure 6.9a-1 Change of the distribution of the soil water potential ψ [cm] on the slope No.1 (Slope angle = 31 degrees, Soil depth = 25 cm), from side view.

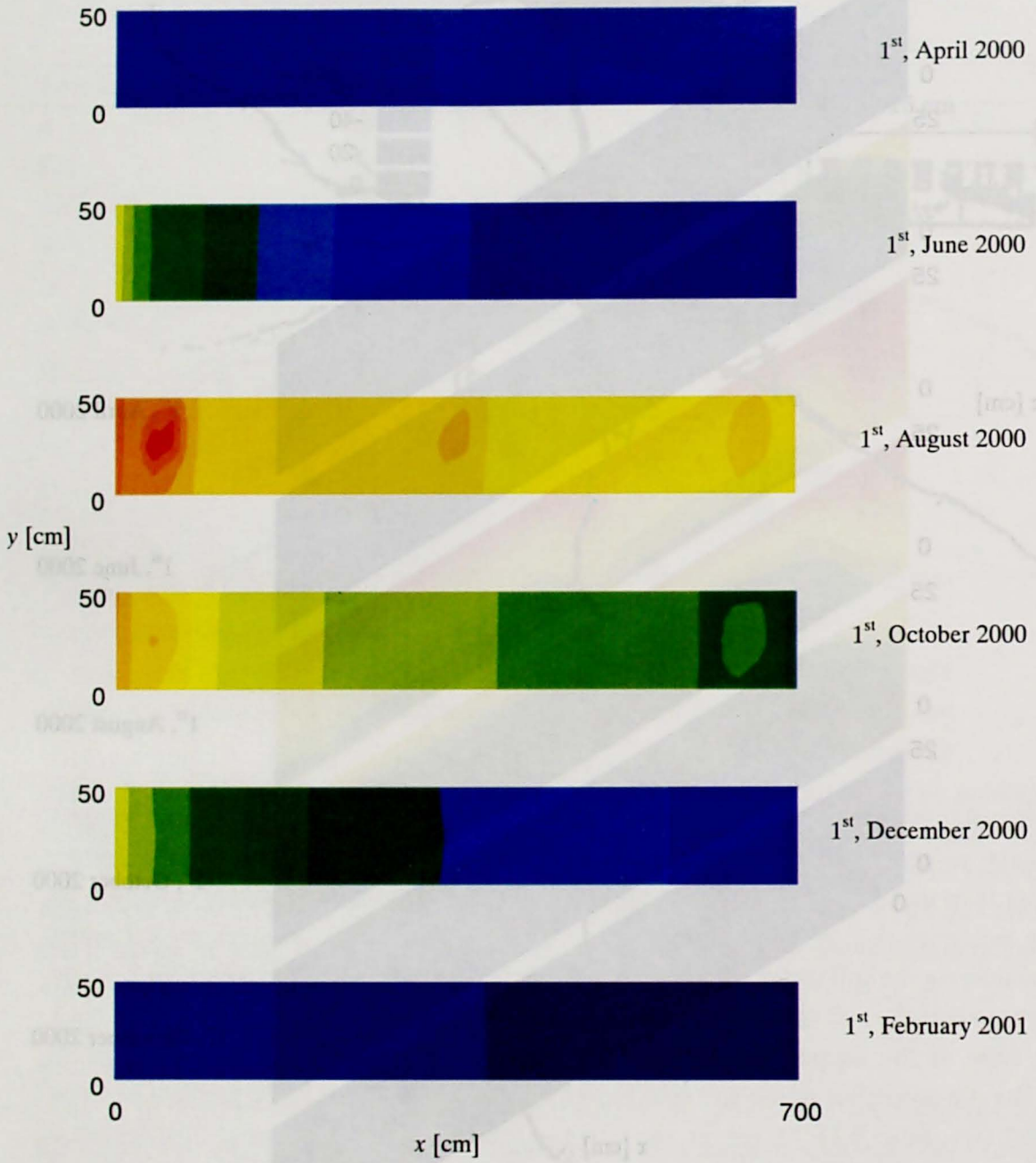

Figure 6.9a-2 Change of the distribution of the soil water potential ψ [cm] on the slope No.1 (Slope angle = 31 degrees, Soil depth = 25 cm), from top view.

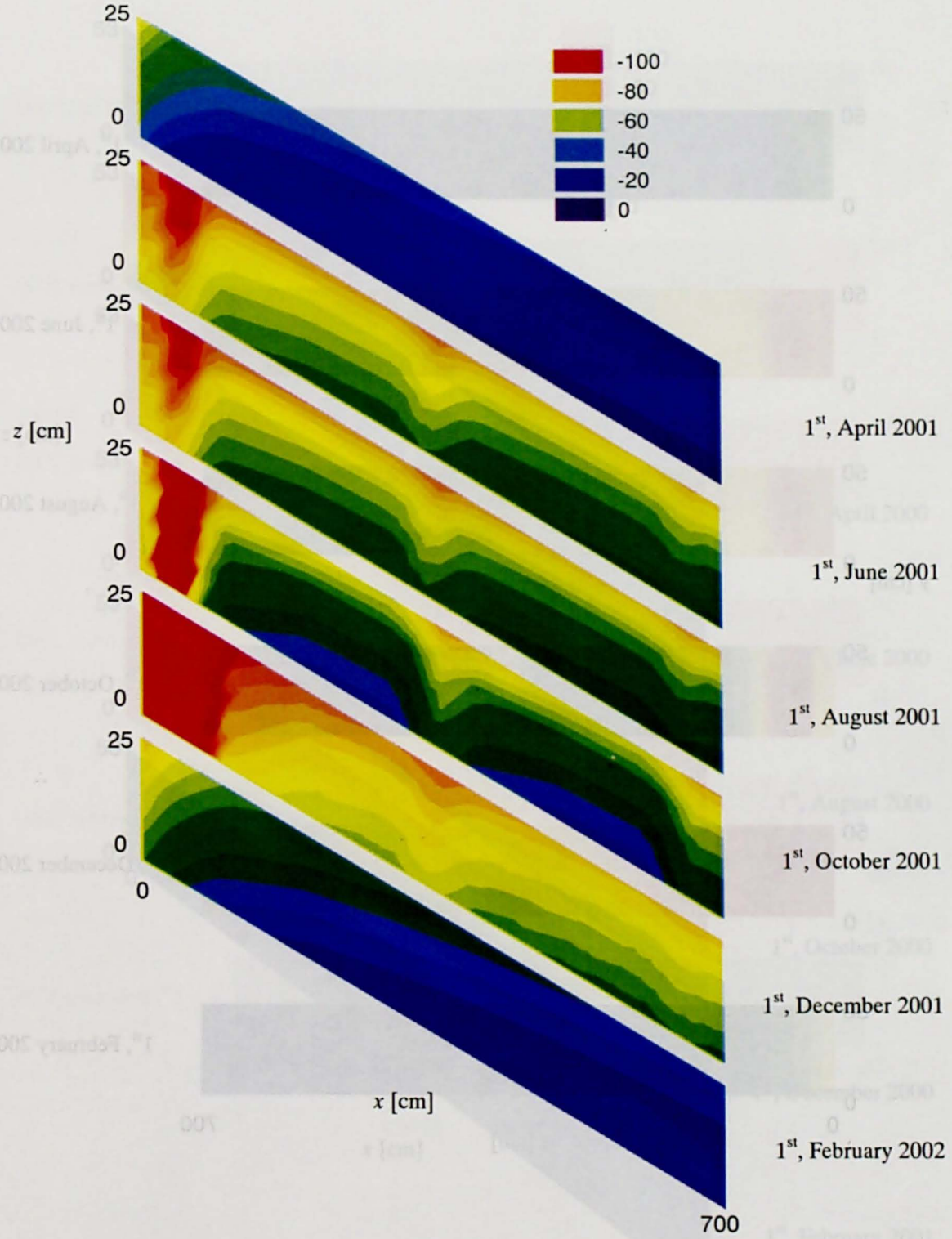

Figure 6.9b-1 Change of the distribution of the soil water potential ψ [cm] on the slope No.1 (Slope angle = 31 degrees, Soil depth = 25 cm), from side view.

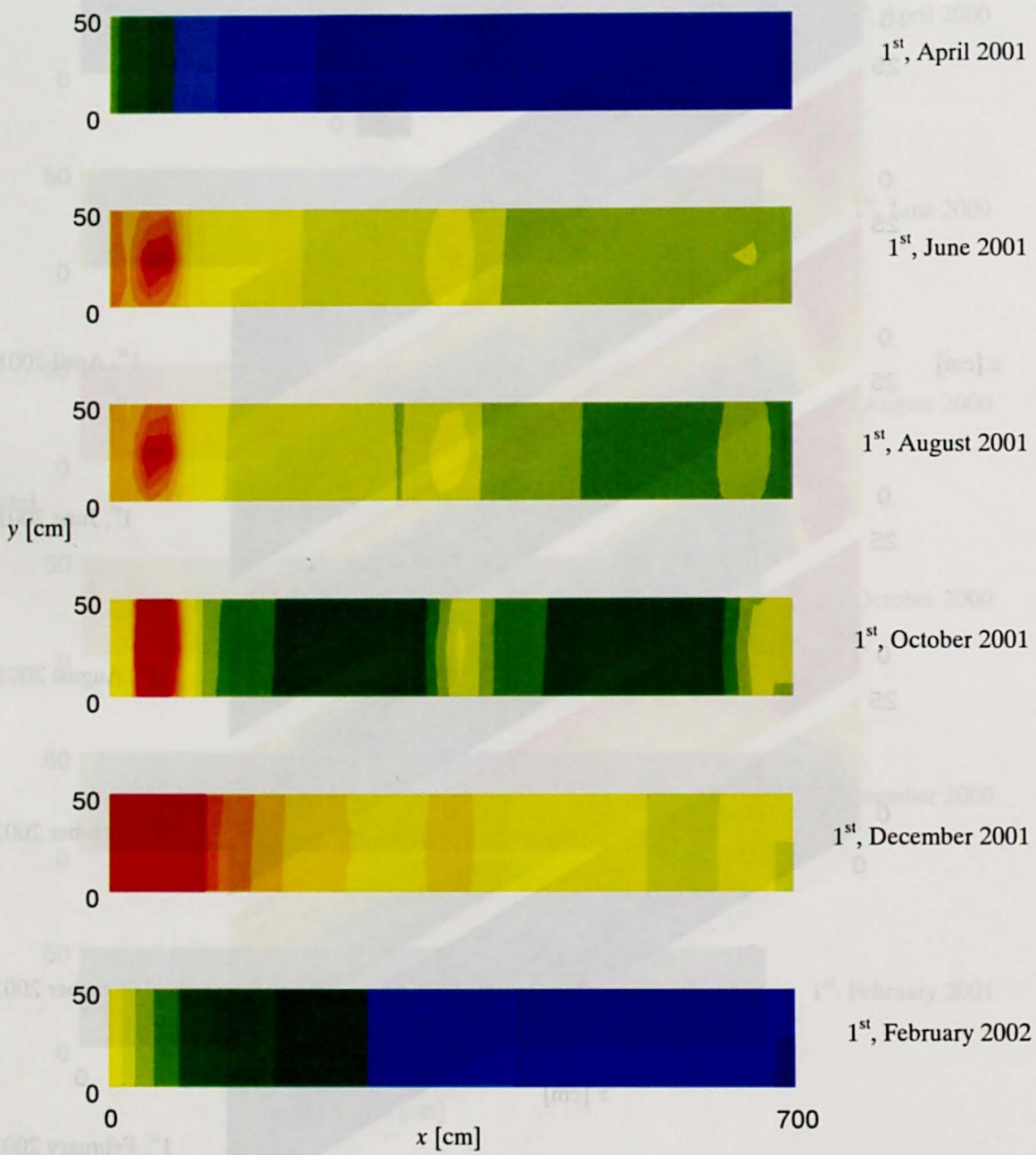

Figure 6.9b-2 Change of the distribution of the soil water potential ψ [cm] on the slope No.1 (Slope angle = 31 degrees, Soil depth = 25 cm), from top view.

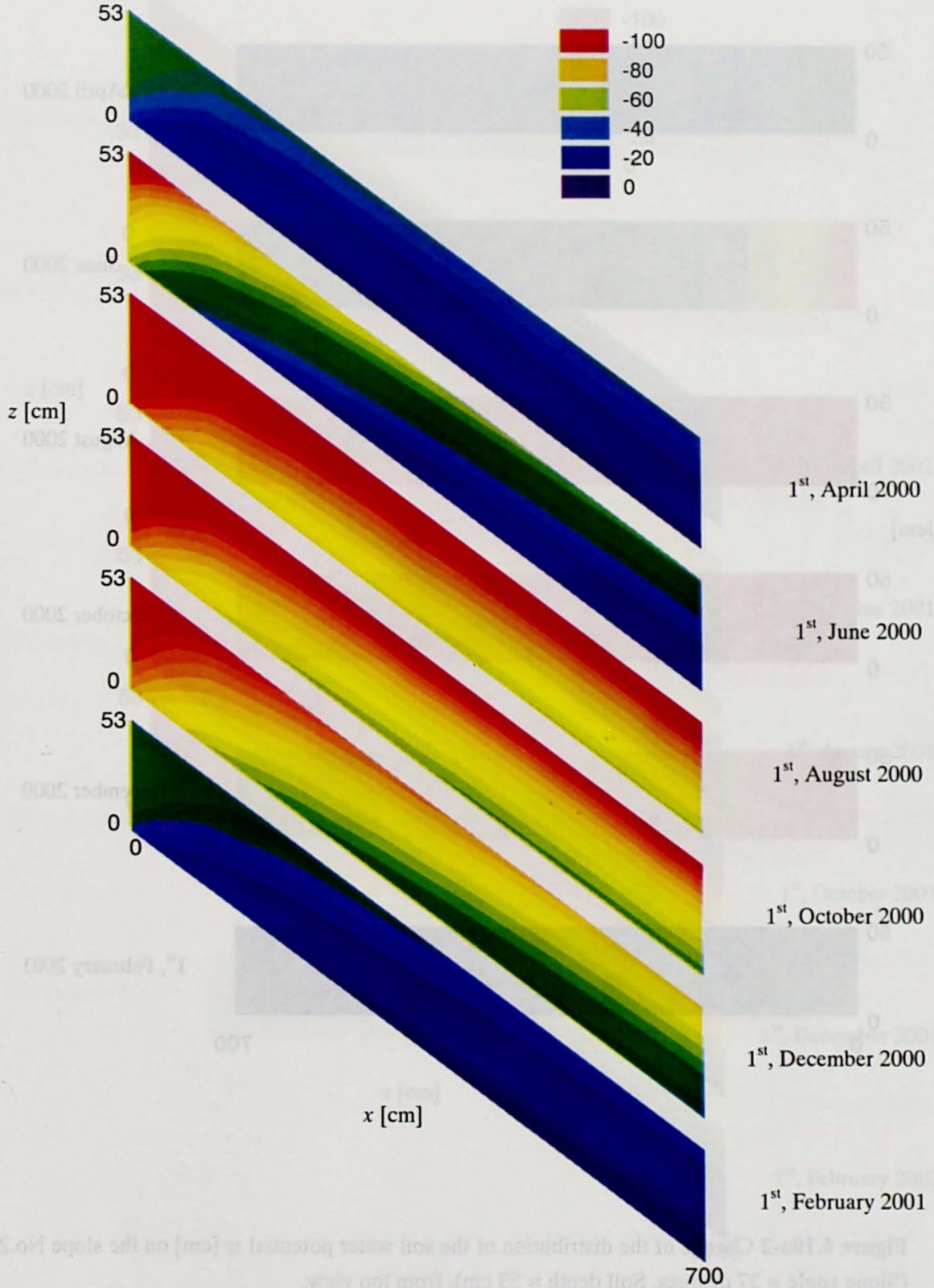

Figure 6.10a-1 Change of the distribution of the soil water potential ψ [cm] on the slope No.2 (Slope angle = 37 degrees, Soil depth = 53 cm), from side view.

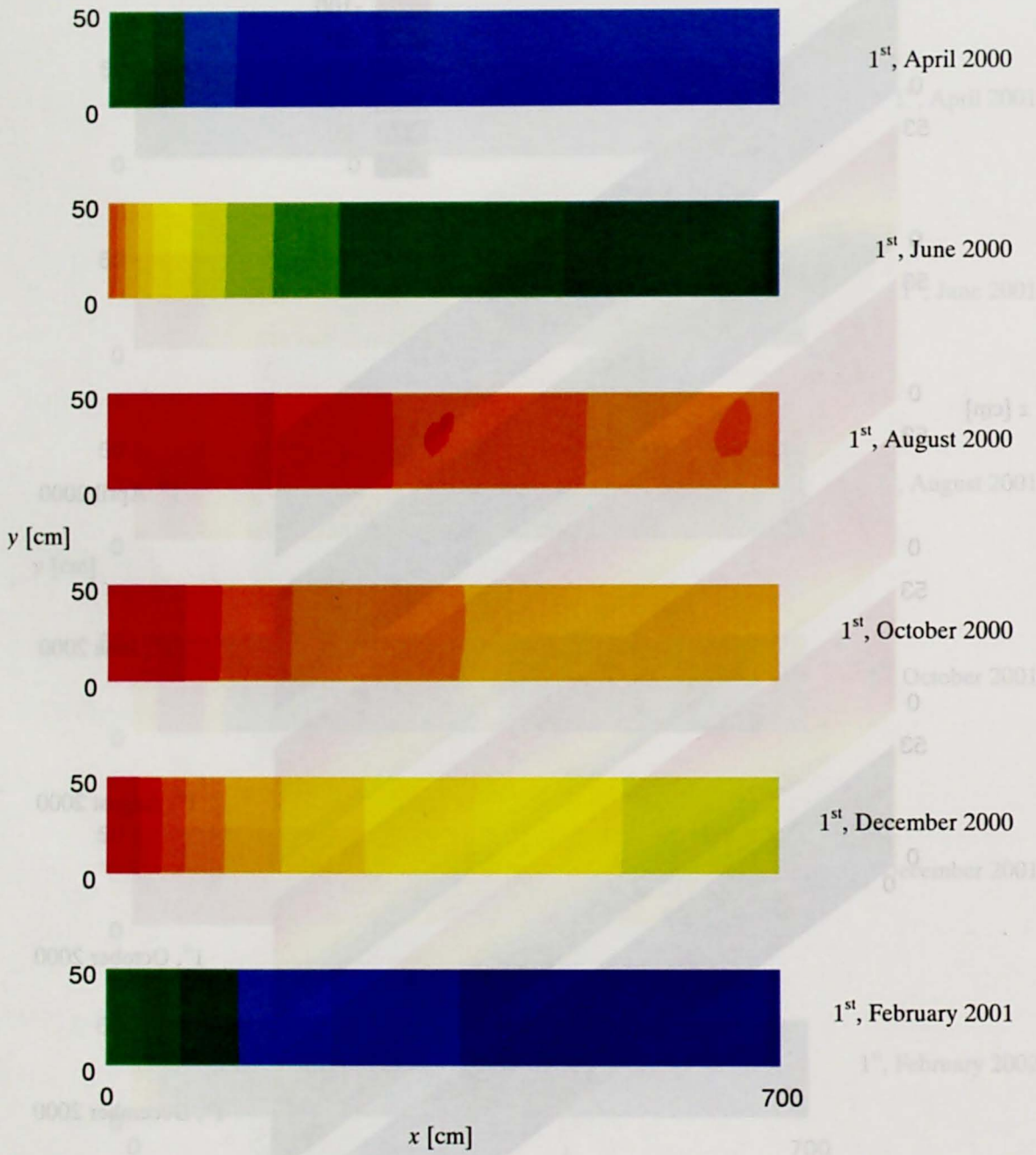

Figure 6.10a-2 Change of the distribution of the soil water potential ψ [cm] on the slope No.2 (Slope angle = 37 degrees, Soil depth = 53 cm), from top view.

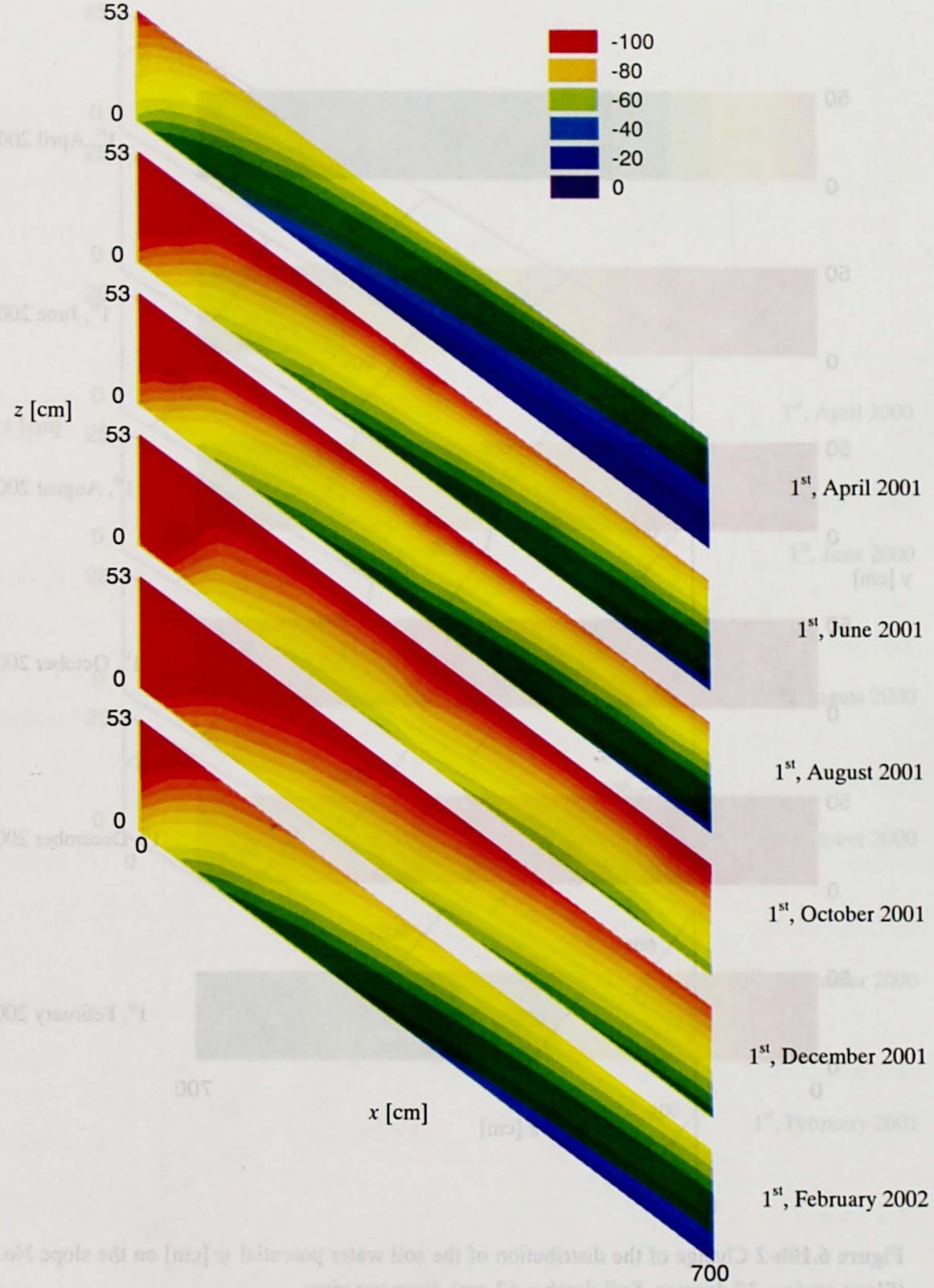

Figure 6.10b-1 Change of the distribution of the soil water potential ψ [cm] on the slope No.2 (Slope angle = 37 degrees, Soil depth = 53 cm), from side view.

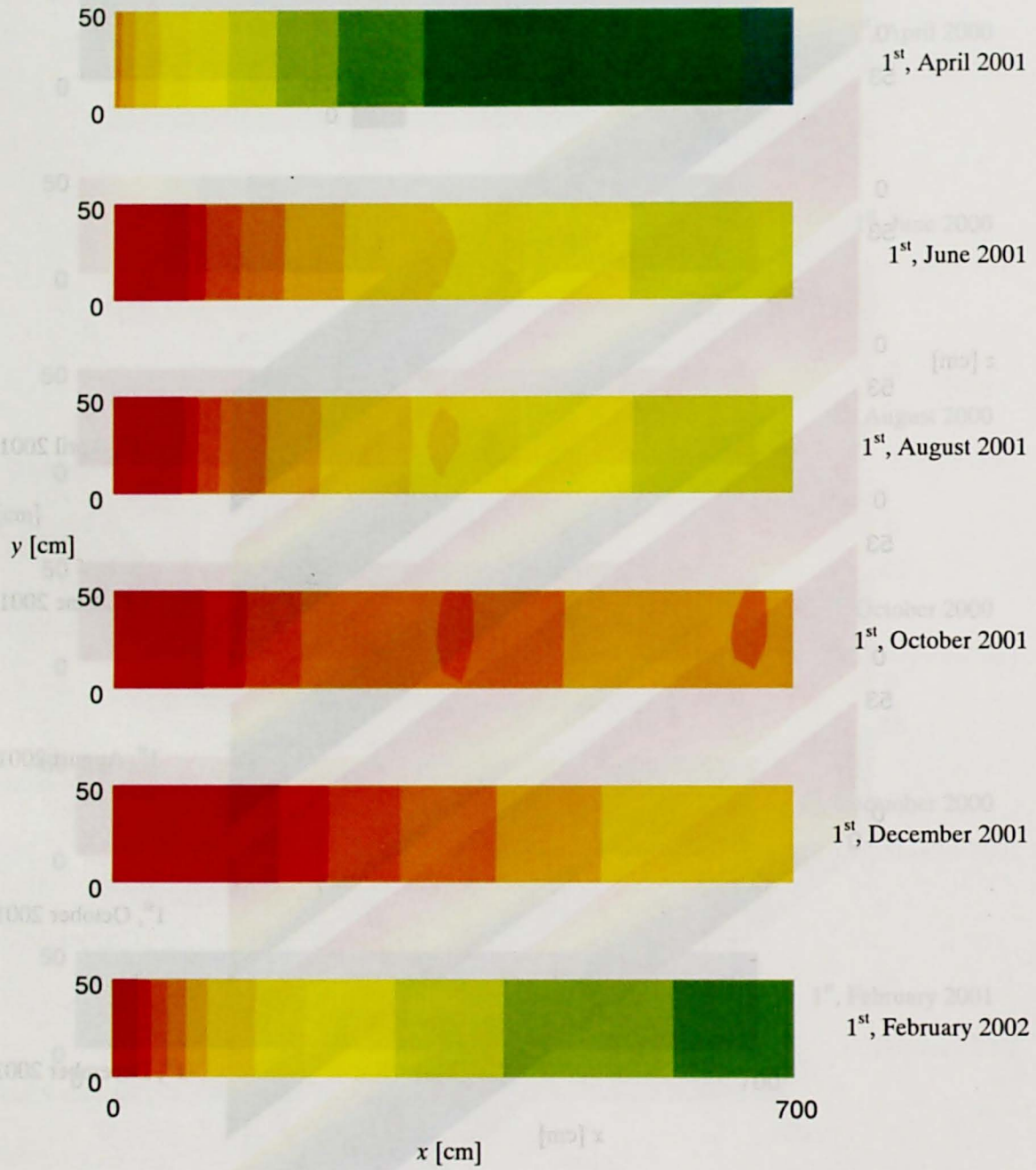

Figure 6.10b-2 Change of the distribution of the soil water potential ψ [cm] on the slope No.2 (Slope angle = 37 degrees, Soil depth = 53 cm), from top view.

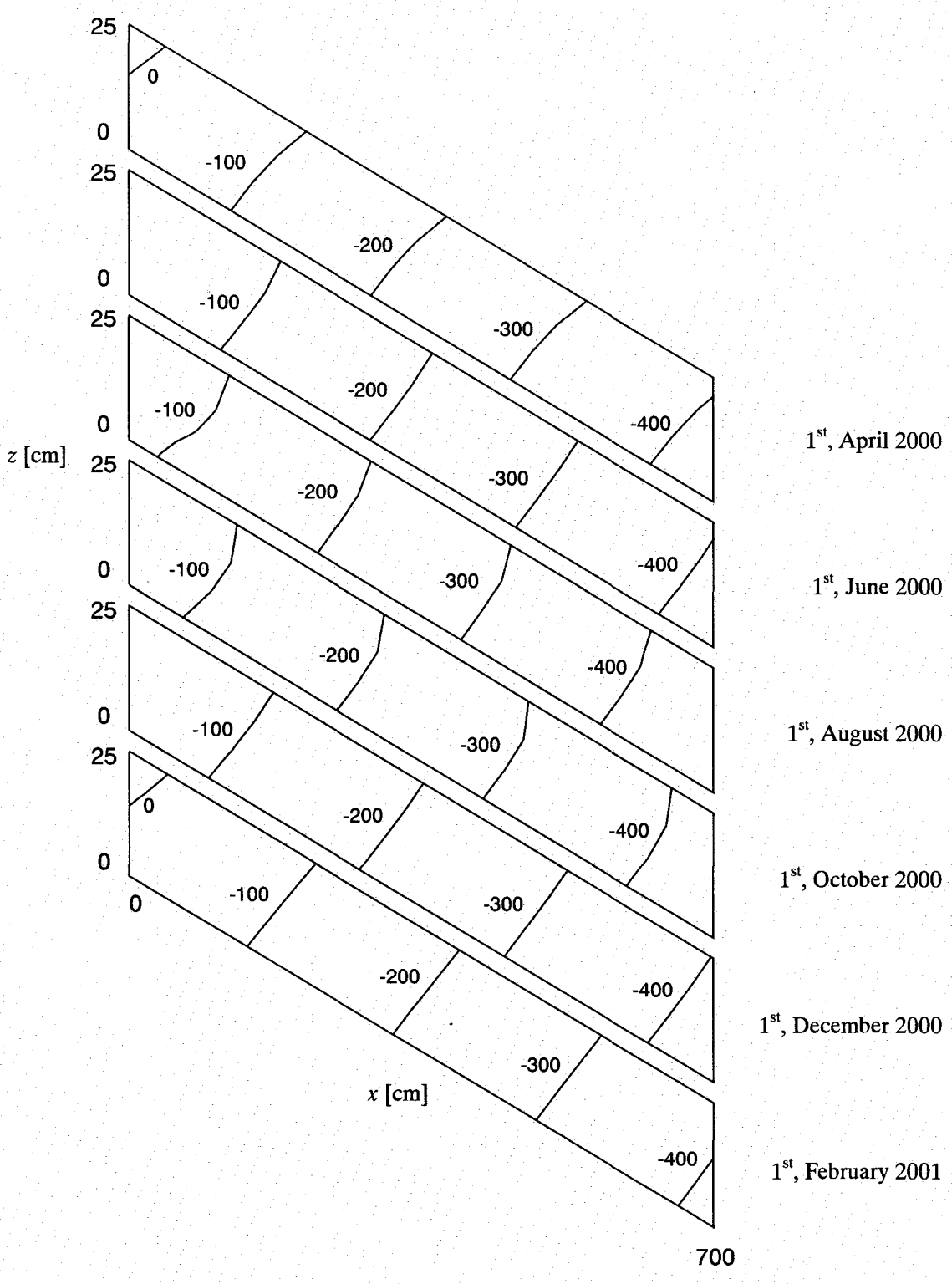

Figure 6.11a Change of the distribution of the hydraulic potential ϕ [cm] on the slope No.1 (Slope angle = 31 degrees, Soil depth = 25 cm).

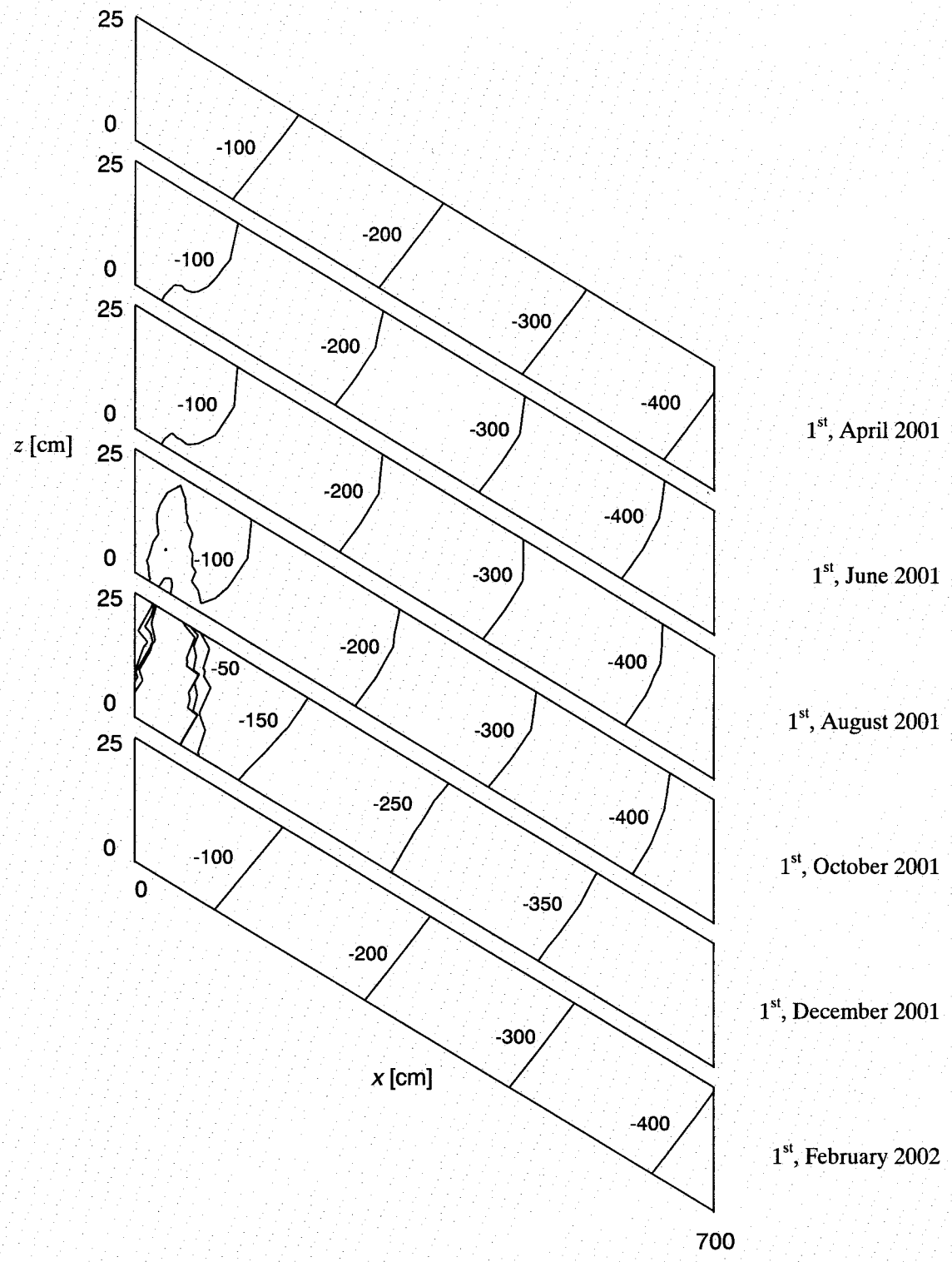

Figure 6.11b Change of the distribution of the hydraulic potential ϕ [cm] on the slope No.1 (Slope angle = 31 degrees, Soil depth = 25 cm).

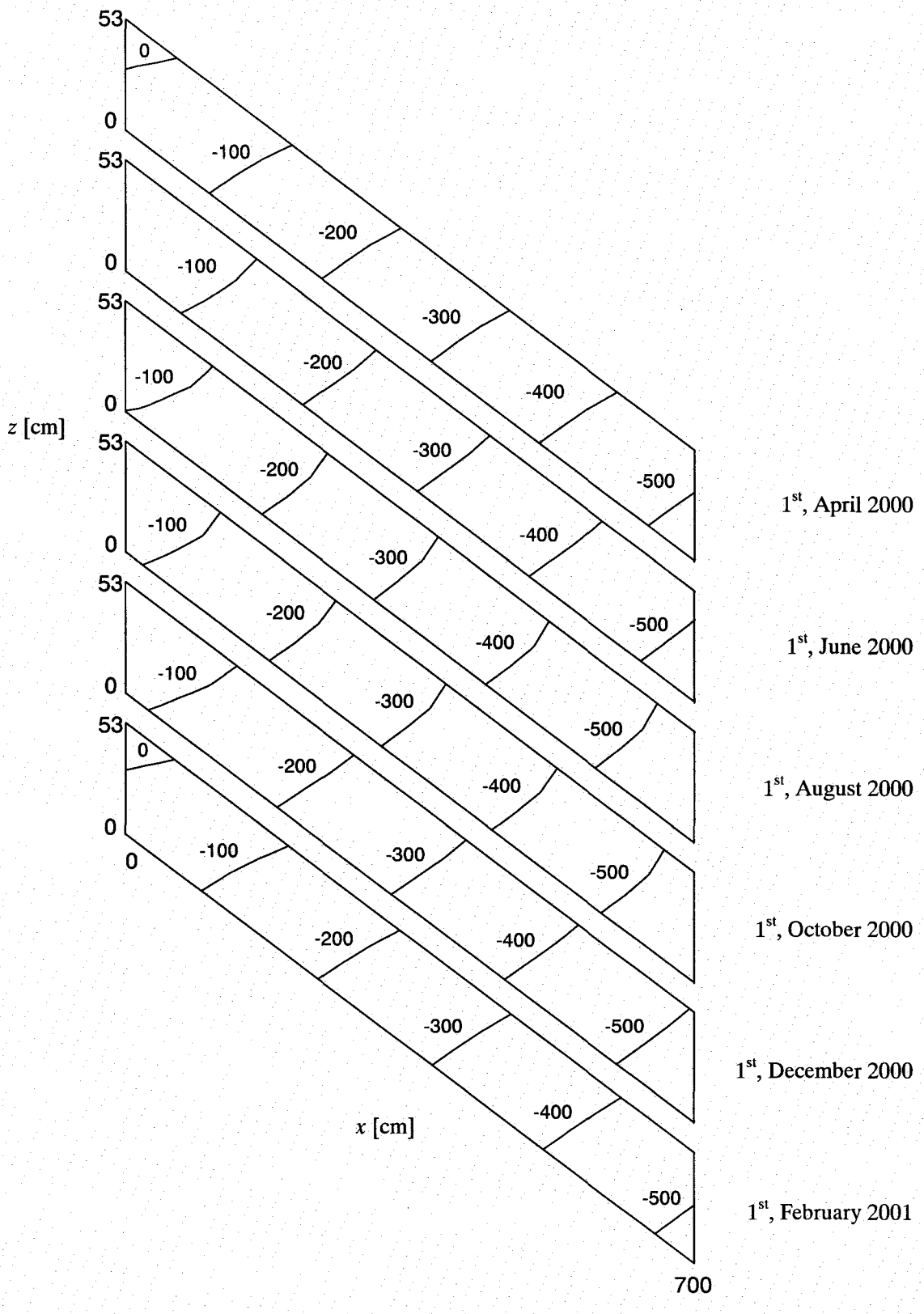

Figure 6.12a Change of the distribution of the hydraulic potential ϕ [cm] on the slope No.2 (Slope angle = 37 degrees, Soil depth = 53 cm).

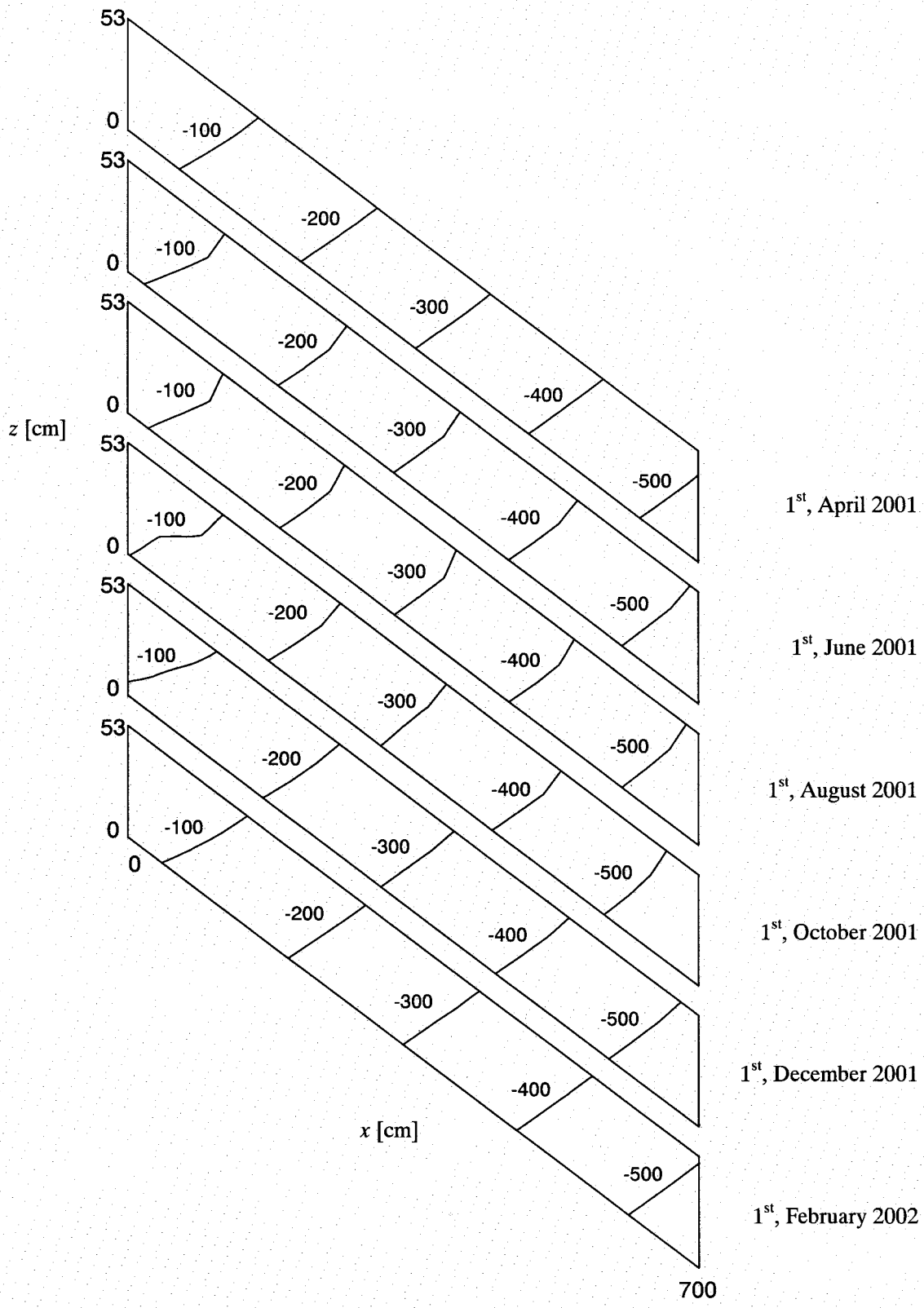

Figure 6.12b Change of the distribution of the hydraulic potential ϕ [cm] on the slope No.2 (Slope angle = 37 degrees, Soil depth = 53 cm).

upstream-end. The former exceptions are due to the higher evaporation from the soil surface, and later exceptions are due to the transpiration in the dry soil. Including these exceptions, the distribution of the hydraulic potential indicates that there exists constant soil water flow along the slope, from the upstream area to the downstream area of the slope. In these figures, no obvious effect of water uptake by roots on the distribution of the hydraulic potential can be seen. Figure 6.13 shows the water balances, the accumulated rainfall, actual evaporation, actual transpiration, and

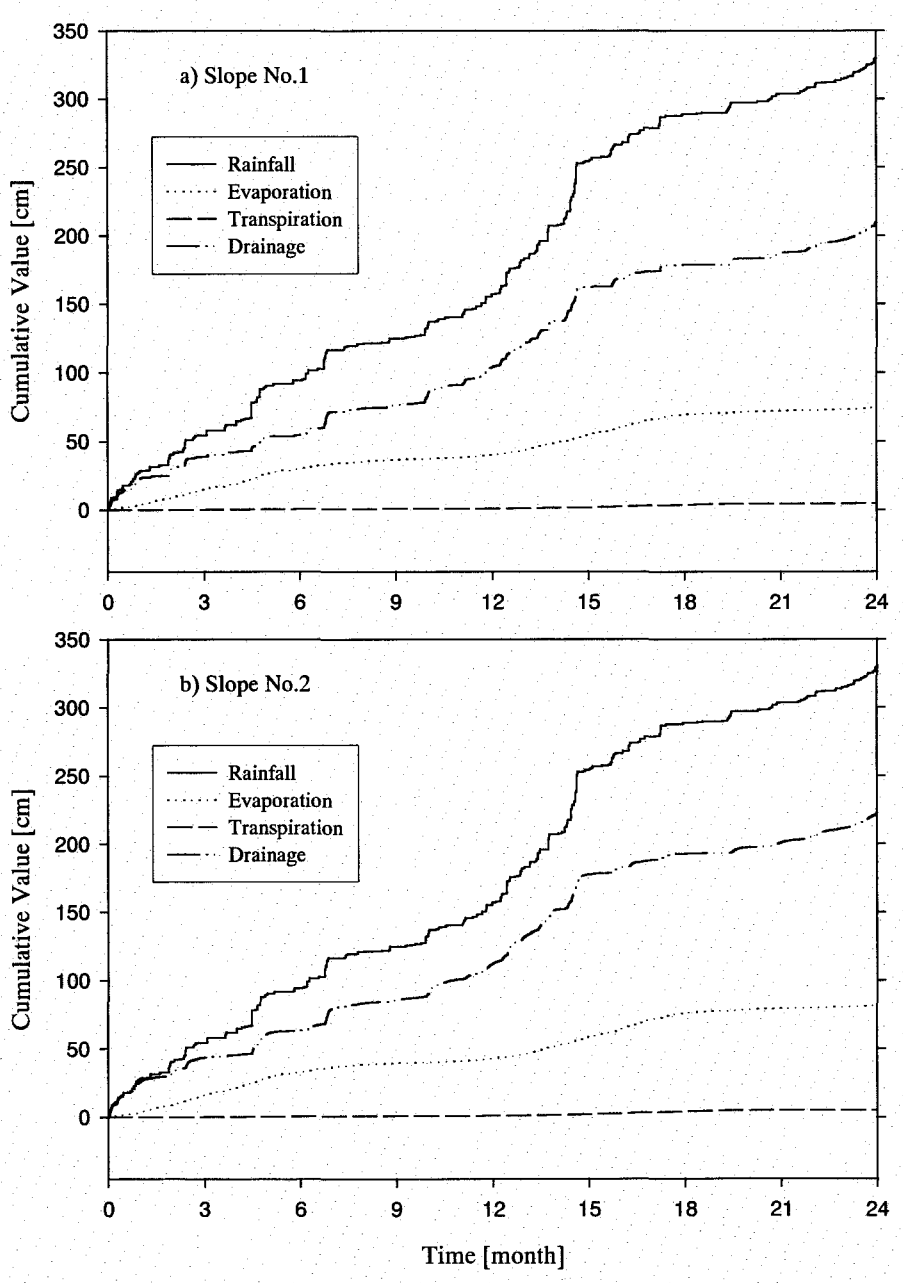

Figure 6.13 Calculated water valance, on a) slope No.1, and b) slope No.2.

drainage from the downstream-end, calculated on slope No.1 and No.2. From Figure 6.13, it is quantitatively clear that the effect of transpiration on the soil water distribution is less than the constant water flow from the upstream area to the downstream area of the slope, which finally flows out as drainage from the downstream-end. Consequently, it may be expected that the water flow from the upstream to the downstream area of the slope strongly affects the development of the root system.

6.5.3 Simulated Plant Root Systems

Figure 6.14 and 6.15 show the simulated morphological architectures of the root system on slope No.1 and No.2, respectively. In each figure, three root systems developed a) close to the upstream-end (upper root system), b) middle of the slope (middle root system), c) and close to the downstream-end (lower root system), are shown as figures projected onto an *x-y* plane and an *x-z* plane. The dotted lines in the *x-z* plane indicate the boundaries of the bottom and the surface of the soil. The elongation behavior of roots being forced to change their orientation when they reached the boundaries, are also modeled and are shown as the figures projected onto the *x-z* plane. On both slope No.1 and No.2, the main root of all root systems elongated straight in the direction of gravity, with a slight helical growth movement. This elongation behavior may be due to the greater elongation rate and the greater effect of gravitropism (see Table 6.2). After reaching the bottom of the soil layer, the main roots were deflected by the mechanical resistance of the bedrock. The elongation of the first order lateral roots in the middle and lower root systems are obviously affected by the effect of hydrotropism. The lateral roots up-slope elongating toward the upper direction, and those down-slope elongating toward the lower direction, in the *x-z* plane. In the *x-y* plane, it also can be seen that the lateral roots tend to grow unequally in the upper direction of the slope. However, the lateral roots in the upper root system elongate equally in all directions in the *x-y* plane. Although the lateral roots which reached the soil surface deflected along the soil surface, the obvious effect of root hydrotropism in forming an asymmetric architecture cannot be seen in the *x-z* plane. These differences of root system development between upper root system and the other two root systems are due to the soil water flow on the slope. Because rain permeates vertically into the soil and then flows downward in the sloped soil layer, the water flux across a section is the accumulation of the rain that permeated the upper part of the slope from the section. Therefore, the water flux in the soil layer increases as the water flows downward. Through the assumption that the elongation rate of hydrotropism is a function of the water flux at the root tip, hydrotropism affects the root system development in the downstream area greater than in the upstream area of the slope. However, the middle root system and lower root system show similar morphologies, and root hydrotropism affects them almost equally. As we have seen previously that

the distribution of soil water potential ψ is almost parallel to the slope (see Figure 6.9a, 6.10a), and the contour lines of the hydraulic potential ϕ distribute at a constant interval (see Figure 6.11, 6,12), the difference between the water fluxes across the middle section and downstream-end section may be slight, in the area lower than the middle of the slope. This similarity in water flow may be the reason for the similar morphologies in the middle and lower root systems. Comparing the root systems on slope No.1 and No.2, the root systems on slope No.1 shows shallower distribution, due to the smaller elongation rate of the main root (see Table 6.2). Comparing the simulated middle and lower root systems and the actually observed root systems, there seems to be a difference, i.e., the root length is over-estimated in the outputs from the model simulation. This may be due to the model not considering the effect of soil impedance, which depends usually on soil depth, and the decay of roots. However, there are many similarities between the simulated and observed root systems. First, the lateral roots up-slope of the main root elongate toward the upper direction, and those down-slope of the main root elongate toward the lower direction. Second, the roots, especially the main roots, elongate with a helical growth movement, as circumnutation. Third, a relatively large number of roots distribute in the up-slope direction. Fourth, the roots that reach the soil surface are deflected and elongate close to the soil surface. As a result, the overall morphologies of the root systems simulated by the model represent the asymmetric architecture observed on the slopes, and show good agreement with the actual root systems. Although there are some developmental behaviors that have not been considered still remaining, the proposed three-dimensional root system development model succeeded in simulating the root system development on a slope with consideration of the effect of soil water flow.

From the simulation results shown above, predictions on the basic morphologies of the root system developed on a slope can be made, as follows

(1) A root system on a slope develops asymmetrically, but a root system close to the ridge of the slope does not.
(2) Because the soil water flux depends on the thickness of the soil layer and slope gradient, the root system development may be affected by these geographical factors.
(3) Because soil water flux depends also on soil hydraulic properties, the root system development may be affected by these soil characteristics.
(4) Although soil mechanical impedance and root decay were not considered in the model, these effects are also important factors in the root system development on a slope.

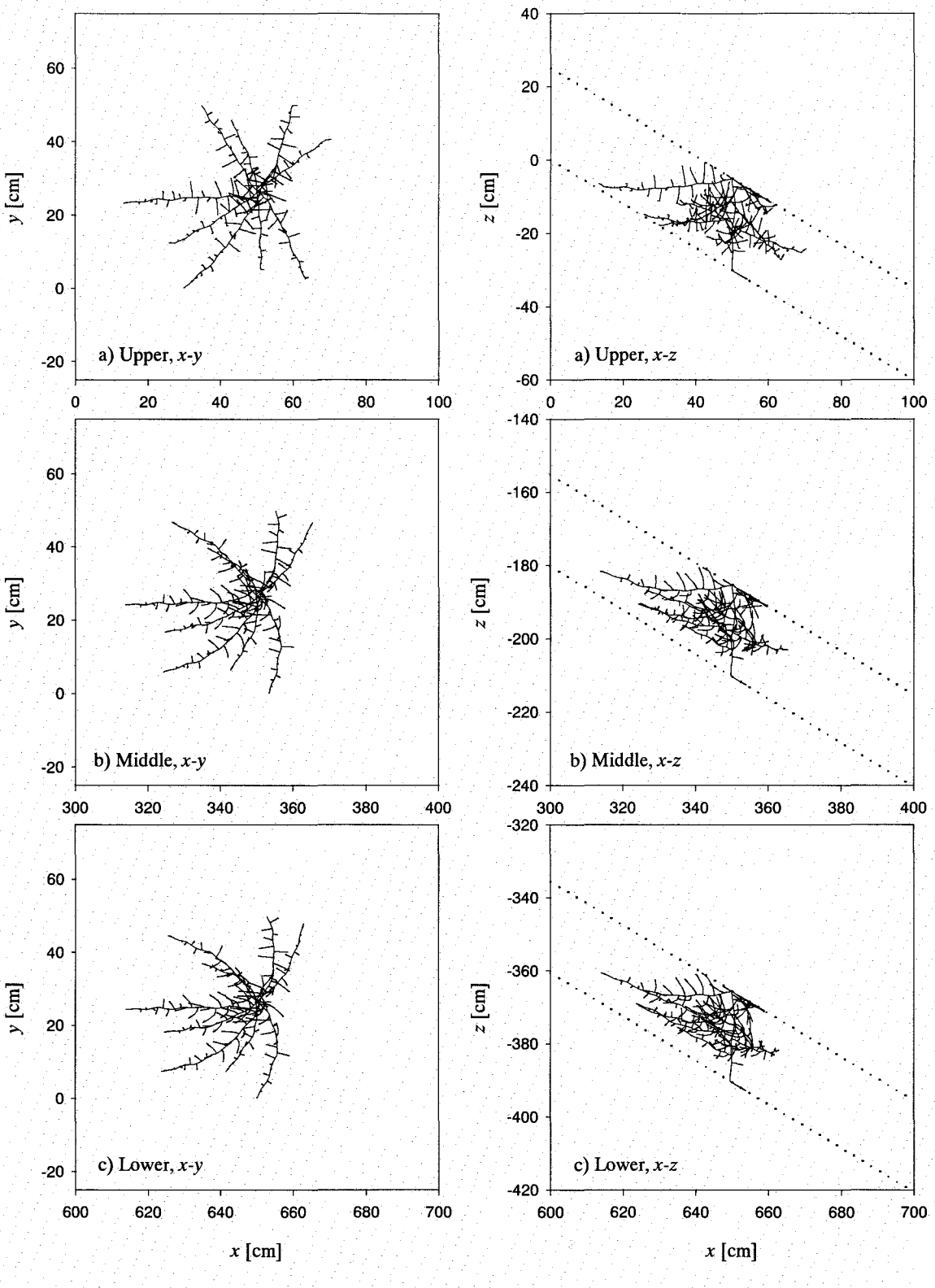

Figure 6.14 Simulated morphological architectures of the root systems (a; Upper, b; Middle, c; Lower) developed on the slope No.1.

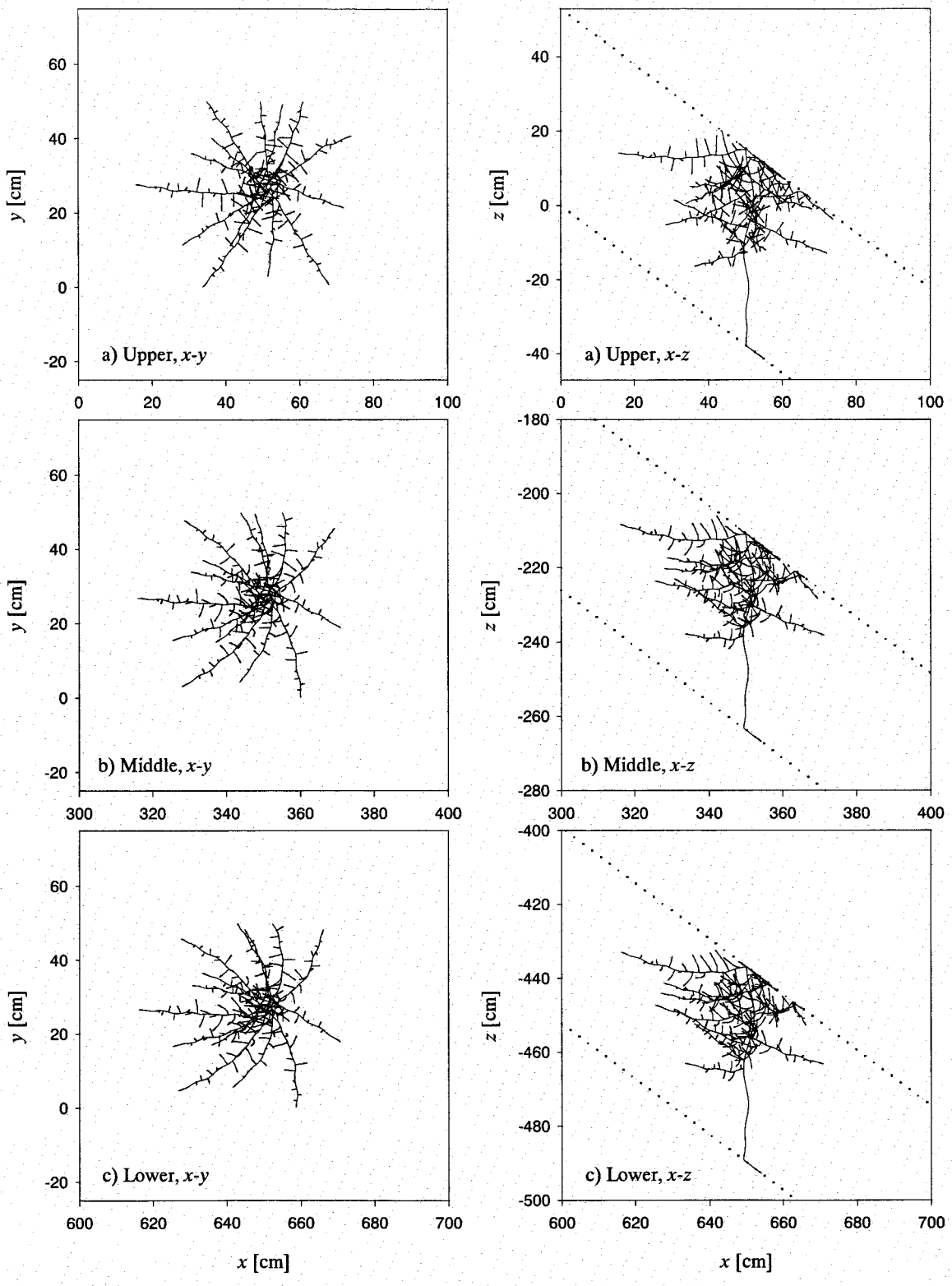

Figure 6.15 Simulated morphological architectures of the root systems (a; Upper, b; Middle, c; Lower) developed on the slope No.2.

6.6 CONCLUSION

In this chapter, a three-dimensional model combining root system development and soil water flow is proposed. The model principle is based on the two-dimensional root system development model proposed in Chapter 3 and Chapter 5. Root hydrotropism was considered as a dominant factor in root elongation as well as gravitropism. In addition to these tropisms, circumnutation was newly introduced in the model. The model simulated the root system development and soil water flow on slopes under actual environmental conditions, i.e., rainfall intensity, evaporation, and transpiration. The model succeeded in simulating the root system architectures that were actually observed on the natural slopes. The simulated asymmetric architecture of the root systems developed on the slope was especially in good agreement with that of the observed root systems, and well represents the characteristics reported in previous studies (Scippa et al., 2001; Yamadera, 1990). It was confirmed that this asymmetric development of the root system was due to root hydrotropism and water flow in the soil layer peculiar to the sloped geography. It was shown that the water fluxes on the sloped soil layer calculated with the actual environmental data affect the root system development stronger than that calculated with the virtually assumed environmental data in Chapter 3, and the root system obviously develops asymmetrically.

The importance of hydrotropism was already suggested in Chapter 3. The hypothesis that root hydrotropism is one of the dominant factor in root system development was not however confirmed, because (1) the model was two-dimensional, (2) actual environmental data was not employed in the simulation, and (3) the simulated root system architecture was not compared to the actual root system sufficiently. In this chapter, root hydrotropism was confirmed as the dominant factor of root system development, because actual environmental data was used for the simulation and the outputs from the three-dimensional model were compared with the actually observed root systems.

Because the primary objective of this study was to understand the mechanism of root system development on slopes, the root elongation and the root system morphological architecture in less than 2-year-old plant root systems were considered. The entire mechanism of root system development through long-term plant growth was not considered, but a very important part of it, i.e., the relationship between the root system development and the soil water flow, was demonstrated. By modifying the model to consider other factors, i.e. soil mechanical impedance, nutrient uptake, and by simulating the longer term growth of plant root systems, it will be possible to use the model for slope stability analysis with an eye for root system structures increasing soil stability.

REFERENCES

Darwin C. 1880 The power of Movement in Plants. John Murray, London

Diggle A. J. 1988 ROOTMAP —a model in three-dimensional coordinates of the growth and structure of fibrous root systems. Plant and Soil 105, 169-178

Doussan C., Pages L. and Vercambre G. 1998 Modeling of the hydraulic architecture of root systems: An integrated approach to water absorption – model description. Annals of Botany 81, 213-223

Dunbabin V.M., Diggle A.J., Rengel Z. and van Hugten R. 2002 Modelling the interactions between water and nutrient uptake and root growth. Plant and Soil 239, 19-38

Feddes R. A., Kowalik P. J. and Zaradny H. 1978 Simulation of field water use and crop yield. Simulation Monographs, Pudoc, Wageningen, The Netherlands.

Ge Z., Ruvio G. and Lynch J.P. 2000 The importance of root gravitropism for inter-root competition and phosphorus acquisition efficiency: results fro a geometric simulation model. Plant and Soil 218, 159-171

Herkelrath W. N., Miller E. E. and Gardner W. R. 1977a Water uptake by Plants: I. Divided root experiments. Soil Sci. Soc. Am. J. 41, 1033-1038

Herkelrath W. N., Miller E. E. and Gardner W. R. 1977b Water uptake by Plants: II. The root contact model. Soil Sci. Soc. Am. J. 41, 1039-1043

Hirota H. 2001 Handbook of roots. Asakura Shoten, Tokyo, Japan 71-72 (in Japanese)

Inuoe N., Amato T. and Khoko K. 1993 Seedling establishment of rice sown directly in flooded paddy field. (2) A model for evaluation effects of movement and elongation of seminal root and apparent weight of seedling on the establishment. Jpn. J. Crop Sci. 62 (Extra issue 2), 39-40

Istoke J. 1989 Grandwater modeling by the finite element method. American Geophysical Union, Washington, DC, USA

Johnsson A. 1997 Circumnutations: results from recent experiments of Earth and in space. Planta 203, 143-158

Kanda M. and Hino M. 1990 Numerical simulation of soil-plant-air system (1) modeling of plant system. J. Jpn Soc. Hydrology and water Resources 3, 37-46

Kimoto A., Uchida T., Mizuyama T. and Li C. 2002, Influences of human activities on sediment discharge from devastated weathered granite hills of southern China: effects of 4-year elimination of human activities. Catena 48, 217-233

Kosugi K. 1996. Lognormal distribution model for unsaturated soil hydraulic properties. Water Resour. Res.32: 2697-2703.

Lubkin S. 1994 Unidirectional waves on rings: Modes for chiral preference of circumnutating plants. Bull. Math. Biol. 56, 795-810

Pages L., Jordan M. O. and Picard D. 1989 A simulation model of the three-dimensional architecture of the maize root system. Plant and Soil 119, 147-154

Scippa G. S., Baraldi A., Urciouli D. and Chiatante D. 2001 Root response to slope condition. Which are the factors involved? Analysis at biochemical and molecular level. Proceedings of the 6th symposium of the international society of root research (Nov. 2001, Nagoya, Japan), Jpn. Soc. Root Res., Nagoya, Japan 128-129

Shimotashiro T., Inanaga S., Sugimoto Y. Matsuura A. and Ashimori M. 1998a Non-destructive method for root elongation measurement in soil using acoustic emission sensors. I. Vertical measurement of single root elongation. Plant Prod. Sci.

1(1), 25-29
Shimotashiro T., Inanaga S., Sugimoto Y. Matsuura A. and Ashimori M. 1998b Non-destructive method for root elongation measurement in soil using acoustic emission sensors. II. Spatial measurement of single root elongation. Plant Prod. Sci. 1(4), 248-253
Somma F., Hopmans J.W. and Clausnitzer V. 1998 Transient three-dimensional modeling of soil water and solute transport with simultaneous root growth, root water and nutrient uptake. Plant and Soil 202, 281-293
Thornthwaite C.W. 1948 An approach toward a rational clcassification of climate. Geogr. Rev. 38, 55-94
Tsutsumi D., Kosugi K. and Mizuyama T. 2002 Observation of 2-dimensional root system development and soil water distribution in a root box. For. Res., Kyoto 74 (in press, in Japanese with English summery)
Tsutsumi D., Kosugi K. and Mizuyama T. 2003. Root system development and water extraction model considering hydrotropism. Soil Sci. Soc. Am. J. (in press)
Yamadera Y. 1990 Experimental study for improving the revegetation technique on steep hillside slopes. Tokyo, Japan (In Japanese)
Zienkiewicz O. C. 1971 The finite element method in engineering science. McGraw-Hill, Berkshire, Englan

CHAPTER 7

GENERAL CONCLUSIONS

Plants uptake water from the soil through their root systems, circulate it through the plant body and return it to the air. The plant root system also prevents hillside slopes from eroding and landslides. These important functions of root systems are related closely to soil water flow. Because both the root system and soil water exist under the ground, there still remain many obscure area in studying the process of root system development and soil water flow. Understanding the mechanism of root system development, which is closely related to soil water flow, is fundamental to understand the physiological and morphological functions of the root systems. A modeling approach may help in understanding the processes of root system development and the soil water flow.

The objectives of this study were (1) to develop a new model, which can simulate and analyze root system development and soil water flow in both the plane and slopes, by considering the effect of hydrotropism which has not been considered in conventional models and (2) to understand the mechanism of plant root system development for the purpose of investigating the effect of soil water conditions on root system development through measurement of the quantitative root system morphological architecture and the distribution of soil water content.

In Chapter 2, root system models were classified into three categories, "development models", "morphometric models", and "distribution models", and the functions of each model were described, in order to clarify the objective of a new model that would be proposed in this study. After classifications, some conventional root system development models were reviewed and the principles of the models were represented. Among those models, the model by Diggle (1988), and the model by Pages et al. (1989) were the pioneers of three-dimensional root system development models, and have been extensively used as the basis of many other models. Common characteristics of these models were that root elongation was modeled by a "vector method" in which rate and direction of root elongation were described as a vector, and that those models were developed to predict root system morphological architectures in crop plant species. As many other models have also been developed in the field of agronomy, those models were applied only for crop plant root system development on the plane. As the result of this review, those items which of necessity must be included

in the new model were summarized. First, the new model could be applied to the development of woody plant root systems. Second, the new model could be applied to root system development on slopes. Third, root elongation would be modeled using a differential-growth mechanism, which reflects actual plant root growth. Fourth, root hydrotropism as well as gravitropism would be included into the root elongation model.

In Chapter 3, the two-dimensional model combining root system development and soil water extraction considering both hydrotropism and gravitropism was proposed, and applied to root system development and soil water flow on both the plane and slopes. In the model, root elongation was modeled not by a vector method but by a differential-growth method, which may be regarded as the actual mechanism of root elongation. The outputs from the model were then compared to those from a conventional model by Pages et al. (1989), in which hydrotropism was not considered. The resulting new model simulated the asymmetric architecture of root systems developed on a slope, i.e. roots on the up-slope tend to grow toward an upper direction and those on down-slope tend to grow toward a lower direction, something which the conventional model cannot do. These results suggest that root hydrotropism is one of the most important factors dominant in root system development. In Chapter 3, however, the comparisons between the simulated and actual plant root system development were not sufficiently carried out.

In Chapter 4, an experiment on root system development in a root box was carried out in order to investigate the effect of hydrotropism on actual plant root growth. In the experiment, soybeans were grown and their two-dimensional root system development was observed. During plant growth, two-dimensional distribution of soil water content was monitored continuously by TDR method. From the morphological architecture of the root systems excavated at the end of the experiment, it was shown that the roots concentrated near the points of water supply, due to root hydrotropic response and the compensatory growth of root system under a reduced effect of gravity. From the monitored two-dimensional distribution of soil water content in the root boxes, it was shown that soil water was distributed according to the root system morphologies and affected the root system developments. Those experimental results proved the hypothesis that root elongation is affected strongly by soil water flow, and therefore the establishment of the whole root system morphological architecture is determined by the surrounding soil water conditions.

The other objective of Chapter 4 was to establish a new experimental system using the root box and the coil type TDR probes. From the results of the experiment, it was shown that the new system was available as a method for quantitatively

investigating simultaneously both root system development and changing soil water distribution.

In Chapter 5, the two-dimensional model that was proposed in Chapter 3 was applied to the root system development and soil water flow in the root boxes, which were presented in Chapter 4. The concept of compensatory growth of root systems was newly introduced into the model. The simulation results, which agreed well with the observed results of root system development and soil water distributions in Chapter 4, demonstrate that the effect of root hydrotropism is a dominant factor in the establishment of root system morphological architecture under the reduced effect of gravity. It was also confirmed that the compensatory growth of the root system plays an important role in root system development, however it alone cannot account for the developmental behavior of roots concentrating to the points of water supply in the root box. The experiment and the model simulation shown in Chapter 4 and 5 suggested that it is possible to apply the model for the design and control of root system architecture under the influence of drip irrigation, or to control of root system development under no gravity conditions, i.e. in a space station.

In Chapter 6, a three-dimensional root system development model was proposed. The model was based on the two-dimensional model previously shown in Chapter 3 and 5. A new concept of circumnutation of root growth was introduced into the model. Actual plant root systems of pine trees that were grown on hillside slopes in the southern part of China (JianXi Province, China) were excavated in order to observe their architecture and to measure the characteristics of root elongation. The soils were also sampled to obtain the hydraulic properties. In the observed root systems, asymmetric architectures were recognized similar to previous studies (Scippa et al., 2001; Yamadera, 1990). The model simulated the development of those actual plant root systems and soil water flow, incorporating actual soil and weather condition data into the model simulation. The simulation results indicate that (1) the water flux from the upstream area to the downstream area existed constantly throughout the calculation period, (2) the asymmetric development of root systems was affected strongly by the water flux from the upstream area to the downstream area, (3) the effect of water flux on root system development was different when comparing root systems close to the ridge of the slope to those at the lower part of the slope, (4) the geography of the slope, i.e. slope gradient, soil depth, and soil hydraulic properties affect the root system development through the various actions of the soil water flow. The observed and simulated root system morphological architectures were in good agreement, especially in the asymmetric architectures. The three-dimensional model simulation incorporating the actual environmental condition data demonstrates that root hydrotropism is the

dominant factor in determining root system architecture on a slope.

Root circumnutation is generally thought to be a movement finding cracks or holes between the soil particles, in order to elongate in compacted soil. In Chapter 6, the detailed effect of circumnutation on simulated root system development has not been discussed sufficiently. However, the preceding model simulations (results not shown) suggested that circumnutation plays an important role not only in representing the natural morphologies of roots but also in emphasizing or reducing the effect of the tropisms, in order to avoid extremely distorted root system development. Further consideration of circumnutation would be possible through experiments and model simulation.

Through the experiment, field observation, and model simulation, the mechanisms of plant root system development have been well-considered. Special attention was paid to the relationship between plant root system development and soil water flow, throughout the study. In the modeling process, gravitropism, hydrotropism, circumnutation, and compensatory growth were considered and introduced as root elongation factors. Above all, the effect of root hydrotropic response on root system development was extensively considered, and it was demonstrated that root hydrotropism is one of the dominant factors in determining the root system morphological architecture. It was shown especially that in determining the asymmetric architectures on slopes root hydrotropism is an irreplaceable elongation factor.

The two-dimensional and three-dimensional models proposed in this study are different from the conventional models, from some view points, (1) modeling root differential growth, (2) consideration of hydrotropism, (3) applicability to root system development on slopes, (4) the modeling not only of root system development but also soil water flow. Therefore, these proposed models are available for simulate root system development and soil water flow under various environmental water conditions, i.e. plant growth by drip irrigation, under no-gravity condition such as in a space station, and woody plant root system development on a hillside slope under natural weather conditions. Furthermore, the model can be used for slope stability analysis of the effect of root systems in increasing the stability of the soil structure. In the future, it will be necessary for models to consider other important effects, such as the effect of the soil mechanical impedance, nutrient uptake, decay of roots, etc., for extensive utilization of the models in various fields.

REFERENCES

Diggle A. J. 1988 ROOTMAP —a model in three-dimensional coordinates of the growth and structure of fibrous root systems. Plant and Soil 105, 169-178

Pages L., Jordan M. O. and Picard D. 1989 A simulation model of the three-dimensional architecture of the maize root system. Plant and Soil 119, 147-154

Scippa G. S., Baraldi A., Urciouli D. and Chiatante D. 2001 Root response to slope condition. Which are the factors involved? Analysis at biochemical and molecular level. Proceedings of the 6th symposium of the international society of root research (Nov. 2001, Nagoya, Japan), Jpn. Soc. Root Res., Nagoya, Japan 128-129

Yamadera Y. 1990 Experimental study for improving the revegetation technique on steep hillside slopes. Tokyo, Japan (In Japanese)

APPENDIX

FINITE ELEMENT METHOD FOR A CALCULATION OF THREE-DIMENSIONAL SOIL WATER FLOW

A.1 Governing Equation

Darcy Equations;

$$q_x = -K\frac{\partial \psi}{\partial x},\ q_y = -K\frac{\partial \psi}{\partial y},\ q_z = -K\left(\frac{\partial \psi}{\partial z}+1\right) \tag{A.1}$$

Equation of Continuity;

$$\left(q_x + \frac{\partial q_x}{\partial x}dx - q_x\right)dy\cdot dz + \left(q_y + \frac{\partial q_y}{\partial y}dy - q_y\right)dx\cdot dz + \left(q_z + \frac{\partial q_z}{\partial z}dz - q_z\right)dx\cdot dy$$
$$-Q\cdot dx\cdot dy\cdot dz = -\frac{\partial \theta}{\partial t}dx\cdot dy\cdot dz \tag{A.2}$$

Substitution of Equation (A.1) into Equation (A.2) gives,

$$\frac{\partial}{\partial x}\left(K\frac{\partial \psi}{\partial x}\right) + \frac{\partial}{\partial y}\left(K\frac{\partial \psi}{\partial y}\right) + \frac{\partial}{\partial x}\left[K\left(\frac{\partial \psi}{\partial x}+1\right)\right] - Q - C_p\frac{\partial \psi}{\partial t} = 0 \tag{A.3}$$

Equation (A.3) is the three-dimensional form for the Richards' equation based on water potential ψ, which describes transient groundwater flow through unsaturated porous media.

A.2 Derive the Approximating Equation (Method of Weighted Residuals)

The contribution of element to the residual at node m to which the element is joined is

$$R_m = \int_\Omega W_m\left\{\frac{\partial}{\partial x}\left(K\frac{\partial \hat{\psi}}{\partial x}\right) + \frac{\partial}{\partial y}\left(K\frac{\partial \hat{\psi}}{\partial y}\right) + \frac{\partial}{\partial x}\left[K\left(\frac{\partial \hat{\psi}}{\partial x}+1\right)\right] - Q - C_p\frac{\partial \hat{\psi}}{\partial t}\right\}dx\cdot dy\cdot dz \tag{A.4}$$

where, W_m is the weighting function for node m, Ω represents the volume of element, $\hat{\psi}$ is the approximate solution for ψ within the element, represented as,

$$\hat{\psi} = \sum_{m=1}^{M} N_m\cdot\psi_m \tag{A.5}$$

where, M is the total node number in the element.
According to Greens theorem and Galerkin Method ($W_m = N_m$), Equation (A.4) is derived as follows,

$$R_m = -\int_\Omega N_m C_p \frac{\partial \hat{\psi}}{\partial t} dx \cdot dy \cdot dz - \int_\Omega \left(\frac{\partial N_m}{\partial x} K \frac{\partial \hat{\psi}}{\partial x} + \frac{\partial N_m}{\partial y} K \frac{\partial \hat{\psi}}{\partial y} + \frac{\partial N_m}{\partial z} K \frac{\partial \hat{\psi}}{\partial z} \right) dx \cdot dy \cdot dz$$
$$+ \int_\Omega N_m Q dx \cdot dy \cdot dz - \int_\Omega K \frac{\partial N_m}{\partial z} dx \cdot dy \cdot dz - \int_\Gamma K \tilde{q} d\gamma \tag{A.6}$$

where, γ is the boundary of the domain, Γ is the surface area of the element which is located on the boundary, and $\tilde{q}$ is normal flux flows out across the boundary. Substitution $R_m = 0$ into Equation (A.6) gives,

$$D_{m,n} \frac{\partial \psi}{\partial t} + B_{m,n} \psi = f_m \tag{A.7}$$

where, the matrix $D_{m,n}$, $B_{m,n}$ and the vector f_m are represented as follows,

$$D_{m,n} = \int_\Omega N_m C_p N_n dx \cdot dy \cdot dz \tag{A.8}$$

$$B_{m,n} = \int_\Omega \left(\frac{\partial N_m}{\partial x} K \frac{\partial N_n}{\partial x} + \frac{\partial N_m}{\partial y} K \frac{\partial N_n}{\partial y} + \frac{\partial N_m}{\partial z} K \frac{\partial N_n}{\partial z} \right) dx \cdot dy \cdot dz \tag{A.9}$$

$$f_m = \int_\Omega N_m Q dx \cdot dy \cdot dz - \int_\Omega K \frac{\partial N_m}{\partial z} dx \cdot dy \cdot dz - \int_\Gamma N_m \tilde{q} d\gamma \tag{A.10}$$

If Δt is small enough, Equation (A.7) is modified as follows,

$$\overline{D}_{m,n} \frac{\psi^{t+\Delta t} - \psi^t}{\Delta t} + \overline{B}_{m,n} \left[\lambda \psi^{t+\Delta t} - (1-\lambda) \psi \right] = \bar{f}_l \tag{A.11}$$

where, $\overline{D}_{m,n}, \overline{B}_{m,n}$ and $\bar{f}_m$ are the means of $D_{m,n}$, $B_{m,n}$ and f_m in time from t to $t+\Delta t$, λ is a constant value ranging from 0 to 1. From Equation (A.11), the unknown value of $\psi^{t+\Delta t}$ is represented as follows,

$$\left(\frac{\overline{D}_{m,n}}{\Delta t} + \lambda \overline{B}_{m,n} \right) \psi^{t+\Delta t} = \left[\frac{\overline{D}_{m,n}}{\Delta t} - (1-\lambda) \overline{B}_{m,n} \right] \psi^t + \bar{f}_m \tag{A.12}$$

In Equation (A.12), the mean values of hydraulic conductivity $\overline{K}$ and water capacity $\overline{C}_p$ are used. $\overline{K}$ and $\overline{C}_p$ are represented as follows,

$$\overline{K} = \lambda K^{t+\Delta t} + (1-\lambda) K^t \tag{A.13}$$

$$\overline{C}_p = \lambda \overline{C}_p^{\,t+\Delta t} + (1-\lambda) \overline{C}_p^{\,t} \tag{A.14}$$

A.3 Assembling the Global System of Equations

We employed the tetrahedral form as the three-dimensional finite element. The approximating function N_m for node m (= i, j, k, and l) are represented as follows,

$$N_m = \frac{1}{6V}\left(a_m + b_m x + c_m y + d_m z\right) \tag{A.15}$$

where, V is the volume of the element, a_m, b_m, c_m, and d_m (m = i, j, k, and l) are the constants represented as follows,

$$a_i = \det\begin{vmatrix} x_j & y_j & z_j \\ x_k & y_k & z_k \\ x_l & y_l & z_l \end{vmatrix}, b_i = \det\begin{vmatrix} 1 & y_j & z_j \\ 1 & y_k & z_k \\ 1 & y_l & z_l \end{vmatrix}, c_i = \det\begin{vmatrix} 1 & x_j & z_j \\ 1 & x_k & z_k \\ 1 & x_l & z_l \end{vmatrix}, d_i = \det\begin{vmatrix} 1 & x_j & y_j \\ 1 & x_k & y_k \\ 1 & x_l & y_l \end{vmatrix},$$

$$a_j = \det\begin{vmatrix} x_i & y_i & z_i \\ x_k & y_k & z_k \\ x_l & y_l & z_l \end{vmatrix}, b_j = \det\begin{vmatrix} 1 & y_i & z_i \\ 1 & y_k & z_k \\ 1 & y_l & z_l \end{vmatrix}, c_j = \det\begin{vmatrix} 1 & x_i & z_i \\ 1 & x_k & z_k \\ 1 & x_l & z_l \end{vmatrix}, d_j = \det\begin{vmatrix} 1 & x_i & y_i \\ 1 & x_k & y_k \\ 1 & x_l & y_l \end{vmatrix},$$

$$a_k = \det\begin{vmatrix} x_i & y_i & z_i \\ x_j & y_j & z_j \\ x_l & y_l & z_l \end{vmatrix}, b_k = \det\begin{vmatrix} 1 & y_i & z_i \\ 1 & y_j & z_j \\ 1 & y_l & z_l \end{vmatrix}, c_k = \det\begin{vmatrix} 1 & x_i & z_i \\ 1 & x_j & z_j \\ 1 & x_l & z_l \end{vmatrix}, d_k = \det\begin{vmatrix} 1 & x_i & y_i \\ 1 & x_j & y_j \\ 1 & x_l & y_l \end{vmatrix},$$

$$a_l = \det\begin{vmatrix} x_i & y_i & z_i \\ x_j & y_j & z_j \\ x_k & y_k & z_k \end{vmatrix}, b_l = \det\begin{vmatrix} 1 & y_i & z_i \\ 1 & y_j & z_j \\ 1 & y_k & z_k \end{vmatrix}, c_l = \det\begin{vmatrix} 1 & x_i & z_i \\ 1 & x_j & z_j \\ 1 & x_k & z_k \end{vmatrix}, d_l = \det\begin{vmatrix} 1 & x_i & y_i \\ 1 & x_j & y_j \\ 1 & x_k & y_k \end{vmatrix} \tag{A.16}$$

where, x_m, y_m, z_m are the x, y, z coordinates of the node m. From Equation (A.15), differentials of N_m are represented as follows,

$$\frac{\partial N_m}{\partial x} = \frac{b_m}{6V}, \qquad \frac{\partial N_m}{\partial y} = \frac{c_m}{6V}, \qquad \frac{\partial N_m}{\partial z} = \frac{d_m}{6V} \tag{A.17}$$

By assuming that C_p is constant in the element, and employing the lumped formulation, Equation (A.8) is represented as,

$$\begin{aligned} D_{m,n} &= C_p \int_\Omega N_m N_n dx \cdot dy \cdot dz = C_p \frac{1!1!0!0!}{(1+1+3)!} 6V = \frac{VC_p}{20} \\ D_{m,m} &= C_p \int_\Omega N_m N_m dx \cdot dy \cdot dz = C_p \frac{2!0!0!0!}{(2+3)!} 6V = \frac{VC_p}{10} \end{aligned} \tag{A.18}$$

Therefore,

$$D = \frac{VC_p}{20}\begin{bmatrix}5 & 0 & 0 & 0\\ 0 & 5 & 0 & 0\\ 0 & 0 & 5 & 0\\ 0 & 0 & 0 & 5\end{bmatrix} = \frac{VC_p}{4}\begin{bmatrix}1 & 0 & 0 & 0\\ 0 & 1 & 0 & 0\\ 0 & 0 & 1 & 0\\ 0 & 0 & 0 & 1\end{bmatrix} \tag{A.19}$$

In transforming Equation (A.18), following law was used (Zienkiewicz, 1971),

$$\int_\Omega N_i^{\,a} N_j^{\,b} N_k^{\,c} N_l^{\,d}\, dx \cdot dy \cdot dz = \frac{a!b!c!d!}{(a+b+c+d+3)!} 6V \tag{A.20}$$

By assuming that K is constant in the element, Equation (A.9) is represented as,

$$\begin{aligned} B_{m,n} &= K\int_\Omega \left(\frac{\partial N_m}{\partial x}\frac{\partial N_n}{\partial x} + \frac{\partial N_m}{\partial y}\frac{\partial N_n}{\partial y} + \frac{\partial N_m}{\partial z}\frac{\partial N_n}{\partial z}\right) dx \cdot dy \cdot dz \\ &= \frac{K}{36V^2}\left(b_m b_n + c_m c_n + d_m d_n\right)\int_\Omega dx \cdot dy \cdot dz \\ &= \frac{K}{36V}\left(b_m b_n + c_m c_n + d_m d_n\right) \end{aligned} \tag{A.21}$$

Therefore,

$$B = \begin{bmatrix} b_i^{\,2} + c_i^{\,2} + d_i^{\,2} & b_j b_i + c_j c_i + d_j d_i & b_k b_i + c_k c_i + d_k d_i & b_l b_i + c_l c_i + d_l d_i \\ b_i b_j + c_i c_j + d_i d_j & b_j^{\,2} + c_j^{\,2} + d_j^{\,2} & b_k b_j + c_k c_j + d_k d_j & b_l b_j + c_l c_j + d_l d_j \\ b_i b_k + c_i c_k + d_i d_k & b_j b_k + c_j c_k + d_j d_k & b_k^{\,2} + c_k^{\,2} + d_k^{\,2} & b_l b_k + c_l c_k + d_l d_k \\ b_i b_l + c_i c_l + d_i d_l & b_j b_l + c_j c_l + d_j d_l & b_k b_l + c_k c_l + d_k d_l & b_l^{\,2} + c_l^{\,2} + d_l^{\,2} \end{bmatrix} \tag{A.22}$$

By assuming that K and Q are constants in the element, and that $\tilde{q}$ is a constant on the boundary, Equation (A.10) is represented as,

$$\begin{aligned} f_m &= Q\int_\Omega N_m dx \cdot dy \cdot dz - K\int_\Omega \frac{\partial N_m}{\partial z} dx \cdot dy \cdot dz - \tilde{q}\int_\Gamma N_m d\gamma \\ &= \frac{VQ}{4} - \frac{d_m K}{6} - \frac{A_{ijk}\tilde{q}}{3} \end{aligned} \tag{A.23}$$

Therefore,

$$f = \begin{bmatrix} \frac{1}{4}VQ - \frac{1}{6}d_i K - \frac{1}{3}A_{ijk}\tilde{q} \\ \frac{1}{4}VQ - \frac{1}{6}d_j K - \frac{1}{3}A_{ijk}\tilde{q} \\ \frac{1}{4}VQ - \frac{1}{6}d_k K - \frac{1}{3}A_{ijk}\tilde{q} \\ \frac{1}{4}VQ - \frac{1}{6}d_l K \end{bmatrix} \tag{A.24}$$

where, A_{ijk} is an area of a triangle consists of three nodes i, j and k, which are located on the boundary.

The area A_{ijk} and volume V of an element are calculated as follows,

$$A_{ijk} = \frac{\left\{\begin{bmatrix}(x_i - x_j)^2 + (y_i - y_j)^2 + (z_i - z_j)^2\end{bmatrix}\begin{bmatrix}(x_i - x_k)^2 + (y_i - y_k)^2 + (z_i - z_k)^2\end{bmatrix} \\ + \begin{bmatrix}(x_i - x_j)(x_i - x_k) + (y_i - y_j)(y_i - y_k) + (z_i - z_j)(z_i - z_k)\end{bmatrix}^2\right\}^{\frac{1}{2}}}{2} \tag{A.25}$$

$$V = \frac{\begin{bmatrix}(x_j y_k z_l + y_j z_k x_l + z_j x_k y_l - x_j z_k y_l - y_j x_k z_l - z_j y_k x_l) \\ -(x_i y_k z_l + y_i z_k x_l + z_i x_k y_l - x_i z_k y_l - y_i x_k z_l - z_i y_k x_l) \\ +(x_i y_j z_l + y_i z_j x_l + z_i x_j y_l - x_i z_j y_l - y_i x_j z_l - z_i y_j x_l) \\ -(x_i y_j z_k + y_i z_j x_k + z_i x_j y_k - x_i z_j y_k - y_i x_j z_k - z_i y_j x_k)\end{bmatrix}}{6} \tag{A.26}$$

A.4 Solve System of Equations

Equation (A.12) is a system of nonlinear equation of the form,

$$[M(X)]\{X\} = \{B(X)\} \tag{A.27}$$

where, $[M(X)]$ is matrix of known coefficients $m_{ij}(x)$, $\{X\}$ is a vector of the unknown x_i, and $\{B\}$ is a vector of known values $b_i(x)$. There are several different numerical methods that can be used to solve equation (A.27). One choice of method that has been widely used for this purpose is the Choleski method (Cook, 1981).

In the Choleski method, the entries within the banded and symmetric matrix $[M(X)]$ can be stored in a vector $\{M(X)\}$. An example is shown as follows,

Full Matrix Storage; Vector Storage;

$$[M(X)]=\begin{bmatrix} m_{11} & m_{12} & 0 & 0 & 0 & 0 \\ m_{21} & m_{22} & m_{23} & 0 & 0 & 0 \\ 0 & m_{32} & m_{33} & m_{34} & 0 & 0 \\ 0 & 0 & m_{43} & m_{44} & m_{45} & 0 \\ 0 & 0 & 0 & m_{54} & m_{55} & m_{56} \\ 0 & 0 & 0 & 0 & m_{65} & m_{66} \end{bmatrix} \qquad \{M(X)\}=\begin{Bmatrix} m_{11} \\ m_{12} \\ m_{22} \\ m_{23} \\ m_{33} \\ m_{34} \\ m_{44} \\ m_{45} \\ m_{55} \\ m_{56} \\ m_{66} \end{Bmatrix}$$

$$,m_{ij} = m_{ji} \qquad \text{(A.28)} \qquad \text{(A.29)}$$

The length of the vector $\{M(X)\}$ is defined as m_{max}, and is calculated as follows,

$$m_{\max} = NW(ND - NW + 1) + (NW - 1)\left(\frac{NW}{2}\right) \qquad \text{(A.30)}$$

where, NW is semi-bandwidth that is the width of the band in $[M(X)]$, ND is number of equation. In the example of Equation (A.28), NW = 2 and ND = 6, then m_{max} is calculated as m_{max} = 11.

An entry of matrix $[M(X)]$, can be assigned to an entry $m_{ij}(x)$ in the vector $\{M(X)\}$ as follows,

$$m_{ij} = j - i + 1 + NW(i - 1) \qquad \text{(A.31)}$$

where, $k = i - ND + NW - 2 \le 0$

$$m_{ij} = j - i + 1 + NW(i - 1) - \frac{k(k+1)}{2} \qquad \text{(A.32)}$$

where, $k = i - ND + NW - 2 > 0$.

The detail of the Choleski method is referable to elsewhere (e.g. Watanabe et al., 1989).

Equation (A.27) is a system of nonlinear equation, because the entry m_{ij} of matrix $[M(X)]$ is a function of one or more values of x_i. In order to predict unknown value $\{X^{(k)}\}$ at time step k, Picard iteration method can be used. The algorithm for Picard iteration is summarized as follows,

(1) Specify initial approximate solution $\{X^{(0)}\}$

(2) For k = 1, 2, 3, …(each value of k is an iteration) do the following

A. Construct the matrix of coefficients $[M(X^{(k-1)})]$, and the vector of coefficients$\{B(X^{(k-1)})\}$
B. Solve the system of linear equations $[M(X^{(k-1)})]\{X^{(k)}\}= \{B(X^{(k-1)})\}$ for $\{X^{(k)}\}$ by the Choleski method
C. Construct the vector of residuals $\{R^{(k)}\} = \{X^{(k)}\}-\{X^{(k-1)}\}$
D. Test for convergence $|\max\{r_i^{(k)}\}|< \varepsilon$?

If convergence criterion is satisfied, use solution $\{X^{(k)}\}$, otherwise set $k = k+1$ and repeat steps A, B, C and D.

A.5 Water flux in an element

x, y and z components of water flux in an element, q_x, q_y and q_z are calculated as follows,

$$q_x = -\overline{K}\frac{\partial \overline{\psi}}{\partial x} = -\overline{K}\frac{\partial}{\partial x}\sum_m \overline{\psi}_m N_m = -\frac{\overline{K}}{6V}\left(\overline{\psi}_i b_i + \overline{\psi}_j b_j + \overline{\psi}_k b_k + \overline{\psi}_l b_l\right) \tag{A.33}$$

$$q_y = -\overline{K}\frac{\partial \overline{\psi}}{\partial y} = -\overline{K}\frac{\partial}{\partial y}\sum_m \overline{\psi}_m N_m = -\frac{\overline{K}}{6V}\left(\overline{\psi}_i c_i + \overline{\psi}_j c_j + \overline{\psi}_k c_k + \overline{\psi}_l c_l\right) \tag{A.34}$$

$$q_z = -\overline{K}\left(\frac{\partial \overline{\psi}}{\partial z} + 1\right) = -\overline{K}\frac{\partial}{\partial z}\sum_m \overline{\psi}_m N_m - \overline{K} = -\frac{\overline{K}}{6V}\left(\overline{\psi}_i d_i + \overline{\psi}_j d_j + \overline{\psi}_k d_k + \overline{\psi}_l d_l\right) - \overline{K} \tag{A.35}$$

REFERENCES

Cook R.D. 1981 Concepts and applications of finite element analysis. 2nd ed, John Wiley & Sons, New York, U.S.A.

Watanabe T., Natori M. and Oguni T. 1989 Numerical calculation software by fortran77. Maruzen, Tokyo, Japan. (in Japanese)

Zienkiewicz O.C. 1971 The finite element method in engineering science. McGraw-Hill, Berkshire, England.

LIST OF SYMBOLS

LOWERCASE ARABIC

a, b, c, d	fitting parameters for the TDR calibration curve
a_m, b_m, c_m, d_m	coefficients for approximating function N_m
a_e	coefficient for the function A_e
a_h	coefficient for the function k_h
a_t	parameter for E_t
b	correction parameter for function S
b_h	coefficient for the function k_h
d	diameter of root
f	global specified flow matrix
f_m	entry of f
k_h	intensity of hydrotropism
l	distance from the beginning point of a main root to a root
m_{max}	length of the vector $\{M(X)\}$
m_{ij}	entry of matrix $[M(X)]$
n, n_o, n_w	exponents which summarize the geometry of the soil
q	water flux
q'	component of water flux q, perpendicular to the root at the root cap
q_x, q_y, q_z	components of water flux q, in x, y, z directions
$\tilde{q}$	normal flux flowing out across the boundary
r	radius of the root tropism
$r_i^{(k)}$	component of $R^{(k)}$
r_T	linearly increasing function of time
t	time
$t_{\max}$	maximum calculation time
w	weighting factor
w_1, w_2	parameters for w
x, y, z	Cartesian coordinate

UPPERCASE ARABIC

A_e	root elongation activity
A_{ijk}	area of triangular consists of node i, j and k
B	global conductance matrix

B	vector of system of linear equation
$B_{m,n}$	entry of matrix B
C_p	soil water capacity
$\overline{C}_p$	temporal mean value of C_p
D	depth of the soil domain
D	global capacitance matrix
D	deflection index in the model by Diggle
$D_{m,n}$	entry of global capacitance matrix D
$\vec{D}$	growth direction
$\vec{D}_{-1}$	growth direction at the previous time step
E_a	diurnally changing function of actual evaporation rate
E_p	potential evaporation rate
E_p'	diurnally changing function of E_p
ER	elongation rate
ER_c	elongation rate of the center of the root
ER_c'	root elongation rate considering elongation activity
ER_g	elongation rate function of gravitropism
$ER_{g,0}$	constant elongation rate of gravitropism
$ER_{g,\max}$	maximum value of ER_g
$ER_{g,\min}$	minimum value of ER_g
ER_h	elongation rate function of hydrotropism
$ER_{h,0}$	constant elongation rate of hydrotropism
$ER_{h,\max}$	maximum value of ER_h
$ER_{h,\min}$	minimum value of ER_h
$ER_{\max}$	maximum root elongation rate around a sectional circle
$ER_{\min}$	minimum root elongation rate around a sectional circle
ER_n	elongation rate function of circumnutation
$ER_{n,0}$	constant elongation rate of circumnutation
$ER_{n,\max}$	maximum value of ER_n
$ER_{n,\min}$	minimum value of ER_n
ER_s	root elongation rate around the sectional circle
$ER_{s,\max}$	maximum value of ER_s
$ER_{s,\min}$	minimum value of ER_s
E_t	potential evapotranspiration rate
G	gravitropism index in the model by Diggle
G	gravitropism parameter in the model by Pages

$\vec{G}$	vertical vector representing gravitropism
I_b	branching interval
I	function for E_t
K	soil hydraulic conductivity
K_s	saturated soil hydraulic conductivity
$\overline{K}$	temporal mean value of K
L	root length density
L_a	apical non-branching zone
L_a/L	primary output of TDR
L_b	basal non-branched zone
L_{cr}	critical value of root length for water extraction
L_x, L_y, L_z	size of the calculation domain
M	total node number in an element
M	matrix of system of linear equation
M	mechanical constraint parameter in the model by Pages
$\vec{M}$	vector representing the mechanical constraints
N_m	approximating function
ND	number of equation
NW	semi-bandwidth
P_1, P_2	elongation points
Q	function of residual normal distribution
Q	source term in the Richard' equation
$R^{(k)}$	difference of obtained values between time step k and k-1
R_c	correction coefficient for the friction loss of water
R_E	division ratio of E_t into E_p
R_m	weighted residual at node m
S	water extraction intensity
S_1, S_2, S_3	coefficients for elongation rate calculation
$S_{a,n}$	actual water extraction intensity from element n
S_n	water extraction intensity for the elemnt n
$S_{p,n}$	potential water extraction intensity from element n
T	transpiration rate
T_i	monthly mean temperature
T_p	potential transpiration rate
T_p'	diurnally changing function of T_p
V	volume of an element
W	width of the soil domain
W_m	weighting function for node m

LOWERCASE GREEK

α	angle of the root tropism
α_E	function of water content ranging from 0 to 1 determining E_a value
α_T	function of water content ranging from 0 to 1 determining $S_{a,n}$ value
β	angle around the root sectional circle from the top point of the circle
β_g	value of β which gives $ER_{g,\max}$
β_h	value of β which gives $ER_{h,\max}$
β_n	value of β which gives $ER_{n,\max}$
β_s	value of β which gives $ER_{s,\max}$
γ	angle between the direction of gravity and root orientation
δ	slope angle
ϕ	soil hydraulic potential
ϕ_i	insertion angle
ϕ_{int}	initial value of soil hydraulic potential
ϕ_v	void ratio
γ	boundary of the domain
κ	dielectric constant
κ_a	dielectric constant of air
κ_{coil}	dielectric constant obtained by coil type probe
κ_p	dielectric constant of probe material
κ_s	dielectric constant of soil particle
κ_{soil}	dielectric constant of soil
κ_w	dielectric constant of water
λ	variable determining subset of the finite difference formulation
θ	soil water content
θ_r	residual soil water content
θ_s	saturated soil water content
ρ	water penetration coefficient of root
σ	dimensionless parameter relating to the width of the pore-size distribution
ψ	soil water potential
ψ_c	water potential of the beginning point of the main root
ψ_e	parameter for the function A_e
ψ_h	parameter for the function k_h
ψ_{int}	initial value of soil water potential
ψ_m	soil water potential corresponding to the median soil pore radius
$\hat{\psi}$	approximated solution of ψ

ω	angle between the $\vec{D}_{-1}$ vector and $\vec{M}$
ω_n	angular velocity of circumnutation

UPPERCASE GREEK

ΔD, ΔW	size of the triangle finite element
ΔER_g	intensity of gravitropism
ΔER_n	intensity of circumnutation
Δt	time step for the root elongation
$\Delta\psi$	difference of water potential between root and soil
Γ	surface area of an element which is located on the boundary
Ω	volume of element

ACKNOWLEDGEMENTS

謝辞

本研究を遂行するに当り、細部から全体の方針に至るまで御指導頂いた、京都大学大学院農学研究科水山高久教授に心からの謝意を表します。また、常に適切な助言をして頂いただけでなく、研究を遂行する姿勢をも示して頂いた京都大学大学院農学研究科小杉賢一朗助手に深く感謝いたします。両先生方の御指導・助言がなければ、この研究を遂行することはできませんでした。重ねてお礼申し上げます。

ともすれば偏った方向に進みがちな研究において、それぞれの御専門の立場から非常に有益かつ鋭い助言を頂いた、京都大学防災研究所藤田正治助教授、京都大学大学院農学研究科里深好文助教授、谷誠教授、大手信人助教授、小杉緑子助手に深い感謝の意を表します。本研究において、先生方の助言全てに沿った結果を示すことは出来ませんでしたが、今後研究を進めるに当り大きな財産となったことは間違いありません。

京都大学農学研究科の山地保全学研究室および森林水文学研究室の緒先輩方、同僚、後輩のみなさんからは、その研究する姿で常によい刺激を与えて頂くと同時に、温かい協力・助言を頂きました。特に、中国大獲村での根系調査における協力は、本研究においてかけがえのないものとなりました。これら全ての方々に心から感謝いたします。また、常に本研究を縁の下から支えていただいた福田路子さんに心から感謝いたします。

最後に、研究を行うことに理解を示し、常に支えてくれた妻と娘、両親に心から感謝します。ありがとうございました。これからもよろしく。

2002年12月

堤　大三